

Old Dominion University

ODU Digital Commons

Sociology & Criminal Justice Theses & Dissertations

Sociology & Criminal Justice

Summer 2011

Prenatal Smoking and Drinking Implications for Subsequent Child Maltreatment

Nicholas Alexander Adams
Old Dominion University

Follow this and additional works at: https://digitalcommons.odu.edu/sociology_criminaljustice_etds



Part of the [Behavior and Behavior Mechanisms Commons](#), [Family, Life Course, and Society Commons](#), [Maternal and Child Health Commons](#), and the [Medicine and Health Commons](#)

Recommended Citation

Adams, Nicholas A.. "Prenatal Smoking and Drinking Implications for Subsequent Child Maltreatment" (2011). Master of Arts (MA), Thesis, Sociology & Criminal Justice, Old Dominion University, DOI: 10.25777/hz97-fk19
https://digitalcommons.odu.edu/sociology_criminaljustice_etds/70

This Thesis is brought to you for free and open access by the Sociology & Criminal Justice at ODU Digital Commons. It has been accepted for inclusion in Sociology & Criminal Justice Theses & Dissertations by an authorized administrator of ODU Digital Commons. For more information, please contact digitalcommons@odu.edu.

LINEAMENT ANALYSIS AND TECTONIC
INTREPRETATION FOR
THE CENTRAL THARSIS REGION, MARS

by

Robert C. Anderson
B.S. May 1979, Old Dominion University

A Thesis Submitted to the Faculty of Old
Dominion University in Partial Fulfillment
of the Requirements for the Degree of

MASTER OF SCIENCE

GEOLOGY

OLD DOMINION UNIVERSITY
December, 1985

Approved by:

Ramesh Venkatakrisnan (Advisor)

G. Richard Whittecar

Randall S. Spencer

ABSTRACT

LINEAMENT ANALYSIS AND TECTONIC INTERPRETATION FOR THE THARSIS REGION, MARS

Robert C. Anderson
Old Dominion University, 1985
Advisor: Dr. Ramesh Venkatakrisnan

Lineament studies conducted for the Central Tharsis Region of Mars (30°N and 30°S latitude; 45°W to 157.5°W longitude) indicate two major events controlled the formation of the Tharsis Dome: 1) a pre-Tharsis fracture system consisting of North-West (315°) trending fractures; and 2) a Tharsian fracture system containing North-South (355°) and East-West (275°) trending fractures. The North-West (315°) trending fractures represent a crustal weakness zone which controlled the early formation of the Tharsis Dome. Analytical studies suggest four centers of uplift: 1) 6°N, 124°W; 2) 0.5°N, 114°W; 3) 5°S, 106°W; and 4) 7°S, 104°W. Each of these uplifting centers is associated with a radial fracture pattern in the Tharsis region of Mars.

Two models explain the tectonic evolution of the Tharsis region-multicentered doming of the crust, and a migrating hotspot.

Dedication

To my Mom and Dad

In recognition of love
and support for 30 years

Acknowledgements

I wish to thank the staff of the Department of Geological Sciences of Old Dominion University for its support and guidance on this project. I am greatly indebted to Dr. Ramesh Venkatakrishnan, my thesis director and good friend, for support, guidance, and most of all faith in me throughout this study.

I would like to thank the other members of my committee, Dr. Randall Spencer and Dr. Richard Whittecar for their assistance. I would like to thank Dr. Whittecar in particular for the many suggestions and useful ideas he offered during this study.

Special thanks goes out to Paul Reynolds of the ODU Computer Center and Britt McMillan for their help with the computer portion of my research.

Last but not least, I am eternally grateful to my parents and my best friend Courtney Reed. Without their love and moral support this thesis would not exist.

TABLE OF CONTENTS

LIST OF FIGURES	vi
LIST OF TABLES	viii
INTRODUCTION	1
Background Information about Mars	2
Research Objectives	4
HISTORY OF THARSIS REGION	6
Geologic Features and Processes	6
Stratigraphy of the Tharsis Area	13
<u>Noachian System</u>	13
<u>Hesperian System</u>	17
<u>Amazonian System</u>	19
EXISTING TECTONIC MODELS	25
Lithospheric Domal Uplift Model	25
Volcanic Construction Model	29
ANALYTICAL TECHNIQUES	31
Lineament Mapping Procedure	31
Analyses	35
<u>Length-Weight Frequencies</u>	39
<u>Fracture Intersections</u>	40
<u>Radial Reconstruction</u>	40

<u>Atypical Fractures</u>42
<u>Density Distribution of Dominant Trends</u>42
RESULTS OF THE DATA ANALYSIS44
Length-Weight44
Fracture Intersection44
Radial Reconstruction47
Atypical Fractures49
Density Distribution52
Projected Centers54
Summary of Analytical Results65
MODELS OF TECTONIC EVOLUTION66
Influence of Pre-Tharsis Fractures66
Proposed Models69
<u>Multiple Doming Model</u>70
<u>Sequential Hotspot Model</u>76
Martian Ridges78
CONCLUDING STATEMENT.80
REFERENCES81
APPENDICES	
1. Terminology of Martian Features93
2. Lineament Data for 10 Degree Intervals.96
3. Lineament Data Divide by Lengths.	115
4. Density Distribution Plots	119
5. Uplifting Experiment.	129

LIST OF FIGURES

Figure	Page
1 Generalized contour map of Tharsis	7
2 Cross Section of Tharsis	8
3 Physiographic Cartoon for Central Tharsis . . .	11
4 Stratigraphic units for Central Tharsis	14
5 Noachian age rocks	16
6 Hesperian age rocks	18
7 Amazonian age rocks	20
8 Banerdt's stress trajectory models	28
9 Composite lineament map for Central Tharsis. . .	33
10 Composite lineament and geologic map for Central Tharsis	34
11 Composite plot of lineaments for Central Tharsis Region	36
12 Composite map of rose diagrams	37
13 Rose diagrams of statistically significant trends	38
14 Length-Weighted frequencies plots	45
15 Fracture intersections frequency plot	46
16 Frequency plots for projected lineaments	48
17 Histogram to calculate atypical fractures . . .	50
18 Frequency plot for atypical fractures	51

19	Density Projections for the Central Tharsis Region	53
20	Resultant density distribution of dominant trends	55
21	Resultant density distribution of dominant trends projected to North-West trend	56
22	Possible candidates for Uplifting Centers	58
23	Radial patterns associated with each Uplifting Center	
	a. Center 1	59
	b. Center 2	60
	c. Center 3	61
	d. Center 4	62
24	Composite map of trends associated with each Uplifting Center	63
25	Comparison of Uplifting Centers	64
26	Illustration of centrifuge model for domal uplift	72
27	Cartoon for the stages of Multiple Doming Model for the Central Tharsis Region.	73
28	Appratus used in fracture experiment	129

LIST OF TABLES

Table		Page
1	Comparison of the Earth and Mars	3
2	Comparison of Martian Volcanoes10
3	Stratigraphic Units24
4	List of Photomosaic Maps32

INTRODUCTION

Ever since its discovery in the 17th century, Mars has captivated the imagination of man. Named after the Greek God of War, Mars, it had remained a shrouded mystery until 1971 when Mariner 9 became the first satellite to orbit another planet. However, the Martian surface still remained a mystery until 1976, when Viking 1 and Viking 2 landed on the surface. Before the project was over, the two Viking orbiters had taken over 50,000 photographs of the Martian surface.

These images opened a new era in planetary exploration by permitting close examination of landscapes and surficial processes active on Mars. Numerous studies discuss the geomorphology, structural geology, and tectonics of much of the planet. Because detailed studies of Martian geology are so new, considerable disagreement has developed over many of the more interesting regions. For example, several conflicting models exist for the tectonic evolution of the Tharsis region.

The primary goal of this research is to reevaluate the tectonic history of the Tharsis region by using improved analytical techniques. The structural grain of the Tharsis region, visible on Viking photographs was not fully exploited in analyses prior to this one due to the

limitations inherent in the procedures used by earlier workers. Also many photogeologic techniques that have been effective in Earth-based photogeologic studies for both interpretation and analysis (e.g. Norman, 1976) have not been used in the mapping of Martian structural and tectonic features. Therefore a secondary objective of this study is to improve upon several interpretative remote sensing techniques.

Background Information about Mars

Although considered to be similar to Earth for centuries (Table 1), Viking photos of Mars revealed a planet substantially different from the other terrestrial planets, Mercury, Venus, and Earth. The Viking Lander found a cold, hostile planet with an atmosphere made up almost entirely of carbon dioxide, plus small amounts of oxygen, nitrogen, and free water (Carr 1980;1981). Unlike the Earth, Mars has no linear mountain ranges or subduction zones to indicate any horizontal motion of lithospheric plates. Vertical tectonics is believed to be the dominant tectonic mechanism on Mars (Carr,1980).

Mutch et al (1976), and Wilhelm (1974) observed that the Martian surface displayed two parts based upon crater

Table 1

Comparison of the Earth and Mars

	Earth	Mars
Diameter (km)	12,756	6,787
Mass ($\times 10^{26}$ gm)	59.8	6.46
Gravitational Acceleration (cm sec ⁻²)	981	373
Average Distance from Sun (10^6 km)	150	228
Mean Density (gm cm ⁻³)	5.52	3.94
Sunlight Intensity (cal/cm ² /sol)	839	371
Length of Year (days)	365	686
Length of day	24h0m	24h40m
Present Inclination	23°27'	23°59'
Present Orbital Eccentricity	0.017	0.093
Period of Rotation (days)	1.00	1.03
Magnetic Field (γ)	60,000	50-100
Atmospheric Pressure (mb average)	1013	7
Known Satellites	1	2
Composition of Atmosphere (major constituents)	N ₂ (79%) O ₂ (21%) H ₂ O ($\frac{1}{2}$ 1%) CO ₂ (0.03%)	N ₂ ($\frac{1}{4}$ 5%) O ₂ (0.1%) H ₂ O (0.1%) CO ₂ (90%)

(Compiled from Carr (1981); Goody and Walker (1972)).

densities: 1) heavy cratered highlands of the high northern and southern latitudes; and 2) the smooth plains material located from 30° south of the equator to the north polar regions. This asymmetrical distribution of features reflects the early evolutionary history of Mars. Wise et al (1979) concluded that the early tectonic history of Mars consisted of two major large-scale events: 1) the degradation of the early crust; and 2) the complex evolutionary history of Tharsis. Numerous authors have since shown, that in order to best understand the tectonic history of Mars, one must first unravel the tectonic history of Tharsis.

Research Objectives

The following are objectives of my research:

- 1) To develop an optimum photo/optical technique for the maximum retrieval of lineament data from the Mariner and Viking images, topographic maps, and geologic maps of the study area.
- 2) To apply and refine a sequence of procedural lineament mapping techniques that have successfully been applied on Earth to better understand the lineament patterns of the Tharsis region.
- 3) To evaluate existing tectonic models to see which

one(s) best fits the mapped and analysed lineament patterns.

- 4) To test the possibility that the Tharsis region is controlled by an underlying basement weakness (planetary fracture pattern)(Hartman, 1973; Katterfel'd, 1974; Felder, 1974; Masson, 1977;1980; Schultz and Malin, 1982; and Whitford-Stark, 1982).

HISTORY OF THARSIS REGION

Tharsis is a dome-shaped (Figure 1) topographically high region centered approximately 105°W , 0°N (Willeman and Turcotte, 1982). Asymmetrical in shape (Figure 2), Tharsis is approximately 8000km in diameter (Solomon and Head, 1982; Wise, 1979; Plescia and Saunders, 1982), 4 to 6 km high and is associated with a strong positive gravity anomaly (Sjogren, 1979). Shown to affect over 25% of the surface area, this region has been the center of most of the major tectonic and volcanic activity that has taken place on the Martian surface (Carr, 1974; Mutch, 1976; Wise, 1979; Plescia and Saunders, 1982; Solomon and Head, 1982).

Geologic Features and Processes

Tharsis contains several large volcanic constructions and gigantic canyon-like features. Most of these features are several magnitudes larger than comparable features on Earth. The largest of the volcanoes, Olympus Mons (see Appendix 1 for definitions of Martian features), is located at 18°N , 134°W . Believed to be the largest shield volcano in our solar system, Olympus Mons is approximately 600 km in diameter, 8 km high, and contains a summit caldera 35 km in diameter (Carr, 1974). Basaltic in

Figure 1

Generalized topographic contour map of the Central Tharsis Region of Mars. Taken from U.S.G.S. #I-1083 Atlas of Mars- Geologic Series. Original map scale 1:25,000,000 (Contour interval in kilometers). om= Olympus Mons; tm=Tharsis Montes; vm=Valles Marineris (These reference labels will be used in following figures.

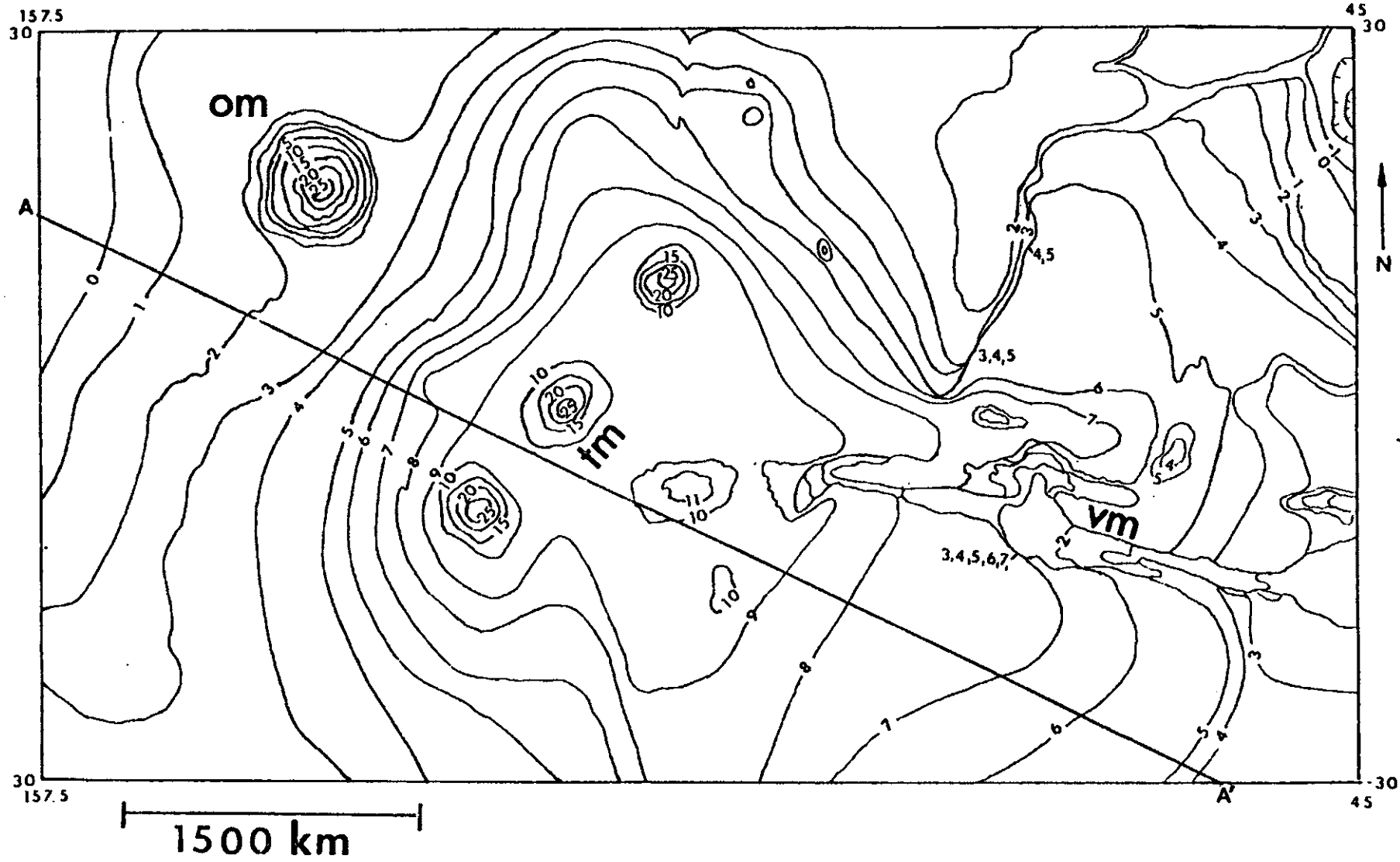
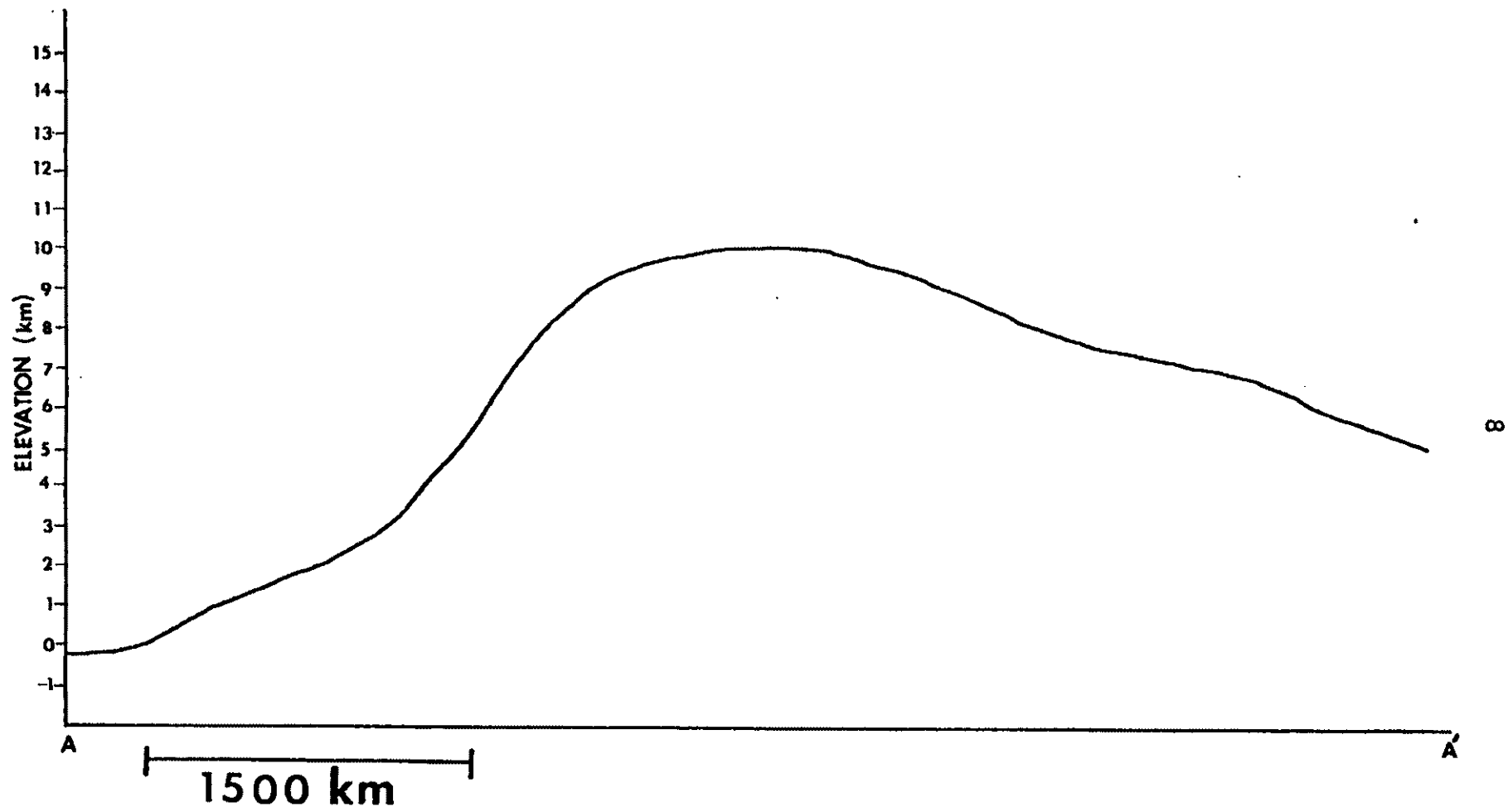


Figure 2 Cross Section of the Central Tharsis Region of Mars. A-A' drawn along general trend of the Tharsis Dome without intersecting major volcanic centers (Figure 1). Elevations measured in kilometers.



composition, this huge volcano played an important role in the evolution of Tharsis.

Just south of Olympus Mons is the Tharsis Montes. This linear (N 40°E) volcanic mountain range is made up of three large shield volcanoes: Arsia Mons (9°S, 120°W), Pavonis Mons (1°N, 104°W), and Ascraeus Mons (11°N, 113°W). Each volcano is approximately 400 km in diameter and 3-5 km above the Martian datum (Carr, 1974). Located throughout the Tharsis region are several small satellite volcanoes. Lying north on the same trend as the Tharsis Montes, three smaller volcanoes have been noted: Uranus Tholus (26°N, 98°W); Ceranius Tholus (24°N, 97°W); and Uranus Patera (26°N, 93°W). East of Ascraeus Mons is yet another small volcano called Tharsis Tholus (13°N, 91°W). On the western side of the Tharsis Montes are three small volcanoes: Jovis Tholus (8°N, 118°W); Biblis Patera (2°N, 124°W); and Ulysses Patera (3°N, 121°W) (Table 2). It is interesting to note that these volcanoes are aligned N45°E (45°) and appear therefore to be structurally controlled (Figure 3).

Also associated with the Tharsis dome is a network of interlocking canyons. The largest canyon in this region is called Valles Marineris. Spanning over 1000 km in length, and 6 km deep, this canyon dominates the south-eastern flanks of the dome. Considered by many to be

Table 2

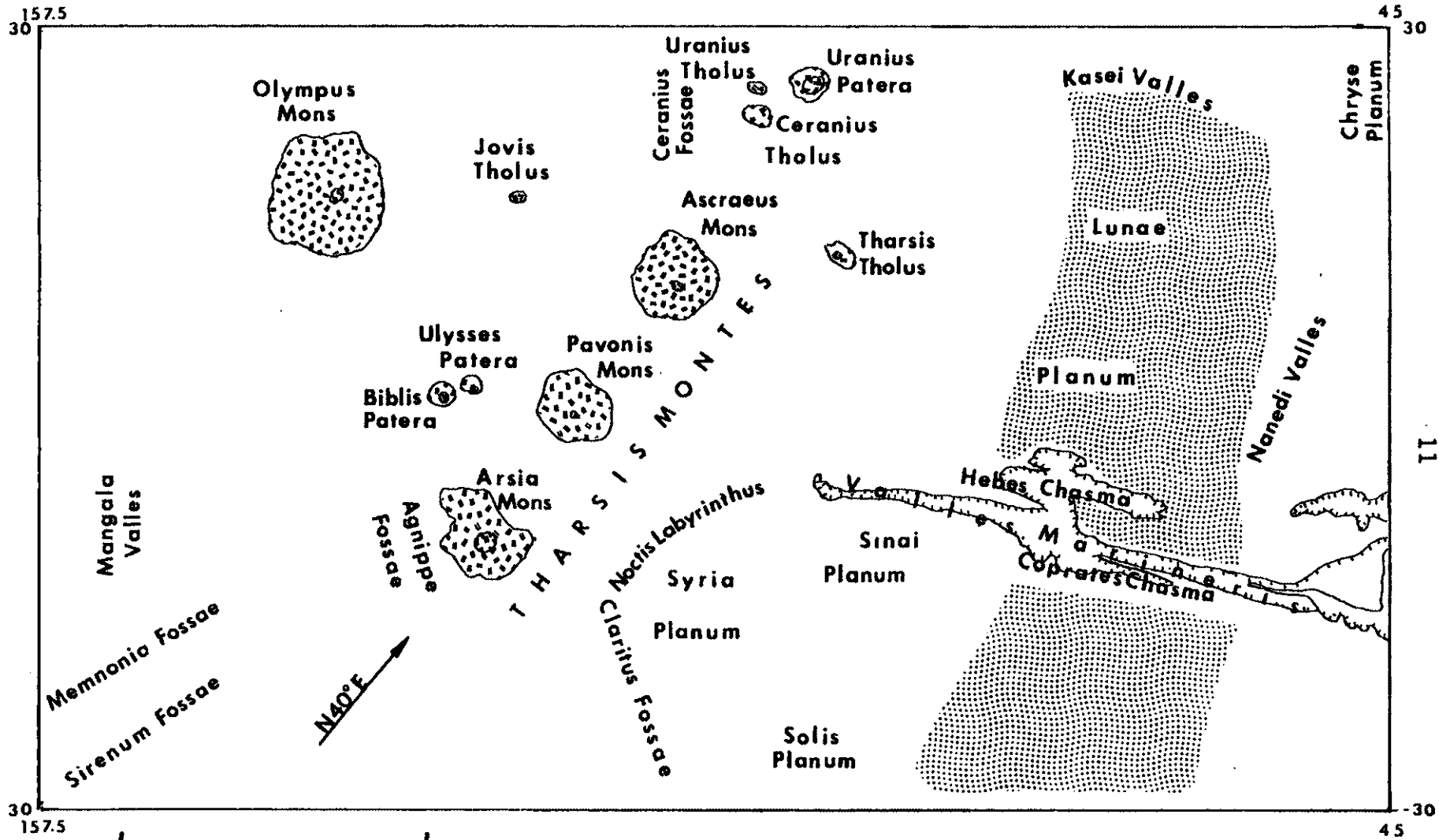
Comparison of Martian Volcanoes

<u>Volcanoe</u>	<u>Avg. Height (km)</u>	<u>Basal Diameter (km)</u>	<u>Avg. Slope (°)</u>
Olympus Mons	23	600	4
Ascraeus Mons	19	300	*
Pavones Mons	17	300	4-6.5
Arsia Mons	12	300	3
Ceraunus Tholus	5	115	9
Uranus Tholus	2	60	7
Uranus Patera	2	240	9
Tharsis Tholus	4	170	*
Jovis Tholus	1	*	*
Biblis Patera	3	100	*
Ulysses Patera	2	100	*

* information not available

Compiled from: Glass (1982), Blasius (1981)

Figure 3 Physiographic reference cartoon for the
Central Tharsis Region of Mars. Dashed
lines=major volcanoes, Dot pattern=ridges.



1500 km

a Martian example of a rift system.

Surrounding the Tharsis dome lies an intricate system of radial fractures, grabens, and compressional ridges. arranged concentrically around the dome.

The geology of the Tharsis region was controlled by alternating periods of volcanism and tectonic deformation (Scott and Carr (1978), and DeHon (1981)). Sequences of lava flows 0.5-3 km thick originate from the major volcanic centers of the Tharsis dome. Between the volcanically active periods, tectonic deformation was controlled by the formation of high fracture systems (fossae) and the appearance of mare-like ridges.

Because Mars has very little free water, landform degradation is dominated at present by eolian processes. Throughout the Tharsis region eroded crater rims, large dune fields, and thick sequences of eolian deposits have been noted. Fluvial activity (Spitzer, 1980) can be documented in some areas on Mars. Supposedly the melting of ground ice during warmer than usual climatic periods in the Martian past generated valleys by both sapping and flooding. The small gravitational force associated with Mars results in a thin atmosphere which is unable to maintain liquid water on the surface for long periods of time. These short-lived fluvial systems most probably were dominated by quick catastrophic events which lasted only a matter of days.

Mass wasting has also played an important role in sculpting the Martian surface (Spitzer, 1980). Landslide debris and slumping features are found throughout this region especially in the south-eastern section of Tharsis which is dominated by the large canyons. Many of the ground fractures associated with slumping features are small however when compared with the regional fracture systems utilized in this study (Kochel, et al, 1982, a,b). They were thus precluded from from the data during initial mapping stages of this study.

Stratigraphy of the Tharsis Area

The Tharsis stratigraphic column has been divided into three Systems (Figure 4): Noachian, Hesperian, and Amazonian (Scott and Carr, 1978). The following discussion is a brief summary of the regional stratigraphy as it pertains to this study.

Noachian System

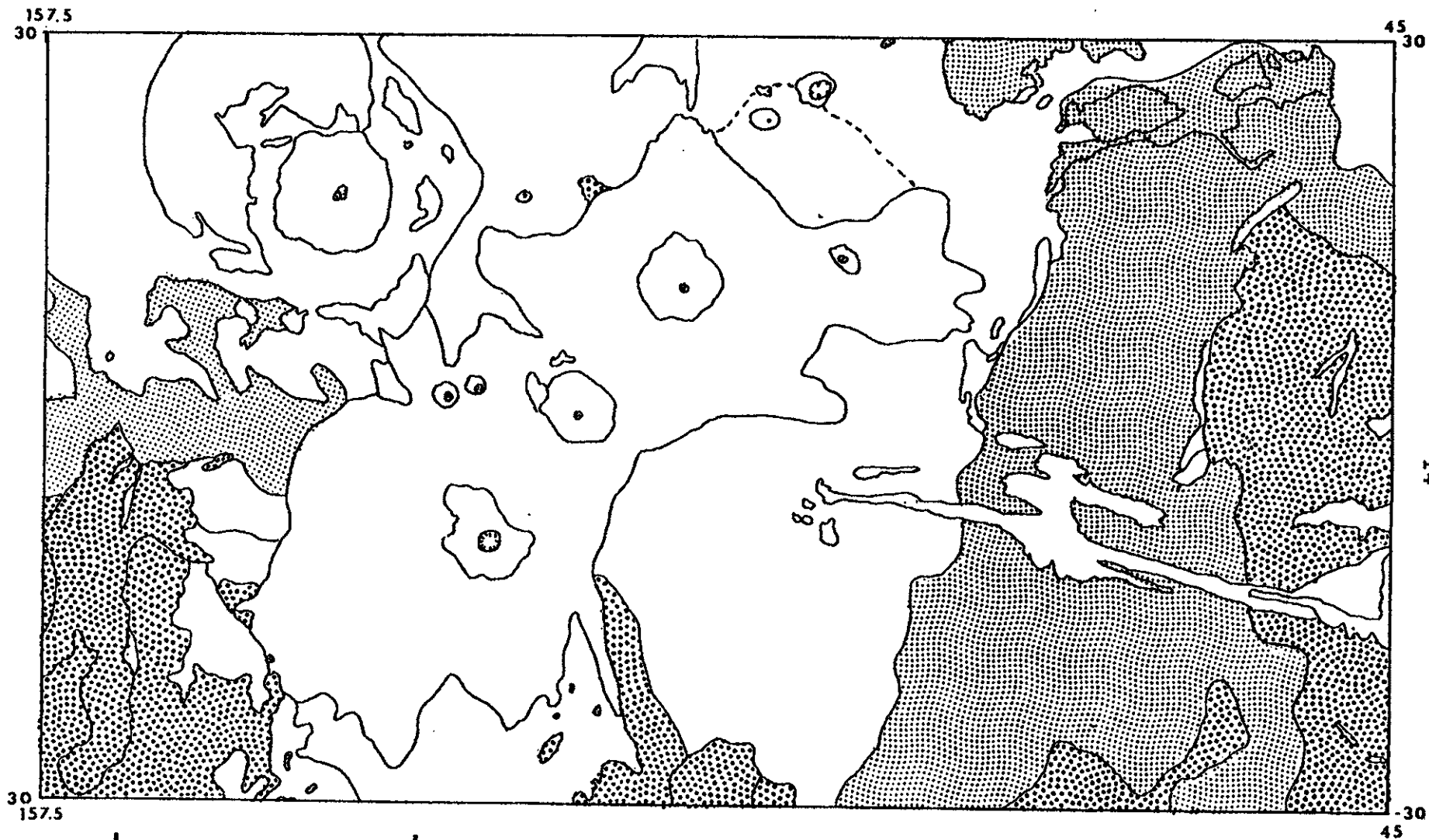
The oldest known rocks on the Martian surface belong to the Noachian System, Nhc. Named after the rocks found in the Noachis Quadrangle, this rock unit consists of the hilly and cratered material on Mars. Scott and Carr (1978) defined Nhc as faulted, highly brecciated, crustal rocks

Figure 4 Stratigraphic units of the Central Tharsis
Region of Mars. Modified from Scott and Carr,
1978; U.S.G.S. #I-1083

Large dot pattern = Noachian Stage

Small dot pattern = Hesperian Stage

No pattern = Amazonian Stage



1500 km

consisting of layers of overlapping and interbedded ejecta-blankets (Figure 5). Formed during a period of high meteorite impact flux on Mars, Nhc covers many of the older, large impact craters.

The next rock unit directly overlying Nhc in the Noachian System are the deflation plains material, Hnpd (Scott and Carr, 1978). Found predominately in the southern polar regions of Mars, this planar unit is normally exposed in erosional windows within younger overlying units.

Directly overlapping the Hnpd and Nhc rock units is Npm, defined by Scott and Carr as mottled plain material which appears mainly in the northern hemisphere of Mars. Wise et al (1979) reported a moderate to high crater count in Npm. Scott and Carr (1978) interpreted this unit to be remnants of old lava plains.

Synchronous with Npm is the rock unit Nplc. This unit has been classified as cratered plateau material by Scott and Carr (1978). Having a crater count of $135/10^2\text{km}$ (Wise, 1979), these ancient lava flows are found in the uplands of the central and southern polar regions. Comprising over a third of the surface rocks, Nplc is frequently dissected with channels and chaotic terrain. Because there are no direct contacts between Npm and Nplc and each exhibit similar crater counts, age determination is presently not possible.

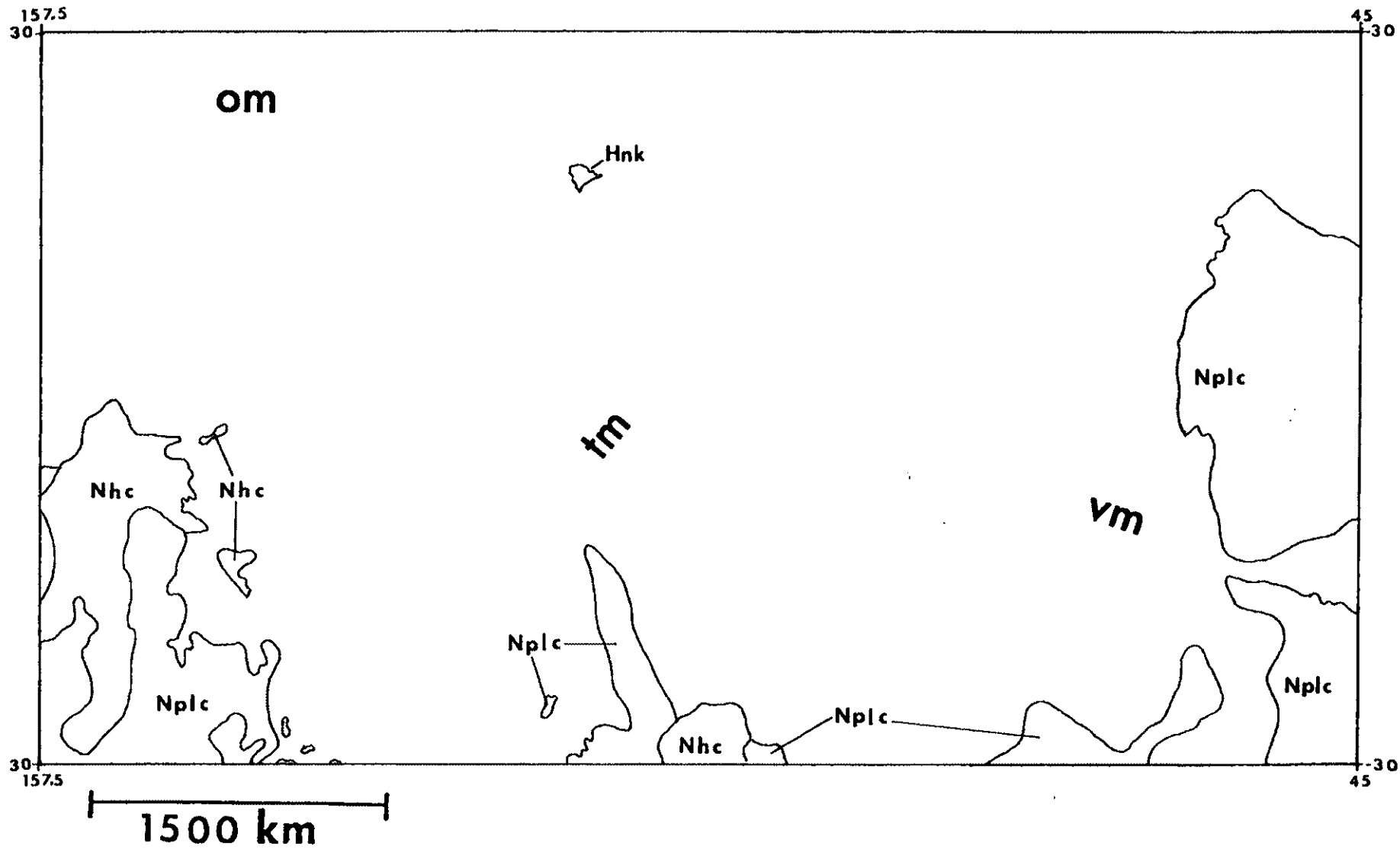
Directly overlying Npm and Nplc rock units is Hnk. Hnk

Figure 5 Rocks of the Central Tharsis Region classified
as Noachian Age. Taken from Scott and Carr
1978 U.S.G.S. #I-1083.

Nhc - Hilly, cratered material

Nplc - Cratered, plateau material

Hnk - Knobby Material



has been classified by Scott and Carr as 'knobby material' and has been interpreted as the erosional remnant of older highland materials. Carr suggested several diverse origins for this unit: material derived from the subsurface collapse due to melting of ground ice, materials left by scarp retreat, materials ejected from impact craters, or materials derived from the erosion of basins and compact crater rims. Scott and Carr (1978), however, concluded that the rocks belonging to Hnk in the Tharsis region are material left behind during scarp retreat.

Hesperian System

The Hnk rock unit is overlain by two units of the Hesperian System (Figure 6). The basal rock unit of the Hesperian System, Hprg, comprises the ridge plains of Mars (Scott and Carr, 1978). Interpreted as ancient lava flows, Martian ridge plains closely resemble lunar maria in appearance. Ridge plains on the Moon and Mars both contain lobate scarps, rills, wrinkle ridges, and similar crater densities of $124/10^2$ km (Wise, 1979).

Directly overlying Hprg is the oldest constructional volcanic unit found on the Martian surface-Hvo. Hvo is commonly associated with the ridge plains material Hprg and forms highly subdued, low-relief volcanic shields.

The third rock unit of the Hesperian System, Hpr has

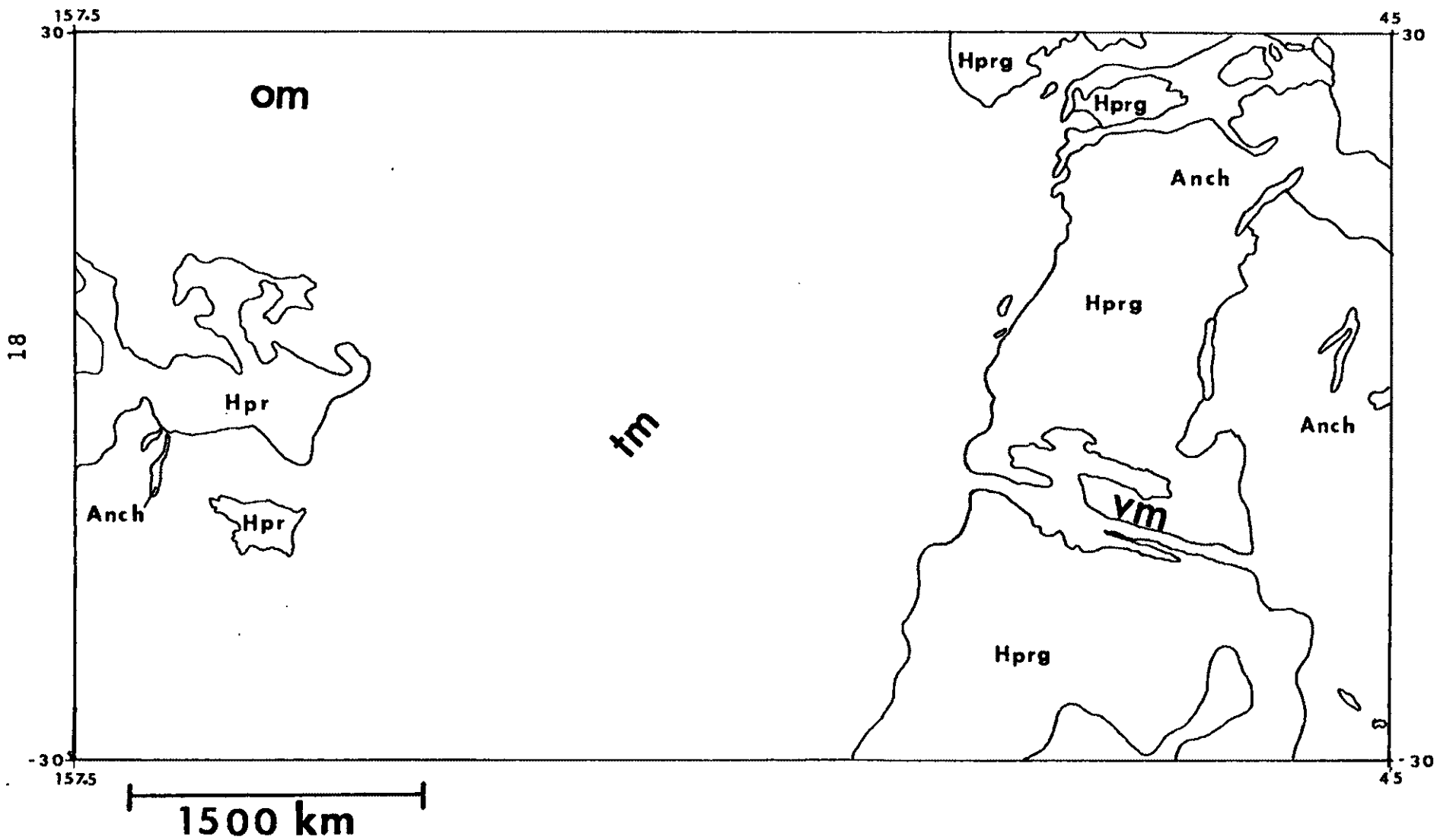
Figure 6

Rocks of the Tharsis Region classified as
Hesperian Age. Taken from Scott and Carr 1978
U.S.G.S. #I-1083.

Hprg - Ridge, plains material

Hpr - Rolling plain material

Anch - Canyon bound material



been classified as rolling plains material (Scott and Carr, 1978). Believed to be volcanic in origin, these flows form relatively flat surfaces. Wise (1979) has determined this rock unit to have crater densities of $73/10^2\text{km}$. Usually more fractured than the cratered plains, this region contains numerous lobate scraps (Scott and Carr, 1978).

Anch rock unit is a canyon-bound unit which first appears in the Hesperian System. Indicating the first appearance of fluvial action, this unit is normally found on the floors of sinuous depressions resembling terrestrial stream beds. Since fluvial activity cannot be attributed to one time zone, this material will appear throughout the younger rock units.

Amazonian System

The youngest period on the Martian surface is called the Amazonian System (Figure 7). Named for rocks found in the Amazonian Quadrangle, this period is dominated by alternating volcanic and eolian events.

The first unit in the Amazonian System is the cratered plains material (Apc). Described by Scott and Carr (1978) as the basal unit for the Amazonian System, Apc has been interpreted as young lava flows covered by a thin veneer of eolian deposits. Similar to the smooth plains material (Aps) in appearance, it differs from Aps only by higher

Figure 7

Rocks of the Central Tharsis Region classified as the Amazonian Age. Taken from Scott and Carr 1978, U.S.G.S. #I-1083.

Apc - Cratered plains material

Aha - Volcanic aureole material

Ahcf - Canyon floor material

Ahct - Chaotic terrain material

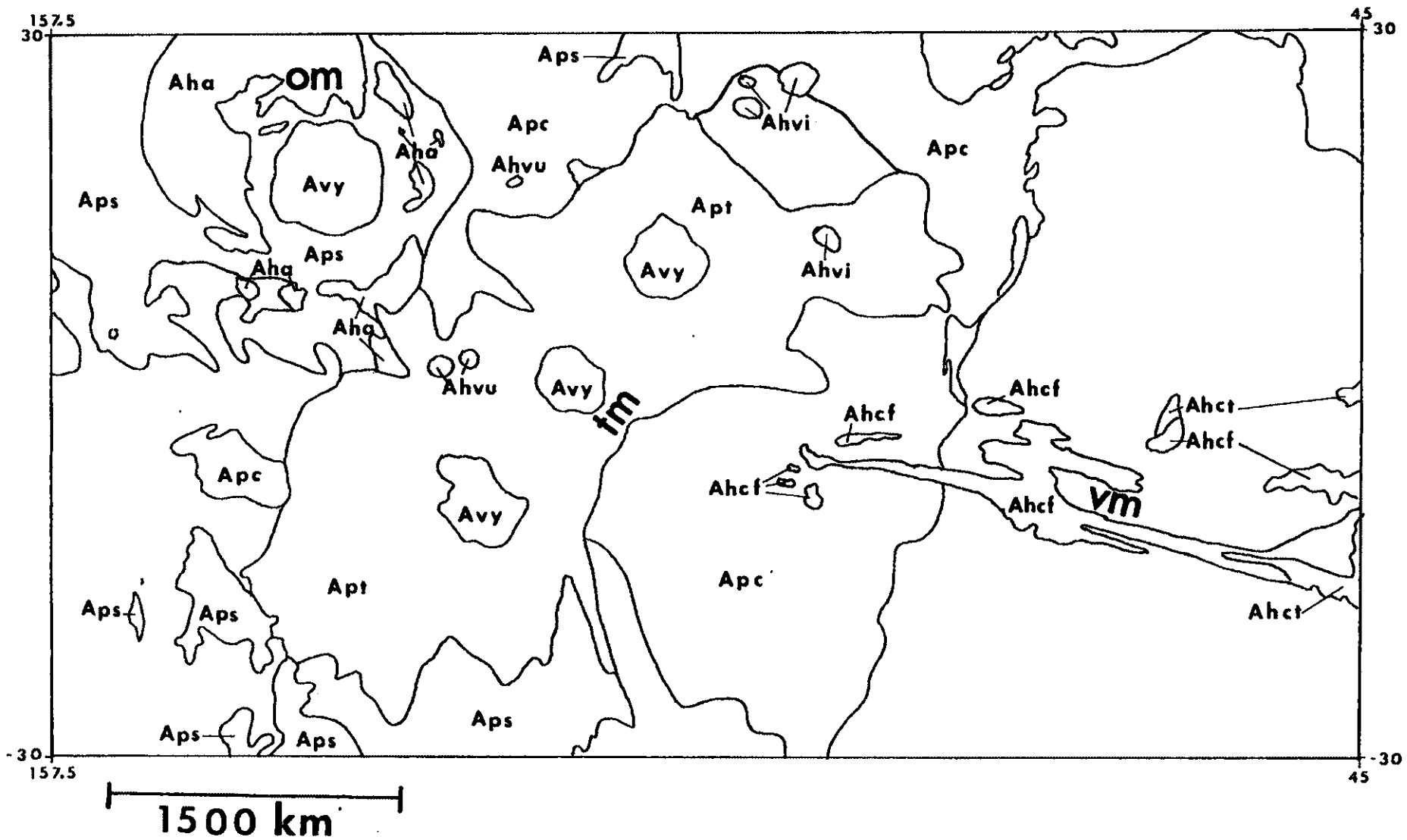
Ahvi - Intermediate aged volcanic plains material

Aps - Smooth plains material

Apt - Young aged volcanic plains material

Avy - Youngest aged volcanic plains material

Ahvu - Young undivided volcanic material



crater counts of $89/10^2\text{km}$ (Wise, 1979) and numerous lobate scraps.

Above the cratered plains material, two diverse rock types are found. The first one Aha, volcanic in origin, has been classified as aureole material. This unit is commonly associated with the major volcanic centers and forms low elongated ridges around the volcanoes. Scott and Carr (1978) interpreted this material as lava flows associated with vents and fissures.

The Amazonian system is characterized by the first appearance of large canyons. The rock unit, Ahcf, has been classified as canyon floor material (Scott and Carr) and is associated with the Valles Marineris canyon. Ahcf usually ranges from smooth to ridged in appearance. Scott and Carr (1978) interpret this unit as landslide debris, and fluvial and/or eolian deposits. Ahcf is usually found in close contact with other rock units of the Amazonian System.

Another rock unit, Ahct represents chaotic terrain material believed to be associated with subsurface collapse from the melting of ground ice. Ahct forms blocky, grooved, fractured terrains which accumulate in topographic lows. In the Tharsis region, it is associated with Valles Marineris region (Scott and Carr).

The later part of the Amazonian System was dominated by the volcanic activity associated with the Tharsis area.

The first rock unit to appear was Ahvi. This unit has been classified by Scott and Carr (1978) as intermediate age volcanic material. Believed to be basaltic in composition, Ahvi dominates the three small volcanoes in the northeastern section of the Tharsis region: Uranus Tholus, Uranus Patera, and Ceranius Tholus (see Figure 1).

The next unit to appear in the Amazonian System is the smooth plains material (Aps). Mapped on a planet-wide extent, Aps is found primarily in the northwestern section of the study area. Scott and Carr (1978) classified Aps to consist of eolian and volcanic deposits which are estimated hundreds of meters thick. With such a thick veneer of material, craters are effectively buried resulting in low crater densities of $59/10^2\text{km}$ (Wise et al 1979).

Overlying this unit is the young volcanic plains of the Tharsis Montes (Apt). This basaltic unit is found primarily around three of the major volcanoes: Ascraeus Mons, Pavonis Mons, and Arsia Mons (Scott and Carr). Apt is sometimes confused with smooth plains material (Aps), but Wise (1979) has determined crater density for Apt is approximately $(15/10^2\text{ km})$, roughly half the count for Aps.

The next unit (Avy) comprises the youngest volcanic landforms on the surface of Mars. Believed to be basaltic in composition, Avy ranges from 200 to 800 m.y. old (Wise, 1979) and is the major constituent of the larger Martian

volcanoes. The last unit Ahvu (young, undivided material) forms relatively small parasite domes and cones associated with the larger volcanic features (Scott and Carr, 1978). Due to the small areal extent of Ahvu, Wise (1979) could not determine the age of this unit (Table 3).

Table 3

Stratigraphic Units

<u>Rock Unit</u>	<u>Description</u>	<u>Crater Counts</u>
Nhc	Hilly, cratered material	
Hnpd	Deflation plains material	
Npm	Mottled plain material	135/10 ² km
Nplc	Cratered, plateau material	
Hnk	Knobby material	
Hprg	Ridge, plains material	124/10 ² km
Hvo	Construational volcanic material	
Hpr	Rolling plain material	73/10 ² km
Anch	Canyon bound material	
Apc	Cratered plains material	89/10 ² km
Aha	Volcanic aureole material	
Ahcf	Canyon floor material	
Ahct	Chaotic terrain material	
Ahvi	Intermediate aged volcanic plains	
Aps	Smooth plains material	59/10 ² km
Apt	Young aged volcanic plains	15/10 ² km
Avy	Youngest aged volcanic plains	
Ahvu	Young undivided material	

EXISTING TECTONIC MODELS

Several tectonic models have been developed for the Tharsis region of Mars. The two models that have received greatest acceptance are based upon either 1) lithospheric domal uplift and concurrent flexure loading of the volcanic crust or 2) volcanic construction.

Lithospheric Domal Uplift Model

A widely accepted model for this region is one of a broad, domal, crustal uplift (Carr, 1974; Frey, 1979; Wise, 1979; Plescia and Saunders, 1982). This model for the Tharsis dome assumes a chemical and/or thermal anomaly in the mantle (Head, 1982). This low density anomaly in the lower mantle rises upward as a plume. Fracturing of the rigid lithosphere occurs above the rising plume resulting in the formation of a radial pattern of intersecting faults. Fracturing is followed by the formation of high volcanoes and the appearance of basaltic volcanic plains. Volcanism probably continues until the magma chamber is depleted. However, since horizontal plate motion is not prevalent on Mars, volcanoes are not expected to migrate horizontally off the 'hot spots'. This lack of plate movement results in the formation of volcanoes which are gigantic compared to terrestrial standards. In comparison,

on Earth, hot-spots form lines of volcanoes (Morgan 1972), such as the Hawaiian-Emperor volcanic chain, in the overriding plate.

Several hypotheses have been developed to explain the mechanism for such a large uplift like Tharsis. Carr (1974) proposed the idea of an upwelling mantle plume located under Tharsis. Wise (1979) developed the idea that two convection cells formed under Tharsis, resulting from convective overturning in the Martian mantle.

However, since the development of Carr's (1974) single uplift model, several authors have tried to extrapolate from it. Wise et al (1979) and Frey (1979) have shown that there were two separate uplifting events responsible for the formation of the Tharsis dome. Plescia and Saunders (1982) examined fracture patterns and defined four major uplifts for the Tharsis region. Several lines of evidence that lend support to the domal uplift model include 1) the broad topographic high of the Tharsis dome; 2) the radial pattern of fractures associated with Tharsis; and 3) the presence of older, hilly and cratered material exposed at the center of the dome (Head, 1982).

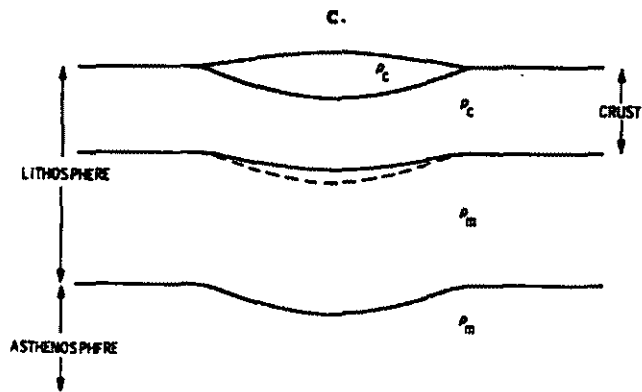
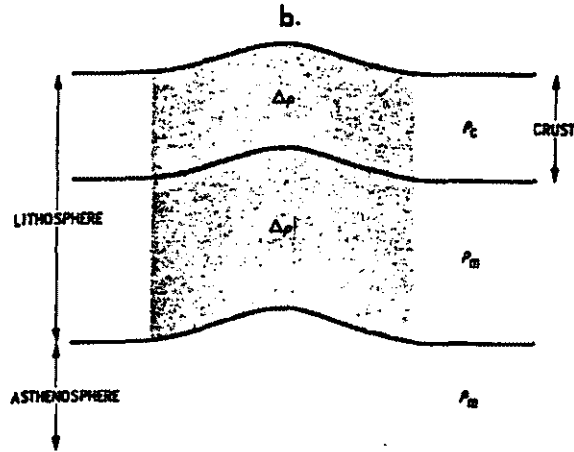
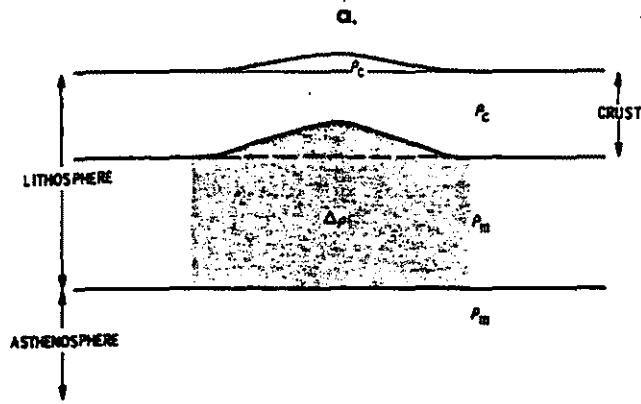
There are however, several questions that this model does not fully explain. Solomon and Head (1982) divided the difficulties into three major categories: 1) stress effects; 2) thermal effects; and 3) compositional effects. They explained that the terrestrial domal uplifts are not

analogous to Martian uplifts. Due to the size of Martian features as compared with the planet's radius, the stresses generated from calculations based on terrestrial analogs are too small. Structures the size of Tharsis generate membrane stresses of a different geometry than those found on the Earth, thereby generating a different stress regime (Turcotte, 1974; Turcotte and Willemann, 1982).

Several studies have attempted to calculate the types of stresses Tharsis would have generated in the Martian lithosphere (Willemann and Turcotte (1982); Banerdt (1982)). Finite element analyses indicated stress trajectories for three types of models (Figure 8): 1) Isostatic model; 2) Flexural uplift; and 3) Flexure loading model (applied load to surface) (Banerdt, 1982). The only model that failed to fit some part of the observed fracture patterns of Tharsis was the Uplift model; the projected stresses generated from this model showed no visible agreement with any observed features found on Tharsis (Banerdt, 1982). The rejection of the Uplift model was supported by the results obtained by Willemann and Turcotte (1982). Banerdt's study, however, did show that the Isostatic model fits the observed pattern of fractures in the area close to the projected center of Tharsis, whereas the Flexural Loading model best explains the area further away from the volcanic center. Banerdt concluded that both the Isostatic and the Flexural Loading models

- Figure 8
- a - Uplift model - Caused by the doming of the lithosphere in response to upward forces (either dynamic or bouyant).
 - b - Isostatic model - Defined as a state of no displacement whereas the load is in balance with the opposing forces from below.
 - c - Flexural loading model - Lithosphere deforms in response to a combination of gravity and topographic loads.

(Taken from Banerdt, 1982)



must have been active during some period of Tharsis formation.

Volcanic Construction Model

Solomon and Head(1980) offered an alternative model to domal uplifting. They proposed a model in which the build-up of volcanic lava flows were responsible for the construction of the Tharsis dome. Solomon and Head (1980) concluded from their model that 1) a thin, heterogenous lithosphere formed in the Tharsis region, 2) this region was the center of localized volcanism; and 3) the domal build-up was the result of the successive accumulation of numerous volcanic lava flows. Their model started with a heteorgeneous, thick lithosphere. Thinning of the lithosphere took place in the Tharsis region either by the generation of global or regional stresses, or by the formation of a high thermal region centered around the volcanic activity. Once the crust thinned, fracturing was restricted around this thin region. Fracture-induced volcanism continued until the development of a broad topographic high. Solomon and Head (1982) pointed out three lines of evidence to support their model: 1) it is not necessary to generate a thermal and/or chemical anomaly in the mantle; 2) there is evidence that loading and subsidence of the lithosphere has taken place by volcanoes

on other parts of the Martian surface (e.g. Elysiumregion);
and 3) gravity profiles agree with observed features found
on the surface.

ANALYTICAL TECHNIQUES

The foregoing section has been an introduction to the stratigraphy and existing tectonic models for the Tharsis region of Mars. The following discussion outlines several analytical lineament studies specifically used for this study that have shown success on Earth. These techniques have been applied to analyze the tectonic evolution of the Tharsis region.

Lineament Mapping Procedure

The area chosen for this study is the central Tharsis region of Mars (30°N. and 30° S. latitude, 45°W. to 157.5°W. longitude). Twenty U.S.G.S. 1:2,000,000 scale photomosaic maps of Mars (Table 4) were examined and lineaments traced onto mylar overlays at map scale. The length and direction of each lineament was accurately measured. The mylar copies for each map were then photographically reduced to a smaller size and assembled to form a composite lineament map (Figure 9).

For the Tharsis region, 6768 lineaments were mapped (Figure 10). Each lineament was then digitized using a Numonics digitizer. The end points of each lineament were measured and recorded in an X-Y reference coordinate frame. Curved segments of otherwise non-rectilinear

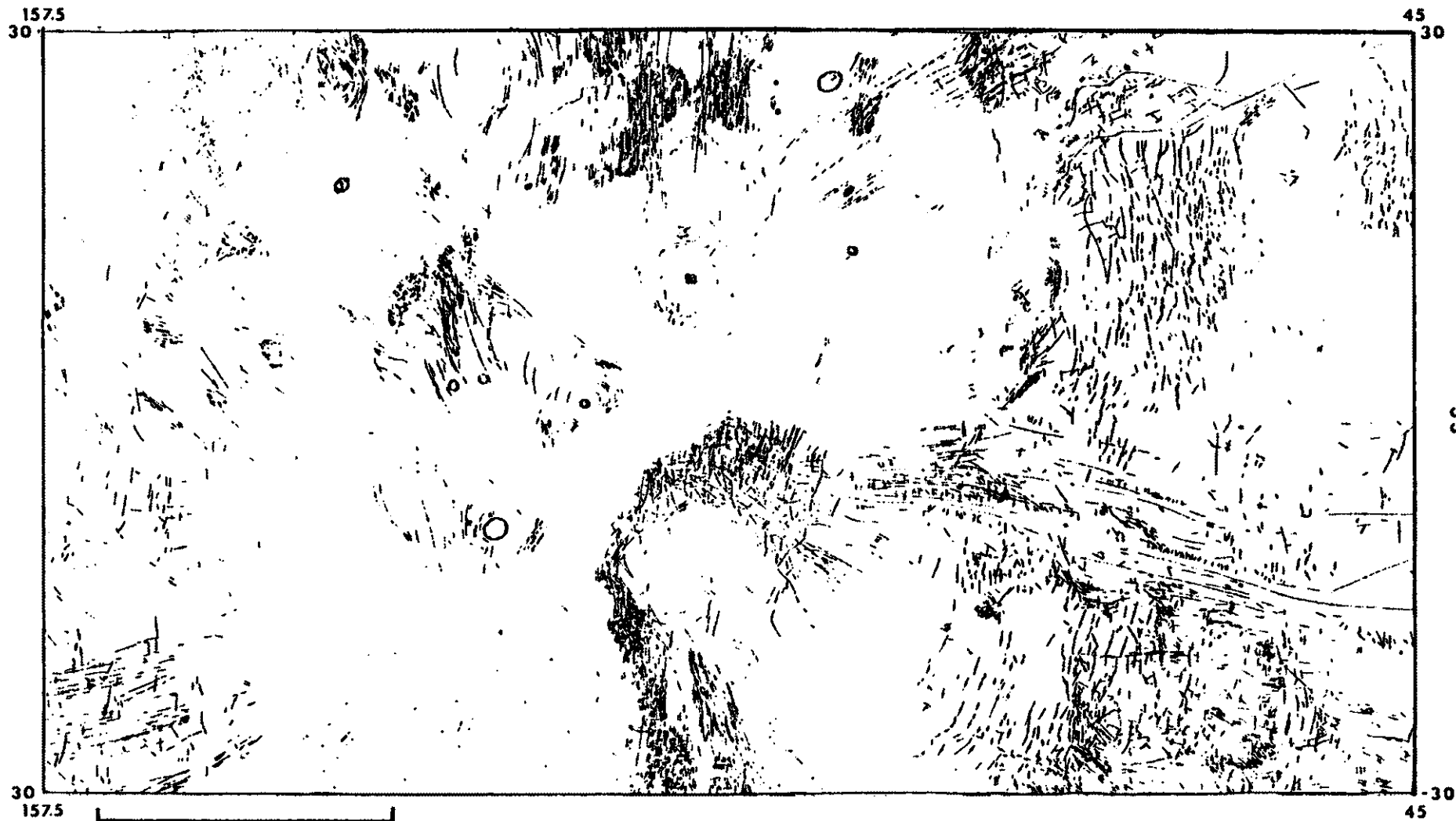
Table 4

List of Photomosaic Maps with Corresponding
U.S.G.S. Index Numbers Used in the Study of
the Central Tharsis Region of Mars

Northeast Amazonis	(MC8-NE)
Southeast Amazonis	(MC8-SE)
Northeast Tharsis	(MC9-NW)
Southwest Tharsis	(MC9-SW)
Northeast Tharsis	(MC9-NE)
Southeast Tharsis	(MC9-SE)
Northeast Lunae Palus	(MC10-NW)
Southwest Lunae Palus	(MC10-SW)
Northeast Lunae Palus	(MC10-NE)
Southeast Lunae Palus	(MC10-SE)
Northeast Memnonia	(MC16-NE)
Southeast Memnonia	(MC16-SE)
Northwest Phoenicis Lacus	(MC17-NW)
Southwest Phoenicis Lacus	(MC17-SW)
Northeast Phoenicis Lacus	(MC17-NE)
Southeast Phoenicis Lacus	(MC17-SE)
Northeast Coprates	(MC18-NW)
Southwest Coprates	(MC18-SW)
Northeast Coprates	(MC18-NE)
Southeast Coprates	(MC18-SE)

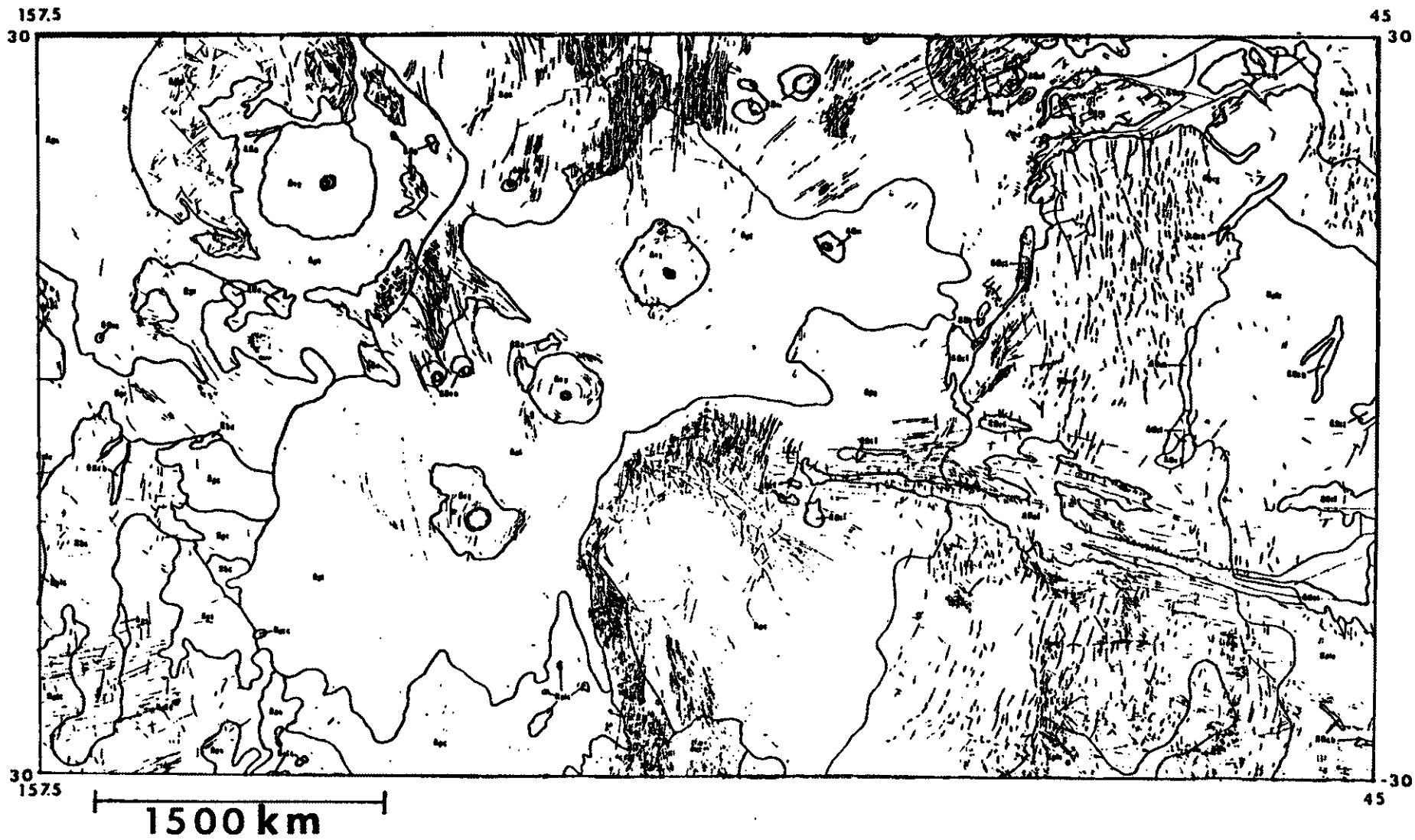
Figure 9

Composite lineament map for the Central Tharsis Region of Mars. Map consists of 6,867 fractures. Fractures smaller than 1 mm (before reduction) were omitted.



33

Figure 10 Composite lineament map superimposed onto the generalized geology map of Scott and Carr (1978) for the Central Tharsis Region of Mars. For detailed map of stratigraphic units see Figures 5,6,and 7.



lineaments were broken into predetermined length segments to facilitate computerization of the data. All analytical procedures were conducted on the Old Dominion University DEC System-10 Computer.

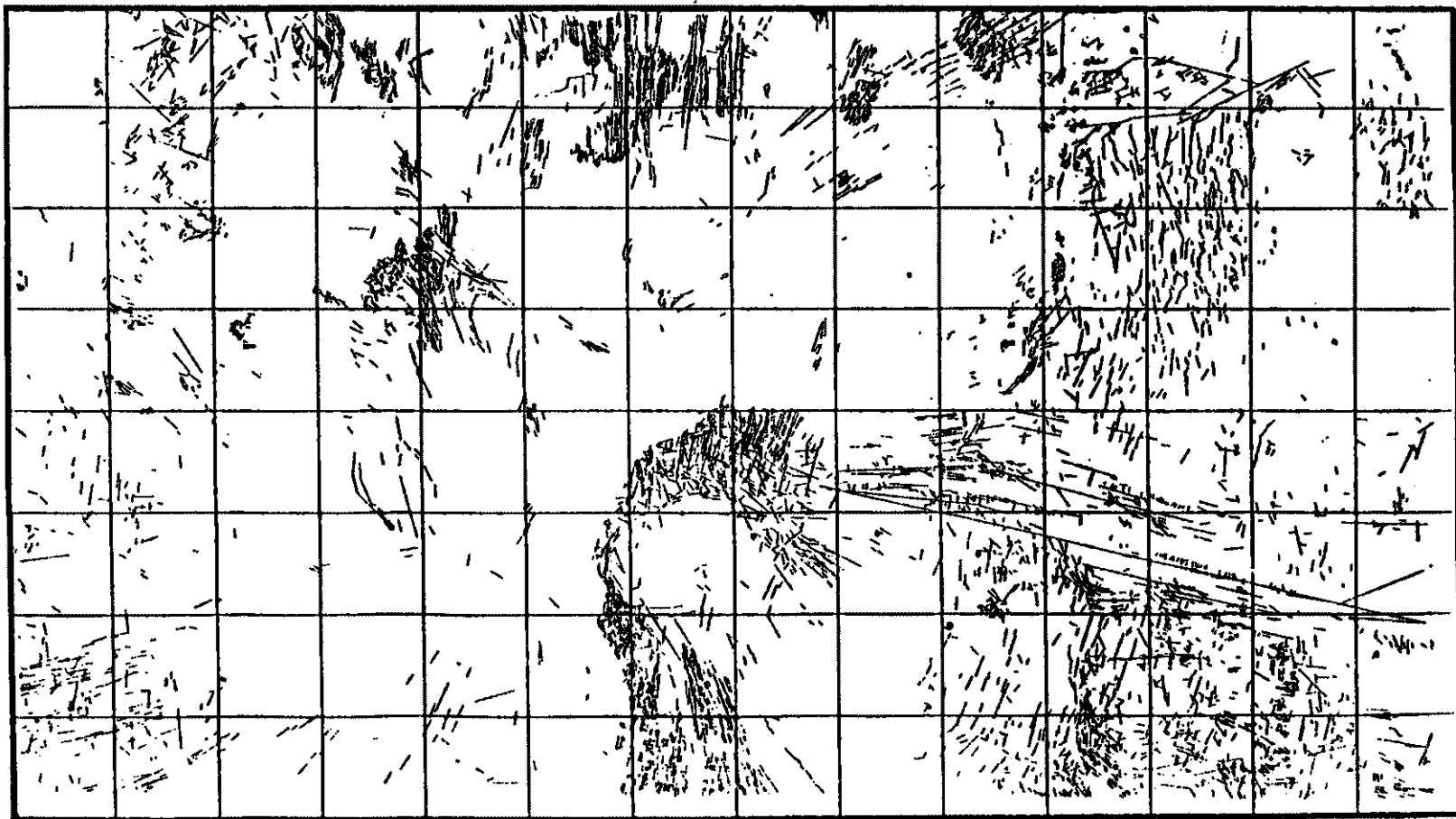
The lineament data was subjected to statistical analyses on a computer program developed by Britt McMillian for statistical fracture trace analysis. This program divided the study area into a predetermined matrix of 14x8 cells; and tabulated the length and direction of each lineament segment for each grid cell. The lineaments were then divided into 5 degree (azimuthal) intervals within their respective grid cells to offset any errors in computation (Abel-Rahman, 1978). The lineament maps were plotted for analysis using a Variant Plotter (Figure 11). Rose diagrams were constructed from the data (Figure 12) for interpretation of the lineament patterns.

Each grid cell was then subjected to statistical analysis to locate dominant trends. Using a 95% confidence interval for lineaments of each grid cell, a map was constructed to obtain statistically dominant trends (Figure 13).

Analyses

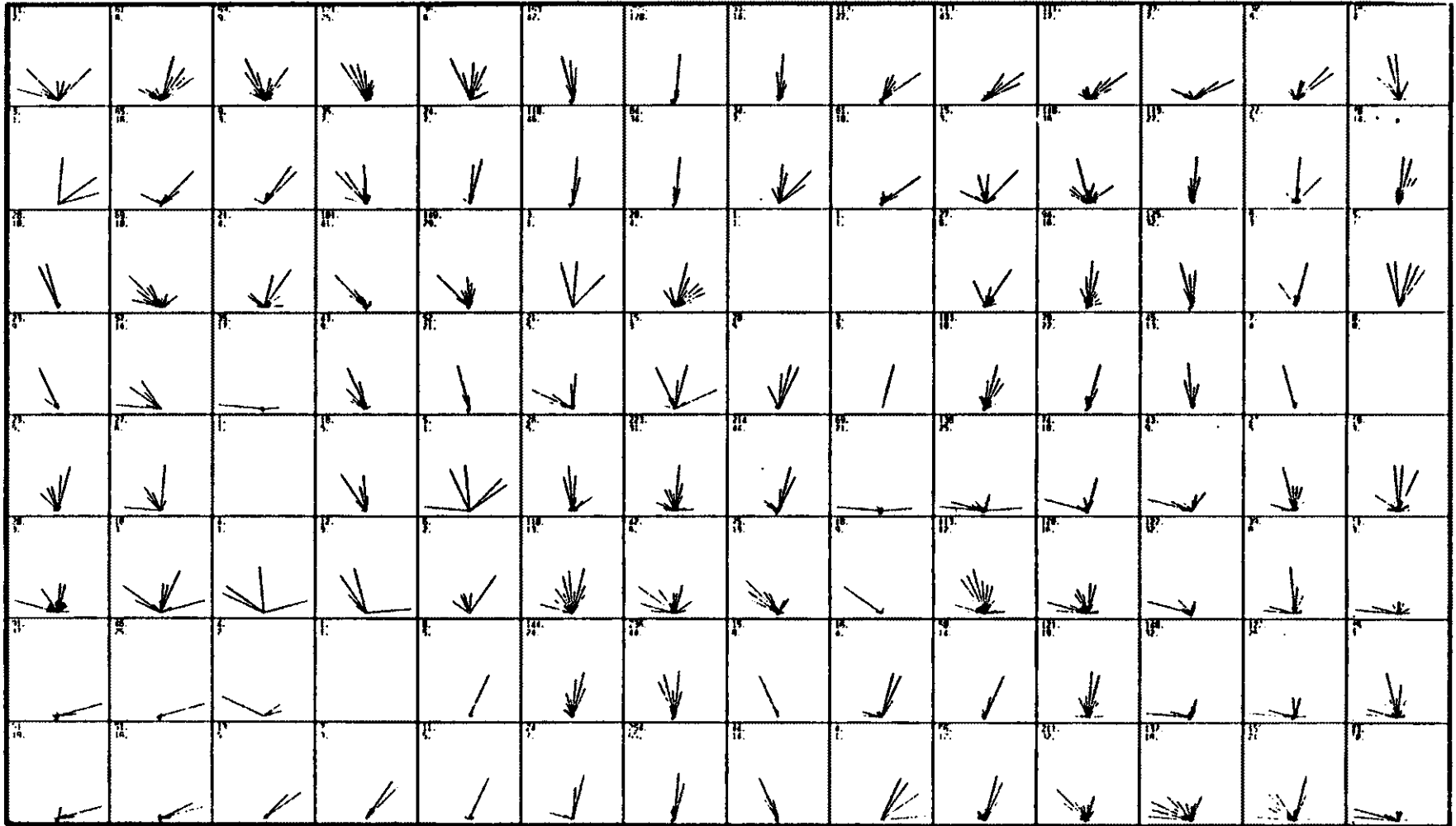
A number of analytical techniques have been developed to examine lineament data on Earth: 1) frequency and/or

Figure 11 Computer generated composite plot of lineaments for the Central Tharsis Region of Mars. (Drawn on a Variant Plotter from a subprogram developed by McMillan, 1984)



1500 km

Figure 12 Computer generated rose diagrams for all lineaments for the Central Tharsis Region.



FRACTURES FOR THE THARSIS REGION / MARS
 ALL FRACTURES

CELL SIZE • 50.0 BY 50.0
 DEGREE RANGE : 0.0 TO 90.0
 LENGTH RANGE : 0.20 TO 0.80

Figure 15 Computer generated rose diagrams for statistically significant lineament directions (based on 95% confidence interval) statistics generated from a computer program developed by McMillan and Venkatakrisnan 1984.

·	↘	↘	↘	↘	↘	↘	↘	↘	↘	↘	↘	·
	↘	·	·	·	↘	↘	↘	↘	·	↘	↘	·
·	·	·	↘	↘		·	·	·	·	↘	↘	
·	↘	·	·	·	·	·	·	·	↘	↘	↘	·
·	↘		↘	·	·	↘	↘	↘	↘	↘	↘	↘
·	↘	·	↘	·	↘	↘	↘	↘	↘	↘	↘	↘
↘	↘	·	·	↘	↘	↘	·	↘	↘	↘	↘	↘
↘	·	·	·	·	·	↘	·	·	·	↘	↘	↘

density contour maps, 2) frequency of fracture intersections, 3) density distribution of dominant trends, 4) atypical fractures, and 5) radial reconstruction. Length-weighted frequencies and fracture intersections techniques will examine regions of lineament concentrations, whereas, density distribution, atypical fractures, and radial reconstruction techniques will outline dominant lineament trends.

Length-Weight Frequencies

Several statistical methods have been developed to interpret directional variations of lineament data. One of the more prominent methods in use is to calculate length-weighted frequencies (Frost, 1977). In this study, length-weighted frequencies were calculated in 18 ten degree intervals; lineaments within each ten degree interval were summed and divided by a predetermined length. A length of 1 unit=10mm was set to simplify the data. These length segments were then divided by the number of lineaments in each interval and given a frequency value. The major advantage of using this method over normal length of weighed frequencies is that long lineaments with small frequencies can be compared with short lineaments which usually occur in significantly larger numbers. When studying a large region such as Tharsis, the length of, or

number of, lineaments alone does not adequately represent the overall lineament pattern. By combining the number and length of lineaments per ten degree azimuthal interval a more realistic scenario appears. Therefore, by using length-weighted frequencies, short (high frequency) and long (low frequency) lineaments can be compared on equal terms.

Fracture Intersection

The lineament data were subjected to an analytical technique developed by Sawatzky and Raines (1978) and modified by McMillan and Venkatakrisnan (1984). The procedure involves counting the number of fracture intersections per predetermined grid cell and then contouring the frequencies of intersections. High concentration areas of fracture intersections represent possible areas of increased volcanic or tectonic activity.

Radial Reconstruction

The shallow intrusion of a magma produces a radial fracture pattern centered on the area of greatest uplift. Interpolation of fractures back to a point therefore should indicate uplifting centers. This technique has been tried on Mars (Salvatori et al (1981) and on Earth

Crosby (1969). Radial reconstruction was applied in the present study to see if one or more radial center existed. In order to use this technique for Tharsis, the following assumptions must be used: 1) that Mars can be considered a one-plate planet (no plate tectonics having ever taken place), 2) that the Martian crust is homogeneous, 3) that the uplifting magmas produce an idealized radial pattern according to the pattern described by Withjack and Schneider (1982) and 4) the greatest concentration of intersections would indicate a prime candidate area for the center of an uplift, since at radial centers of uplift-fracture intensity increases as all fractures converge on the domal center.

Due to the large number of fractures for this region, the data were reduced using a plotting subprogram designed to draw lineaments of particular lengths (10 mm, 10-25 mm, etc; map scale: 1mm= 33.8 km) as well as for a particular degree interval (0-10,10-20, etc) (Appendix 2). This subprogram divided the lineaments into four categories of length: 1) fractures less than 10mm in length; 2) fractures 10-25mm in length; 3) fractures 25-50mm in length; and 4) fractures greater than 50mm in length (Appendix 3).

Fractures in class 2 (10-25mm) were used to project the radial centers of fractures for the Central Tharsis region. This class was used because of the following reasons : 1) to reduce the data to a workable smaller set;

2) there is an adequate statistical representation of the entire population in this class; and 3) a sufficient number of lineaments were available to project back to possible volcanic centers.

Atypical Fractures

Pretorius and Partridge (1974) developed a technique that could be used to recognize the atypical (secondary) fracture pattern of an area. To analyse atypical fractures, 1) calculate the lengths of lineaments in an angular interval for the whole area; 2) plot the data as a histogram; 3) calculate L, where L=frequency level between highest and lowest value on the histogram; 4) calculate the proportion of lineaments for each grid cell with atypical lengths; and 5) contour. High contour concentrations represent regions controlled by secondary fracturing.

Density Distribution of Dominant Trends

Another technique used in lineament directional studies is one of projecting major trends (Boorder, 1981). This technique has been successful when looking for older preexisting trends which have been overlain by younger sedimentary layers. To calculate the dominant trends for a region, the number of lineaments per specified degree

interval are computed and the density (frequency) of each interval contoured. Projection lines are then drawn from each region of high concentration along the average degree interval of the lineaments. By connecting each region of high concentration, long fractures can be interpolated across regions covered by younger volcanic layers.

RESULTS OF THE DATA ANALYSIS

Length-Weight

Length-weighted frequency data constructed and contoured for the central Tharsis region of Mars (Figure 14) suggest the existence of seven lineament concentration zones (LCZ). It is believed that each lineament concentration zone (LCZ) was controlled by one or more tectonic events on Mars.

Fracture Intersection

Fracture Intersection frequency data were contoured for the Central Tharsis region (Figure 15). A comparison of the contour pattern from Figure 15 with the LCZ obtained from Figure 14 shows a similar frequency pattern. LCZ 3,4,5, and 7 maintain a relatively high frequency of intersections whereas LCZ 1, and 6 (possibly 2) show major reduction in the frequency of intersections. The reduction in frequency can be attributed to one of the following causes: 1) control by local tectonism resulting in the increase in the number of fractures; 2) control by one dominant stress trajectory trend; or 3) higher quality resolution of images.

For the Central Tharsis region the reduction in

Figure 14 Computed Length-Weight frequency diagrams for
the Central Tharsis Region of Mars.
Calculated from a computer program developed
by McMillan, 1984. Dot pattern = Areas of
Projected Lineament Concentration Zones
(LCZ). Numbered LCZ are discussed in the text.

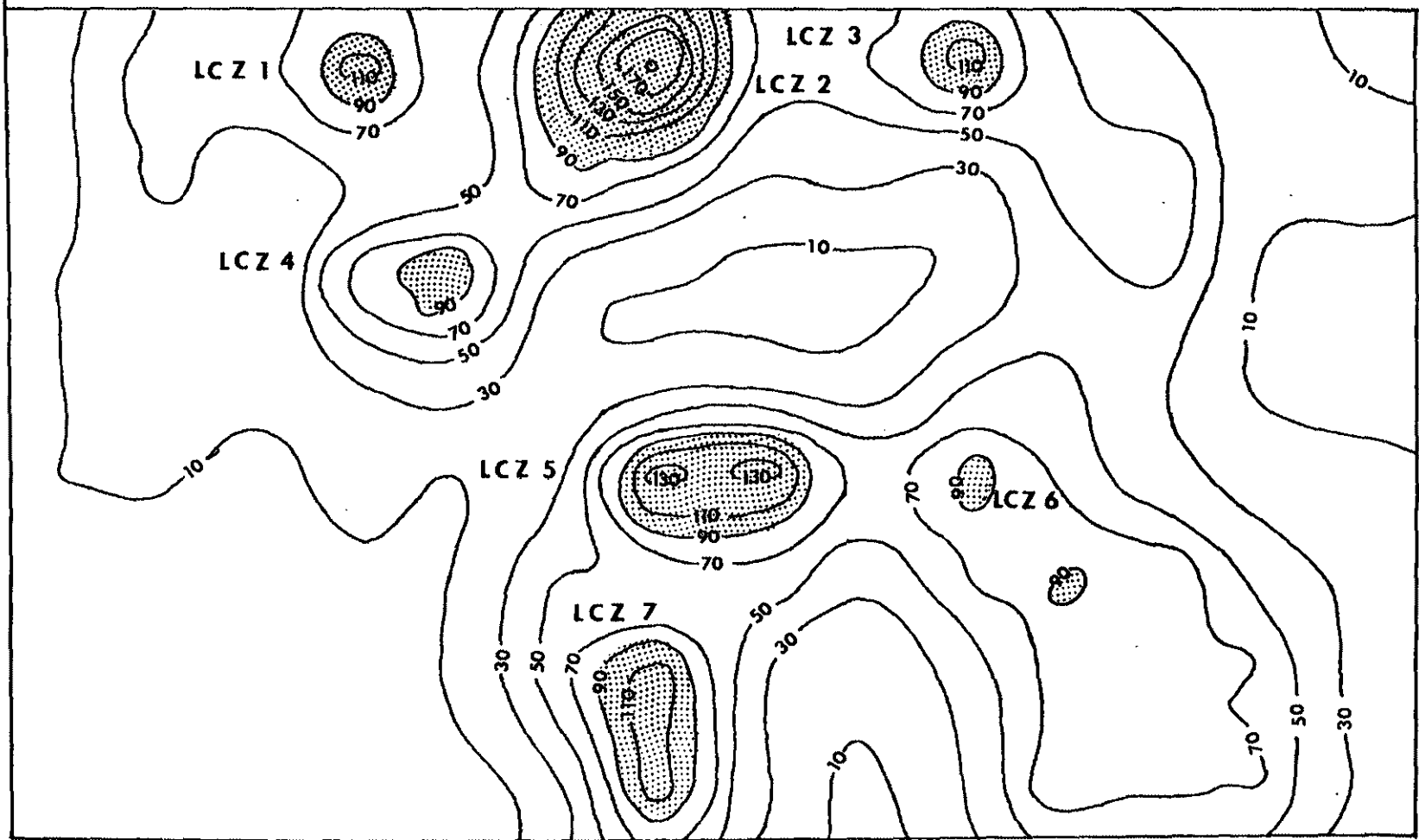
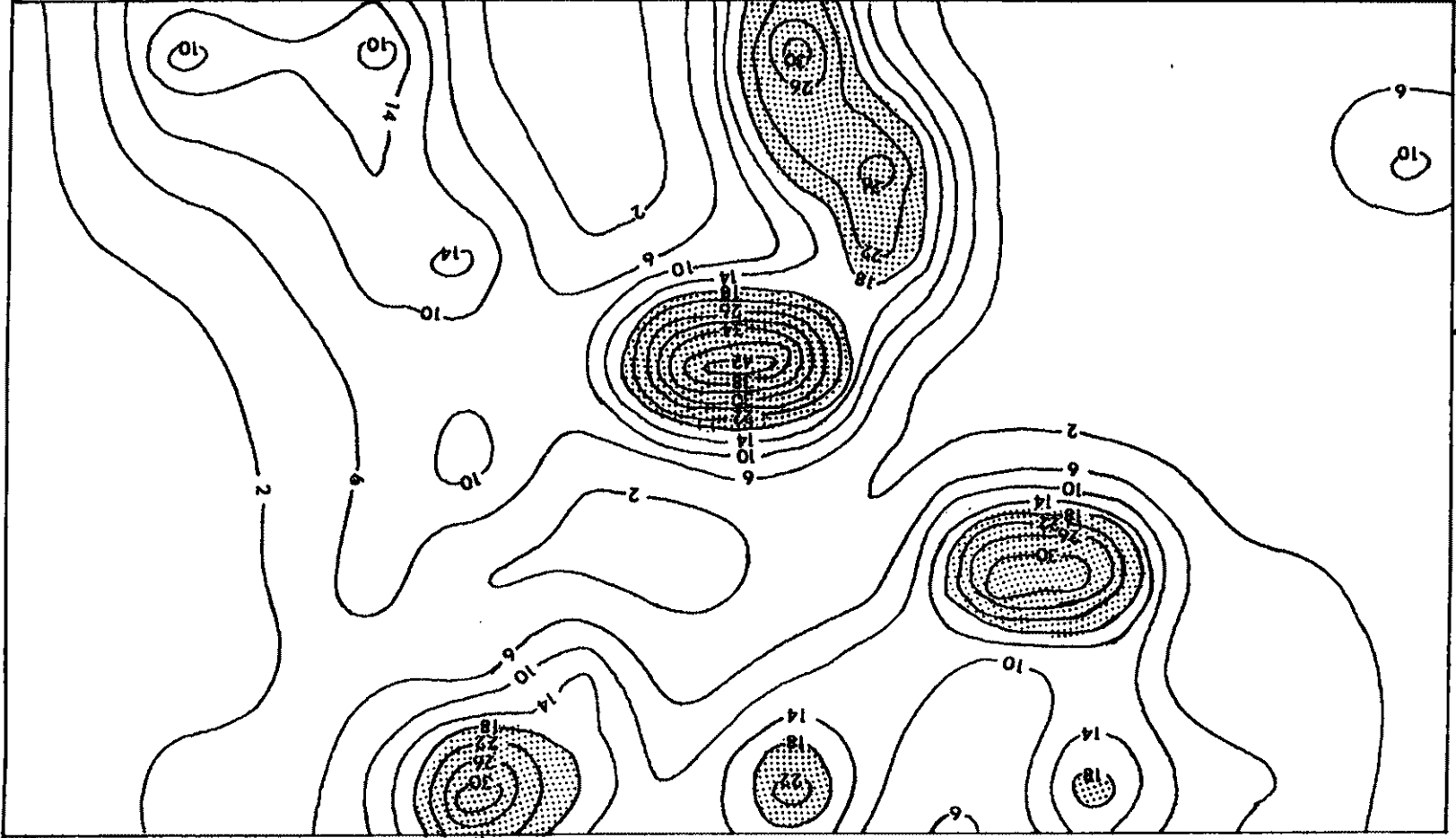


Figure 15 Frequency diagram constructed for the intersection of lineaments for the Central Tharsis Region of Mars. Procedure modified from Sawatzky and Raines (1979) by McMillan and Venkatakrisnan (1984). Dot patterns = areas corresponding to LCZ's



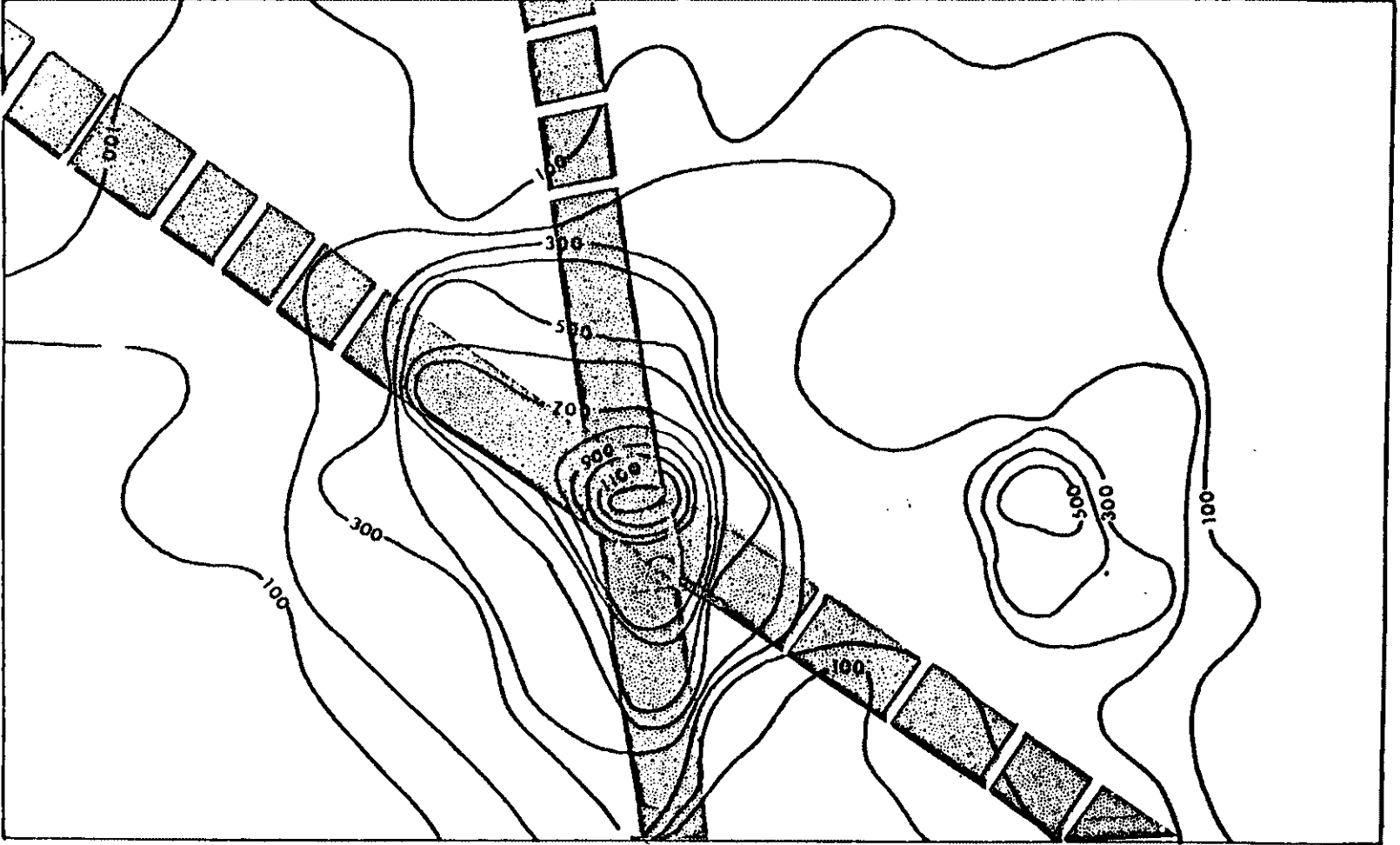
frequency between LCZs' generated for Length-Weight data versus the contour pattern generated from the analysis of Fracture Intersections suggest that LCZ 1 and 6 are dominated by single tectonic events. The lineaments of LCZ 1 are attributed to the formation of Olympus Mons; the lineaments of LCZ 6 are dominated by the presence of Valles Marineris.

Assuming lineament intersections of different lineament-zones or azimuthal peaks increases in areas where repeated volcano-tectonic activity has caused superposition and overprinting of lineaments, LCZ 3,4,5, and 7 are regarded as areas controlled by multiple tectonic events. Each tectonic episode need not generate a "new" fracture trend, since reactivations of preexisting fractures are possible depending on the change in stress directions.

Radial Reconstruction

Figure 16, constructed from the data generated by the Radial Reconstruction analyses, illustrates contoured frequencies of intersections. The map shows two strong trends: 1) a North-South (355°) trend between LCZ 5 and LCZ 7; and 2) a minor trend North-west (315°) between LCZ 4 and LCZ 5. Close examination of the computer generated rose diagrams (Figure 12 and 13) confirm the possible existence of the two trends.

Figure 16 Frequency diagram for the projected lineaments
(10 -25mm class) for the Central Tharsis
Region of Mars. Two areas of possible
dominant lineament trends are found.



Atypical Fractures

Figure 17 is a histogram constructed from the atypical fracture data. From Figure 17, four trends are classified as typical trends; 275-280, 355-0, 0-5, 5-10, and 10-15. This conclusion is in agreement with the results obtained by Salvatori et al (1981). Their study indicated the Tharsis region was controlled by dominant North-South (355°) and East-West (275°) trending fractures.

Figure 18 is a contour plot of the atypical lineaments for the Tharsis region. From the plot, using proportional values greater than 70%, two prominent regions of atypical lineaments were obtained: a North-West trending region corresponding south of a traverse between LCZ 4 and LCZ 5 and the southwestern section of Tharsis.

A comparison of the results obtained from the Radial Reconstruction analyses and the Atypical Fracture data verify the existence of two trends; a strong North-South (355°) from the typical data, and a minor North-West (315°) trend from the atypical lineament pattern. The only discrepancy between the two techniques is the appearance of the East-West (275°) trending lineaments. This East-West trend can be attributed to concentric fracturing resulting from the formation of the Tharsis dome. Due to the nature of the Radial Reconstruction technique (projecting centers with radial patterns), the

Figure 17 Histogram of atypical fractures for the Central Tharsis Region of Mars. Calculated mean average equal 251; fractures above the mean are considered typical and removed from the data. (Pretorius and Partridge, 1974)

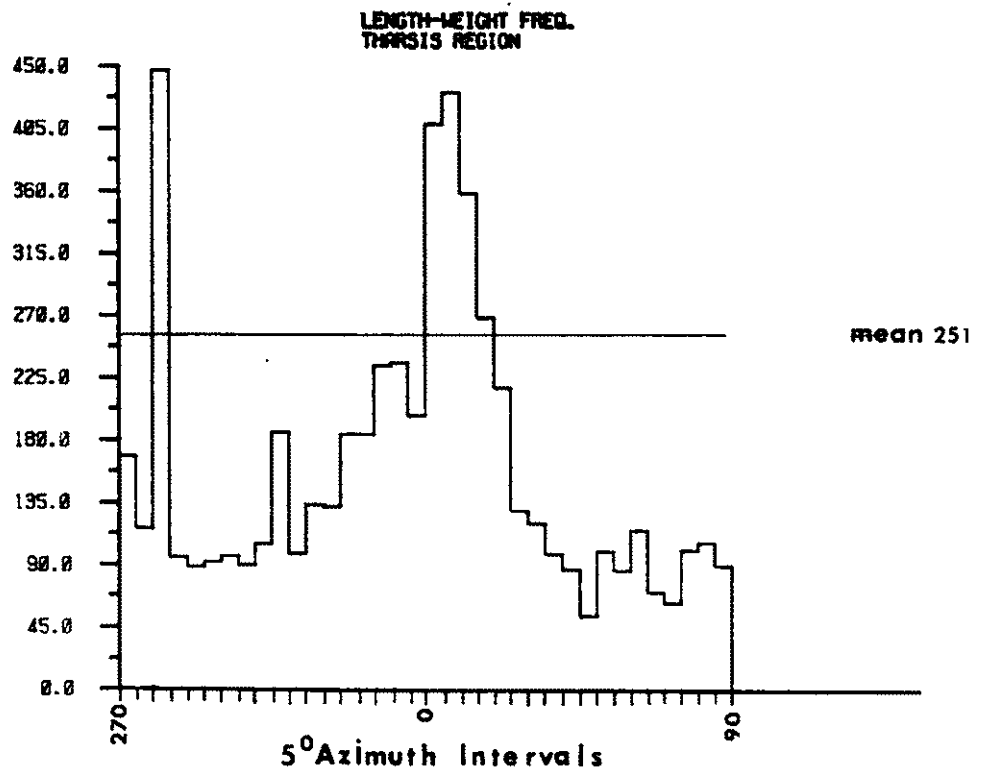
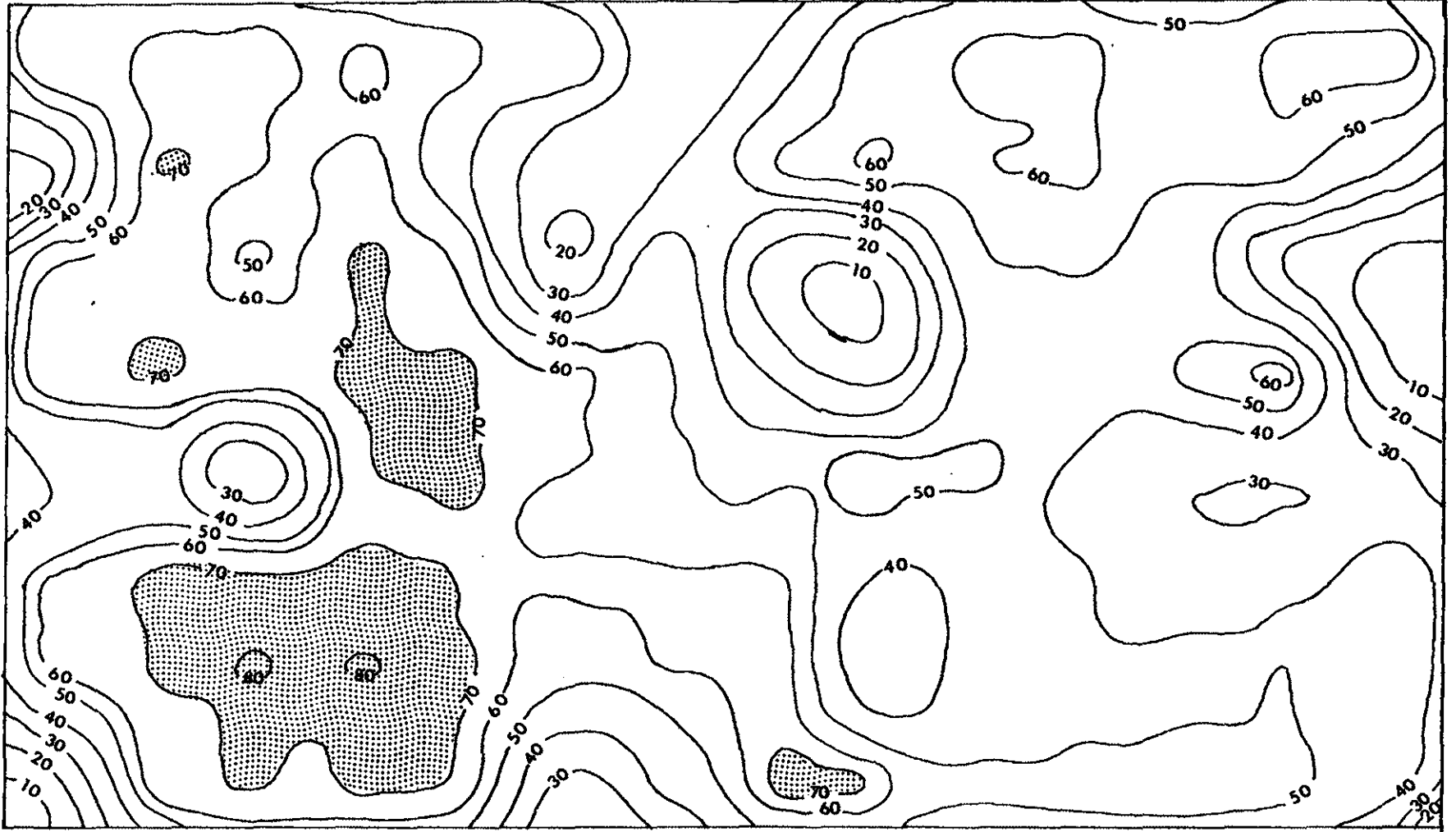


Figure 18 Frequency diagram constructed for atypical fractures of the Central Tharsis Region of Mars. (Following the procedure developed by Pretorius and Partridge, 1974). Dot pattern = areas of atypical concentrations greater than 70%



East-West (275°) trend would not appear on the frequency plot.

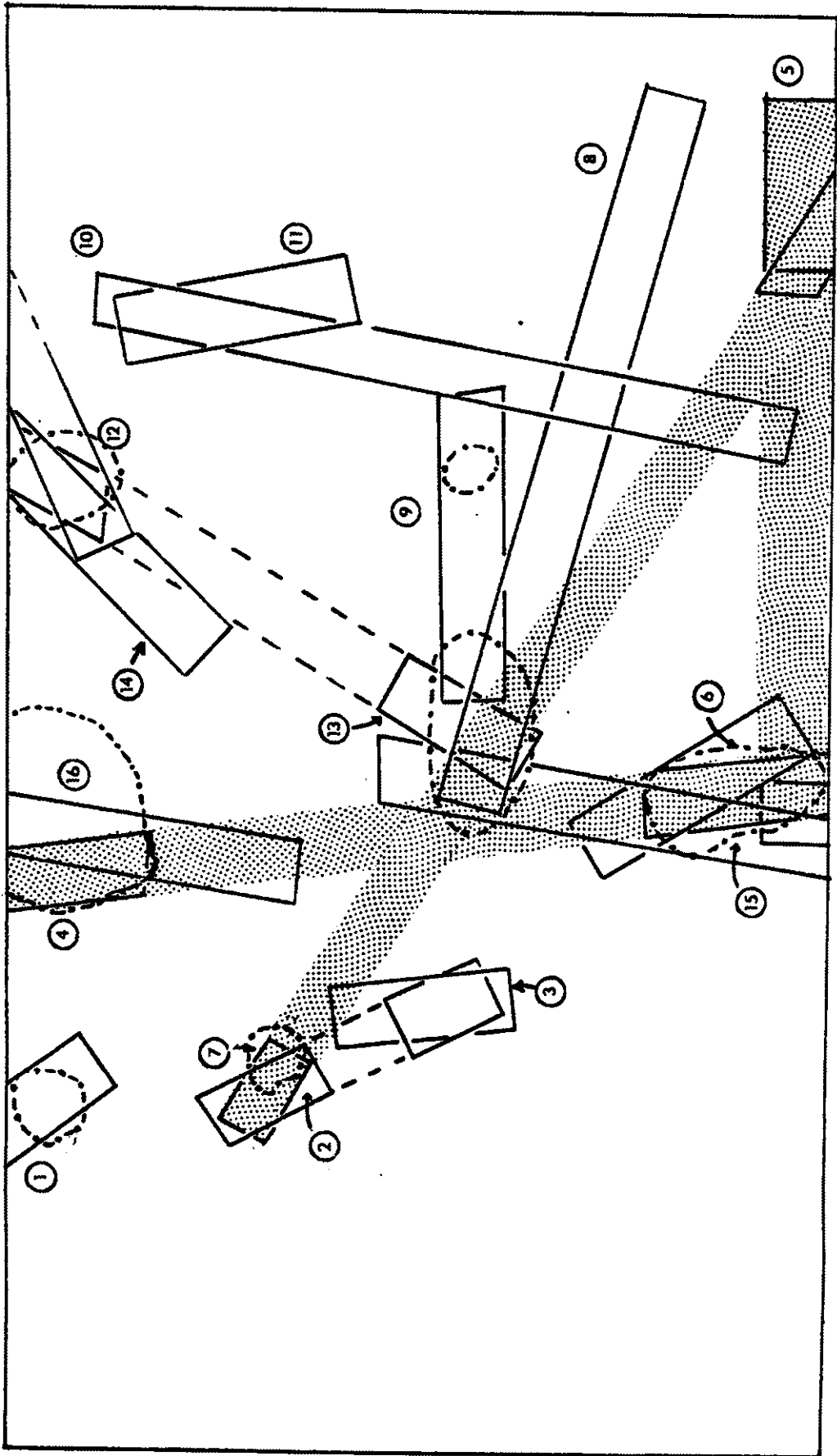
Density Distribution

Density distribution plots were constructed for the Central Tharsis region. For this region, a 20 degree interval was used (Appendix 4). Each contour plot was then examined for major trends or regions of high concentration of lineaments (Figure 19). Figure 19 illustrates fourteen dominate trend directions compiled from the nine density plots. From Figure 19 several lineament directions can be interpreted. Regions 1 and 2 are attributed to the lineaments resulting from the formation of Olympus Mons. Regions 8 and 9 are the lineaments associated with Valles Marineris. The Martian ridges are associated with regions 10 and 11.

A closer examination of the lineaments responsible for Region 3 reveals the existance of a minor, weak crustal zone between Arsia Mons, Biblis Patera, and Ulysses Patera. The presence of this weak zone indicates that Biblis Patera and Ulysses Patera may be satellite volcanoes of Arsia Mons.

Regions 4,5, and 7 coincide with the three dominant trends described in the Radial Reconstruction and Atypical Fracture analyzes: Region 4 corresponds to the North-South

Figure 19 Density distribution of the dominant trends for the Central Tharsis Region. From this technique, 16 dominant trend directions were recognized. Dot pattern = dominant lineament trends associated with the Tharsis dome. Dot-Dashed pattern equals LCZ pattern.



(355°) trend; Region 5 is associated with the East-West (275°) trend; and Region 7 relates to the minor North-West (315°) trend.

Figure 20 was compiled from the remaining six unexplained regions: 6, 12 thru 16. These regions are believed to be the direct result of the formation of the Tharsis dome.

Projected Centers

It has been hypothesized by several authors (Wise, 1979; Solomon and Head, 1982; Plescia and Saunders, 1982; Felder, 1974; Harp, 1976; Roth et al, 1980) that the Tharsis uplift was not a single event, but the result of several smaller uplifts. To test the hypothesis that Tharsis region was controlled by multiple uplifting centers, Regions 6, and 12 thru 16 were projected such that they intersected with one of the three major lineament directions: North-South (355°), East-West (275°), and North-West (315°) (Figure 21).

The North-West (315°) trend was chosen over the North-South (355°) and East-West (275°) trends for the following reasons: 1) Previous authors have found this North-West (315°) trend (Katterfel'd, 1974; Harp, 1976) in other parts of the Martian surface and believed it to be an older preexisting Tharsis trend. If the North-South

Figure 20

Six unidentified trends calculated from the Density Distribution analysis. Each of the six trends are believed to have resulted from the formation of the Tharsis Dome.

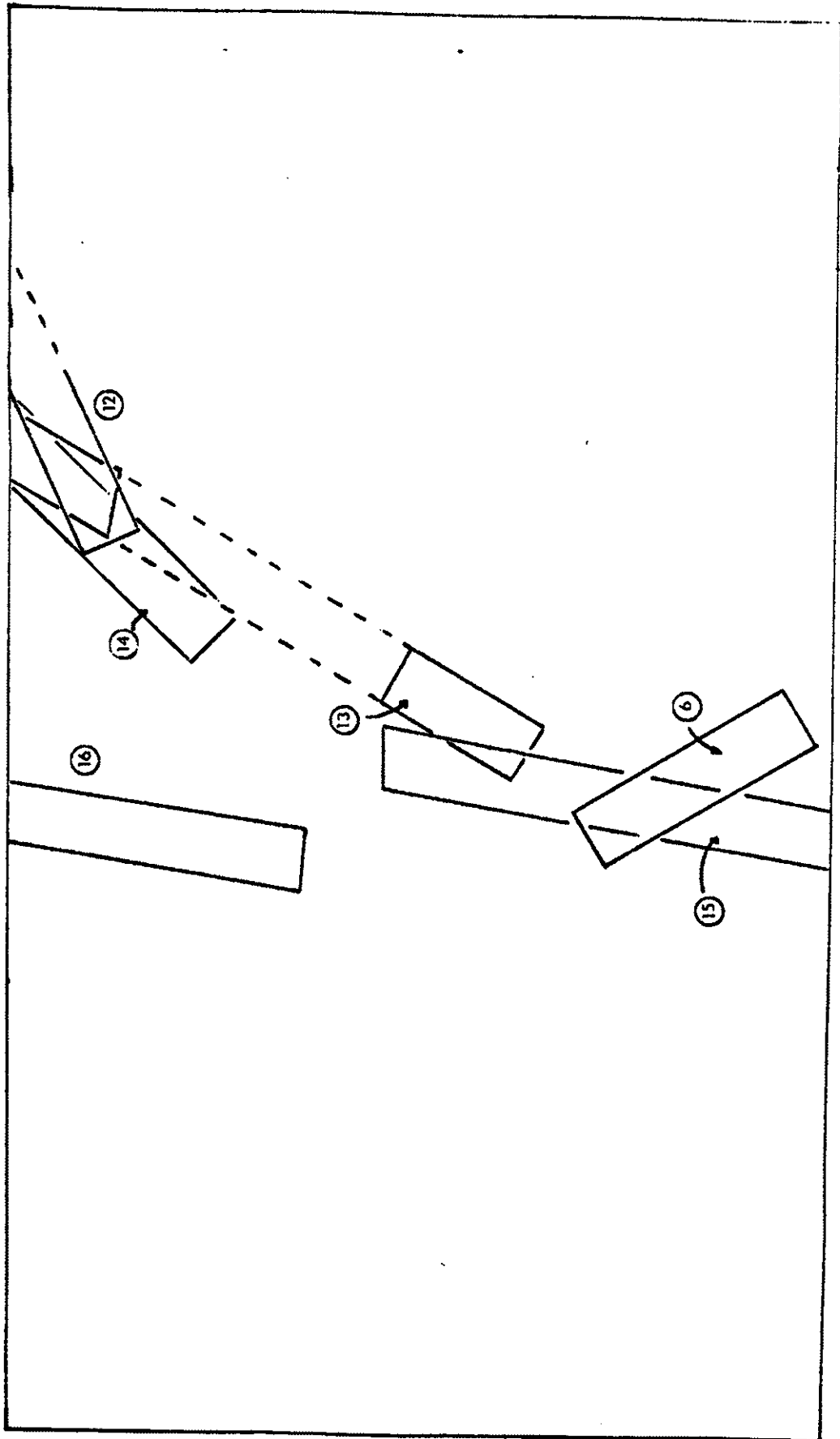
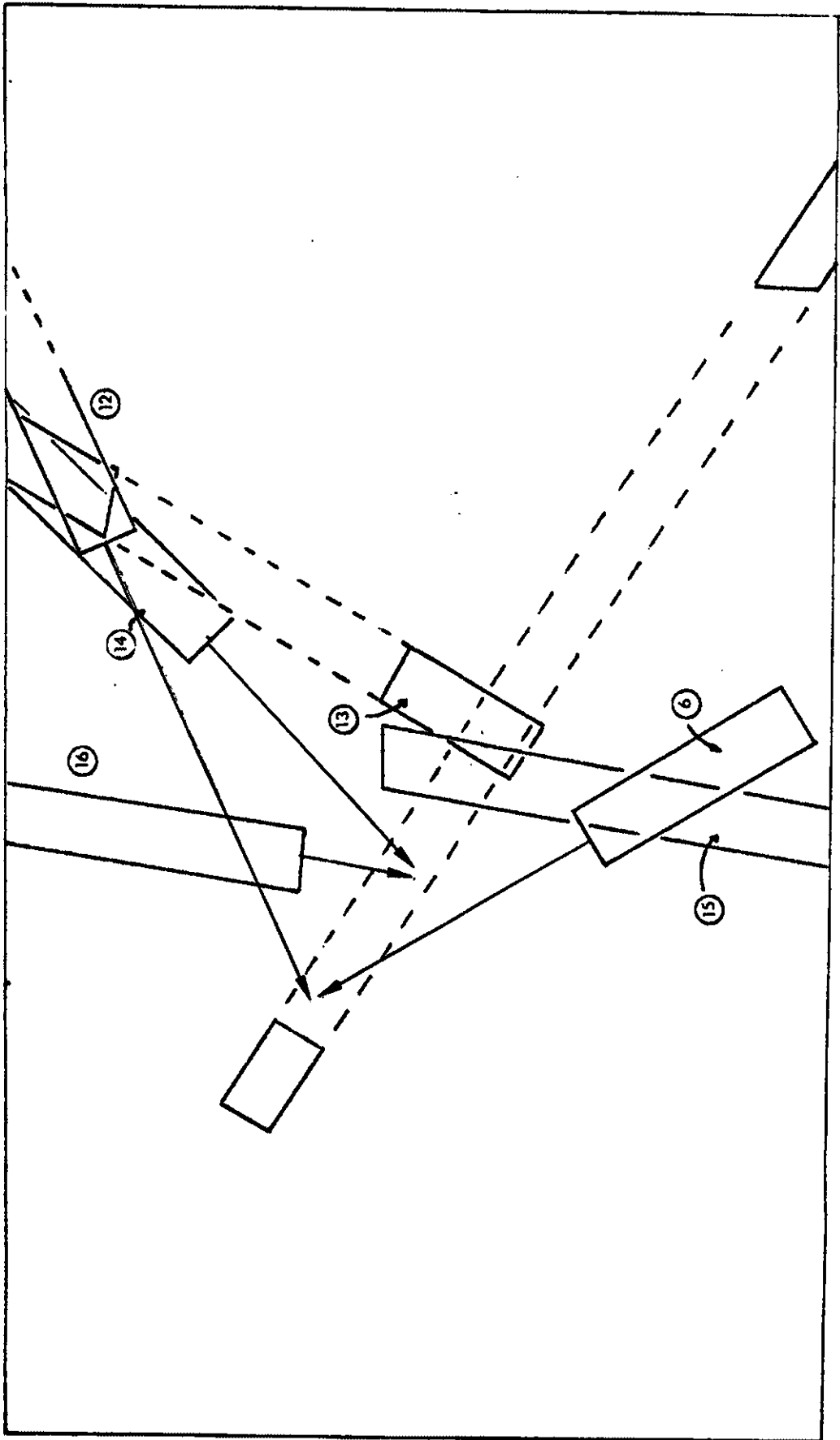


Figure 21 Six unknown density distribution zones
projected to the North-West trend.
Arrows indicate possible sources for
uplifting centers.



(355°) trend is a result of the younger Tharsis dome (Salvortari, 1981), the North-West (315°) trend could be considered the older planetary fracture. 2) Not all the statistically dominant trends associated with each LCZ and density distribution analysis intersect the North-South (355°) or the East-West (275°) trends. 3) The general trend of the Tharsis dome is in the North-West direction. 4) Olympus Mons follows the North-West trend from Noctis Labyrinthus through Pavonis Mons.

Figure 22 shows four candidates as possible centers for the Tharsis region uplift: 1) 6°N, 124°W; 2) 0.5°S, 114°W; 3) 5°S, 106°W; and 4) 7°S, 104°W. Assuming an "ideal" radial pattern, lineaments that projected to any of these centers were plotted. (Figure 23 a,b,c,d). Each uplift center was assumed to be an area of 400 sq. km. Figure 24 is a composite map of all lineaments associated with the four uplifting centers (UC). By using this method, 65 percent of all fractures mapped in the Tharsis region can be explained to align with one of the four uplift centers.

As indicated earlier, numerous authors have associated the Tharsis dome with multiple uplifting. Figure 25 demonstrates a comparison of the uplifting centers (UC) calculated from this study and the uplifting centers recognized by earlier studies.

Figure 22 Possible candidates for uplifting centers (UC's) following the 315° trend. Triangle's correspond to uplifting centers identified from this study.

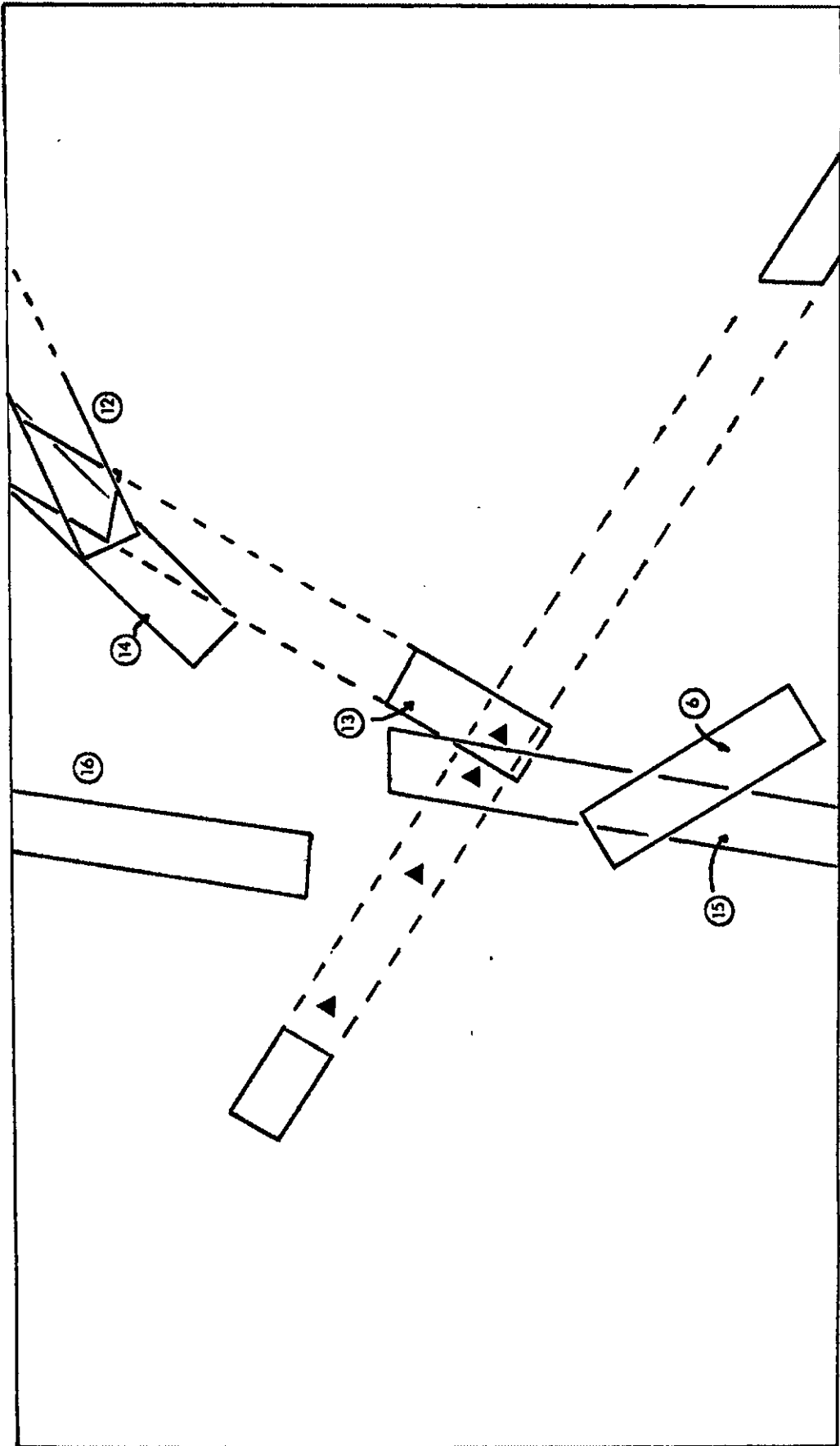
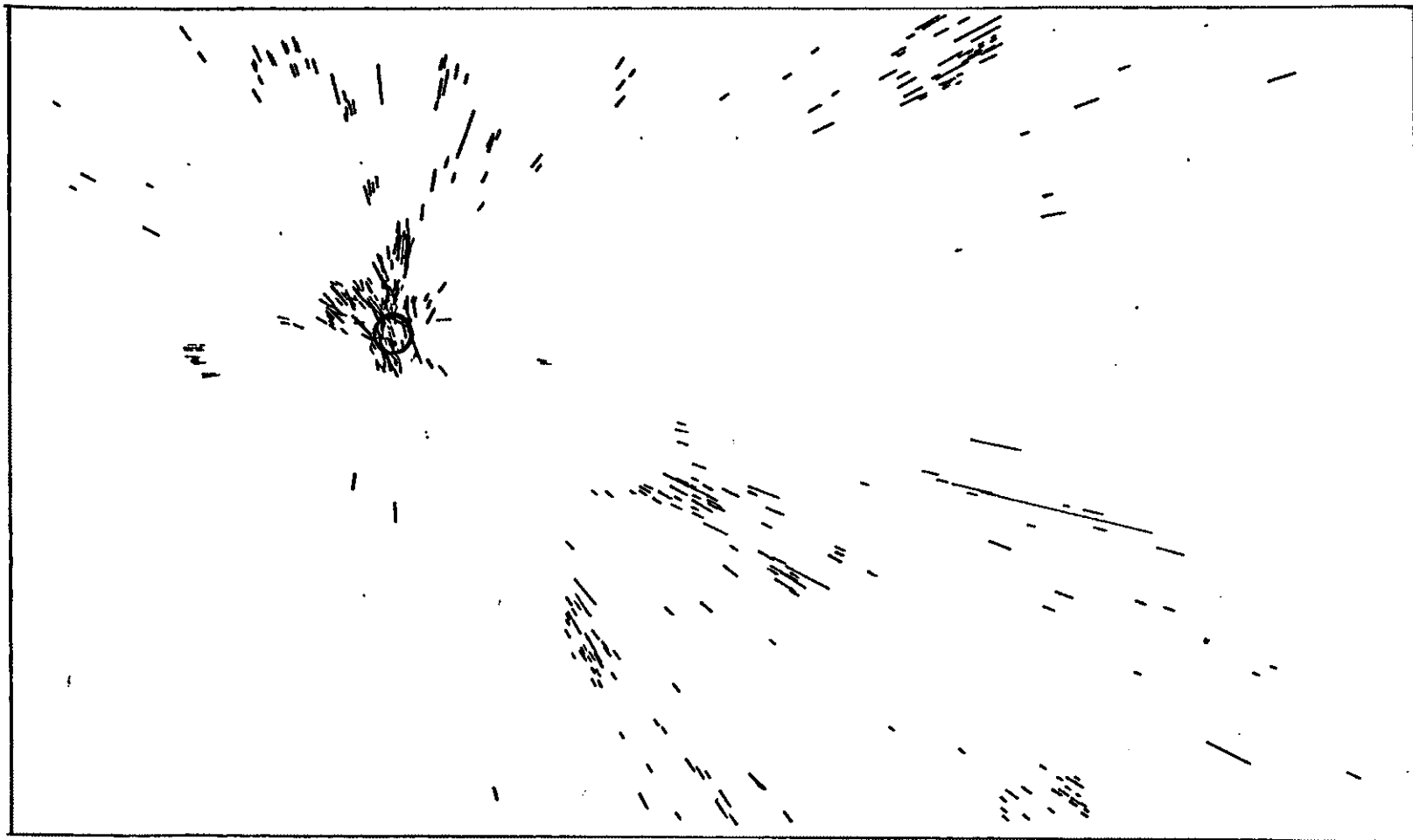
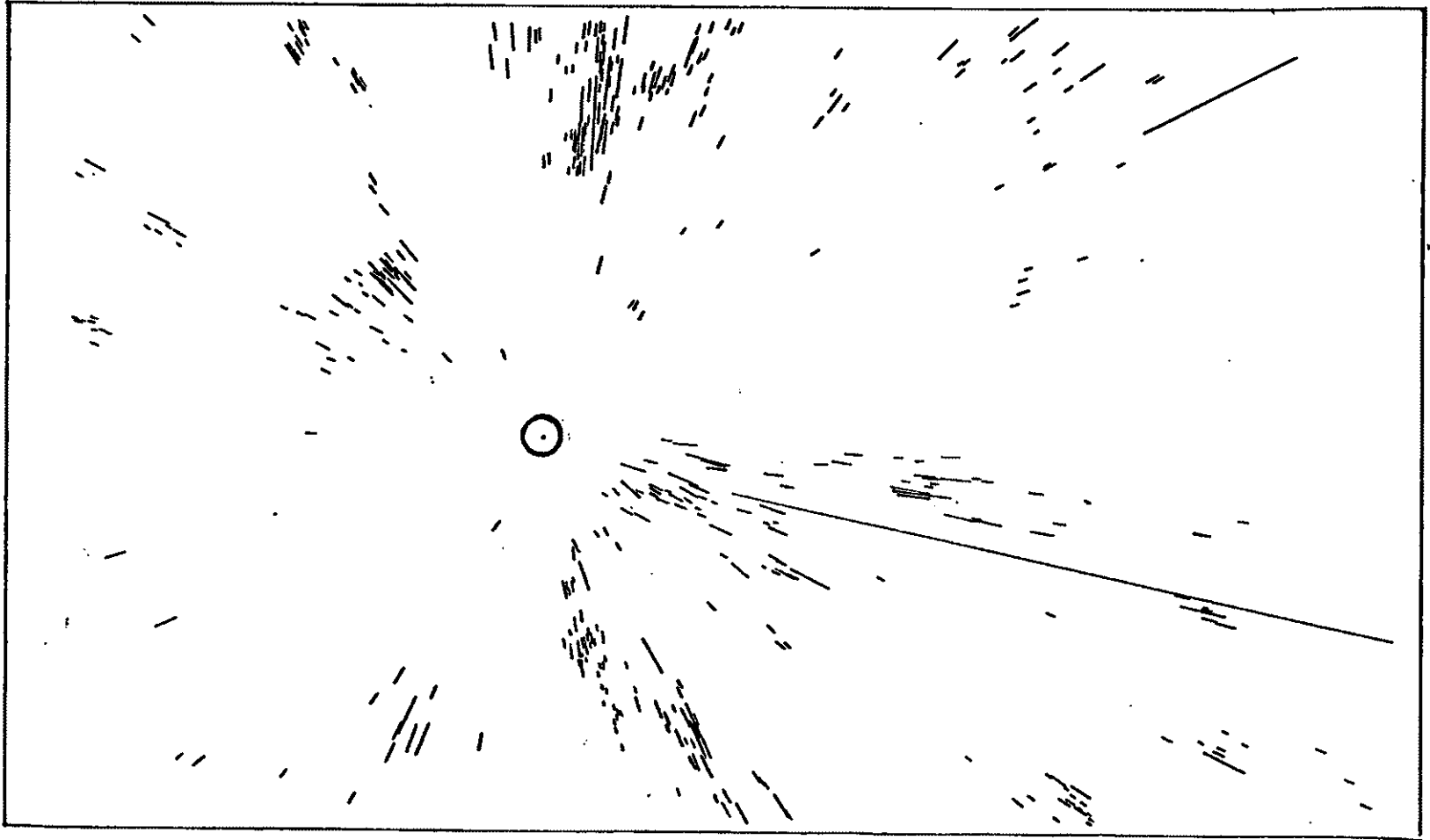


Figure 23a Radial fractures associated with Uplifting
Center No. 1; 6°N, 124°W.



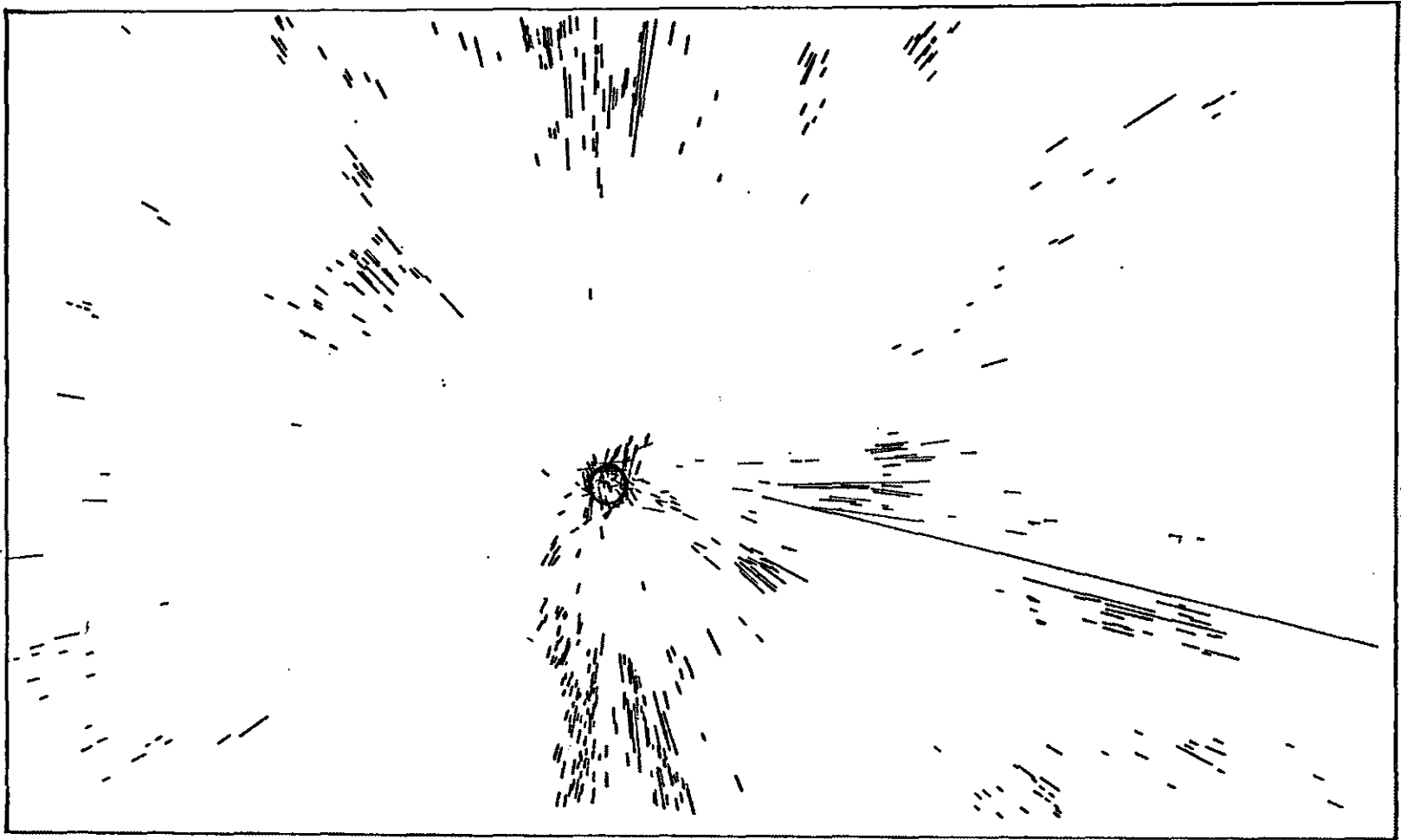
6° N, 124° W

Figure 23b Radial fractures associated with Uplifting
Center No. 2; 0.5°S, 114°W.



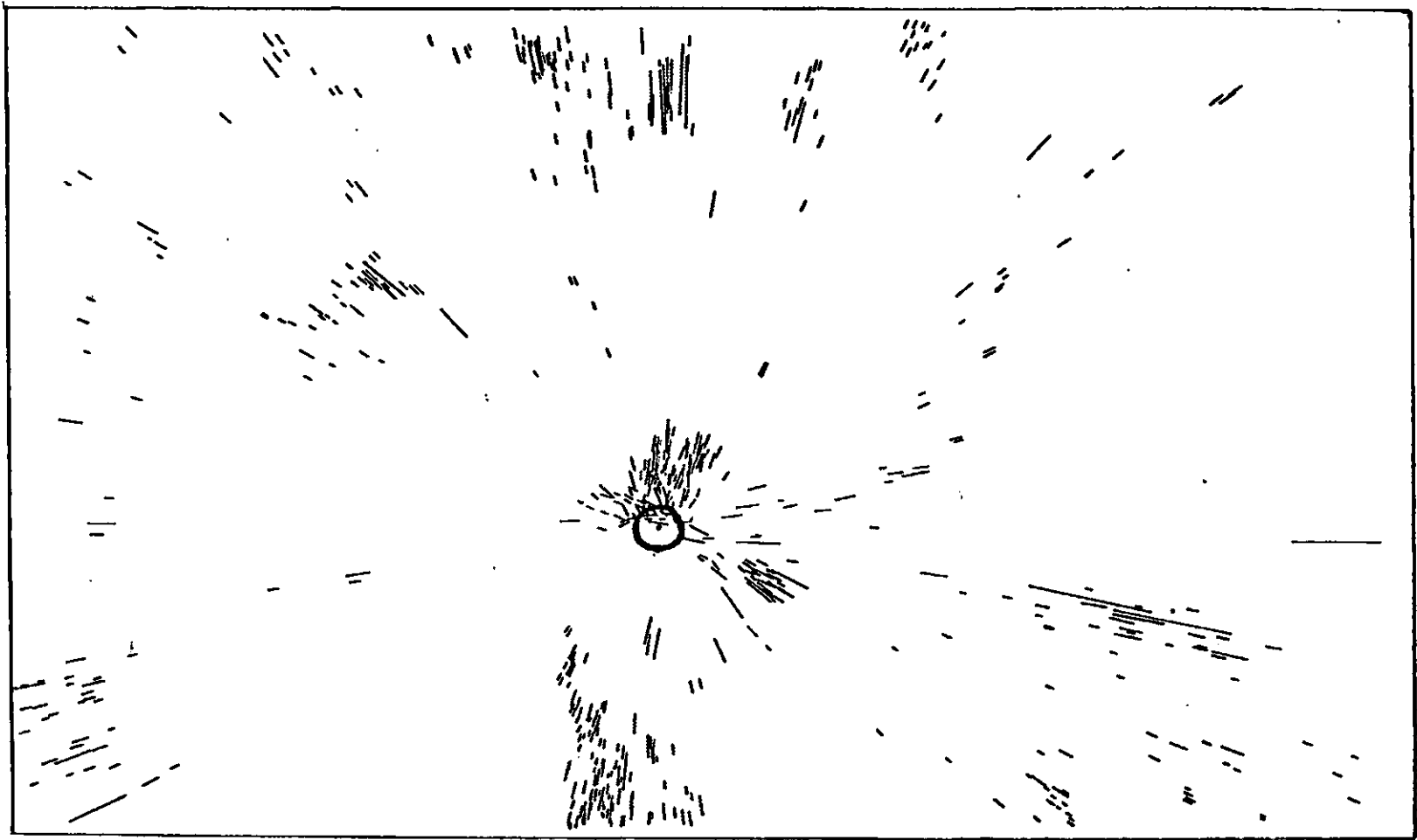
0.5° S, 114° W

Figure 23c Radial fractures associated with Uplifting
Center No. 3; 5°S, 106°W.



5 S, 106 W

Figure 23d Radial fractures associated with Uplifting
Center No. 4; 7°S, 104°W.



° °
7 S, 104 W

Figure 24 Composite map of radial projected lineaments associated with all the major Uplifting Centers. This pattern explains 65 percent of all Tharsis area fractures mapped in this study.

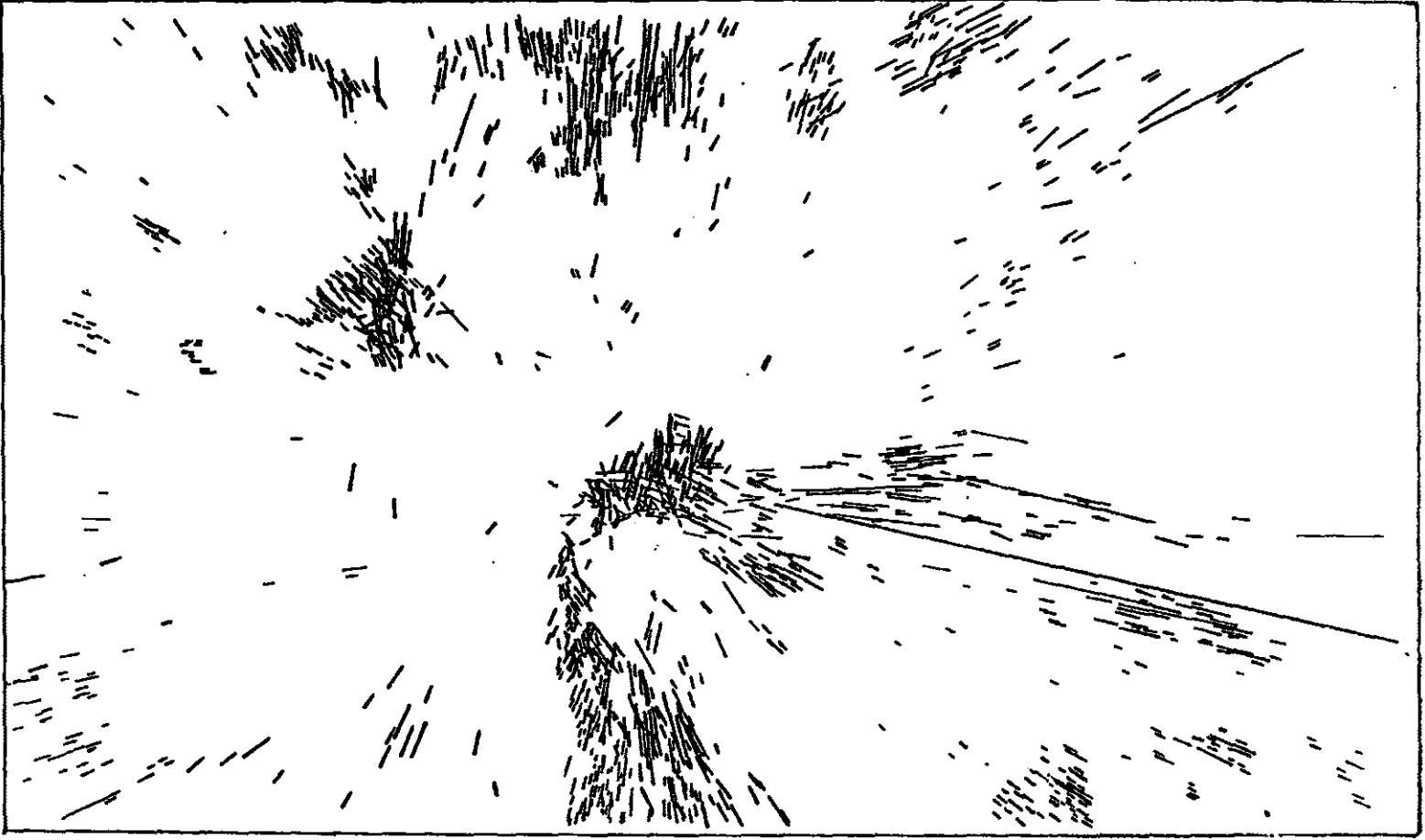


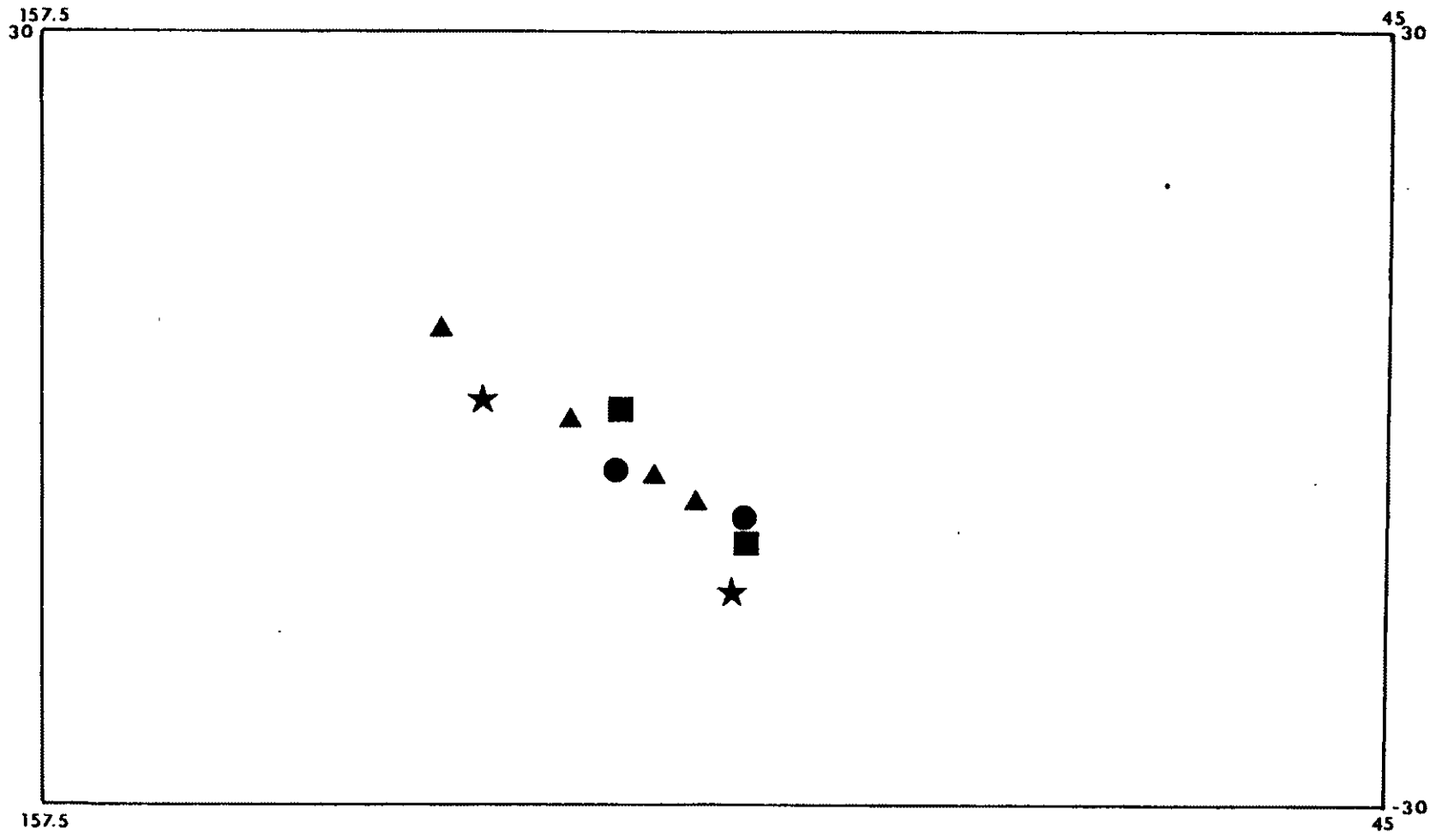
Figure 25 A comparison of major uplifting centers for the Central Tharsis Region of Mars.

Legend

Projected alignments of centers

Solomon & Head:	315°
Plescia & Saunders:	339°
Wise:	322°
This study:	315°

Triangles = This study
Squares = Solomon & Head
Circles = Plescia & Saunders
Stars = Wise



Summary of Analytical Results

From this analytical study of the central Tharsis region of Mars several conclusions emerge:

- 1) Seven lineament concentration zones exist in the central Tharsis region;
- 2) Two of the LCZ appear to be associated with local tectonic events (e.g. formation of Olympus Mons (LCZ 1), and the formation of Valles Marineris (LCZ 6));
- 3) LCZ 2,3,4,5 and 7 indicate that the Tharsis Dome is not the result of a single central uplift but a complex, multiple series of magmatic movements;
- 4) The Tharsis Dome was controlled by two events:
 - a. Pre-Tharsis fracturing which resulted in the formation of two trends (315° and 45°);
 - b. Uplift in at least four centers creating radial fracturing, the 355° and 275° trends forming the most strongly concentrated zones.
- 5) The 315° trend was the controlling feature in the initial development of the Tharsis Dome.

MODELS OF TECTONIC EVOLUTION

The results of the analytical techniques suggest that two separate tectonic events controlled the formation of the Tharsis Dome—a pre-Tharsis fracturing and fracturing associated with the Tharsis uplift.

Influence of Pre-Tharsis Fractures

Crustal fractures formed prior to generation of the Tharsis volcanic features may have controlled the location of magmatic activity. From two of the analytical studies (Radial Reconstruction and Density Distribution), the dominant trend for the Tharsis region is shown to be North-South (355°). These results are in agreement with the results of Salvatori et al (1981) in which they concluded North-South (355°) and East-West (275°) fracture trends are dominant for the Tharsis region.

However the dominant fracture trend(s) of a region is not necessarily the most ancient tectonic control. For example, the North-South and East-West trending fractures align with uplifting centers and thereby appear, either radially or concentrically, to be the result of the dome formation (uplift or subsidence). Many authors consider the North-West trend which I observed in the Tharsis area plus an North-East trend to pre-Tharsis

axes of crustal weakness (Hartman, 1973; Harp, 1976; Katterfel'd, 1974; Binder and McCarthy, 1972; Felder, 1974; Masson, 1977 and 1980; Schultz and Malin, 1982; and Whitford-Stark, 1982). They all believed that most of the Martian surface exhibits a global set of North-West and North-East trending fractures in a planetary "grid". Katterfel'd (1974) concluded the Martian surface was dominated by four global fracture trends: NW and NE; NS and EW; and regional trends of NNW and NNE. Harp (1976) concluded the surface of Mars was dominated by two orthogonal sets of fractures: $N40^{\circ}-50^{\circ}W$, and a $N40^{\circ}-50^{\circ}E$ trend. Masson (1977) reported the fracture pattern of the Tharsis terrain consisted of three tectonic directions: NNE/SSW; NNW/SSE; WNW/ESE or EW; and NS or NNW/SSE. Whitford-Stark (1982) concluded that a NNW trend appeared relatively early in the planet's history and diminished during later periods. Perhaps the crustal weakness zone was the result of fracturing associated with lithospheric contraction (Bonatti and Harrison, 1976) or by the generation of "membrane stresses" (Anguita and Herman, 1975) associated with the curvature of the planet.

The North-West trend shown throughout the three lineament trend analytical techniques used in this study probably controlled the early evolution of the Tharsis region. However, the stratigraphic evidence for dating fractures in the study area is weak. Presumably the oldest fracture pattern should only be found in the oldest rocks

hence pre-Tharsian fractures should be seen only in Noachian and Hesperian age rocks. Unfortunately there are very few rocks of this age in the study area. The only evidence of pre-Amazonian rocks which contain substantial fractures occur in a small area of Hesperian rocks near Kasei Valles (LCZ 3-Figure 14) (Scott and Carr (1978), located on the northeastern flanks of the the Tharsis dome. However, this region shows no evidence of the 315° fracture trend. Even so, because Noachian and Hesperian rocks outside the study are dominated by North-West and North-East fractures and almost no other area of uplift are known on Mars, the North-West and North-East fractures probably underlie the Tharsis region. The extensive volcanism associated with the Central Tharsis region during the Amazonian period certainly covered fractures which developed prior to domal uplift. Apparently, the 315° trend found in the Amazonian rocks of this region relates to reactivation of the older planetary fracture pattern during domal uplift.

Reactivation of buried North-East trending fractures may have controlled the position of the volcanoes of the Tharsis Montes. Even though the North-East (40°) trend of the Tharsis Montes has not appeared in this study, its existence can not be ruled out. On the contrary, this orthogonal fracture trend may exist buried by younger sediments, only to emerge beyond the boundaries of the study area.

Proposed Models

The early stage of Tharsis is proposed to consist of a series of either coincidental or sequential domal uplifts. These small domal uplifts are believed to be the result of diapirs rising from a magmatic plume which followed the pre-Tharsis North-West (315°) (planetary) crustal weakness trend. Deposition of extensive volcanic lava plains (Downs 1982) combined with the uplifts to form the present Tharsis rise.

The Tharsis region of Mars resembles a Martian analog to a "hotspot". Hotspots on Earth are regions of lower mantle magmatic upwelling. Many authors recognize hotspots on Earth (Morgan, 1972; Wilson, 1973; Burke and Wilson, 1976; Vogt, 1974 and 1976; Crough, 1978). Wilson (1973) established the following crustal feature for identifying an underlying hot spot in the mantle: 1) it is an area of topographic uplift; 2) it an area of active volcanism; 3) there is a possibility of a positive gravity high associated with the region; 4) there exist two lateral ridges often radiating from the center; and 5) the area is believed to be an area of increased heat flow. Most of these criteria are met in the Tharsis region. As previously noted, the Tharsis area is topographically high, probably due to uplift (Carr, 1974; Frey, 1979; Plescia and Saunders, 1982). With active volcanism existing in the

recent past (approximately 20 m.y.). Sjogren (1979) developed a gravity map showing the Tharsis dome to be associated with a strong positive gravity anomaly. The only criteria established by Wilson (1973) not readily recognized is the presence of the associated lateral ridges. Their absence in the Tharsis region can be attributed to the great thickness of Tharsis lavas flows (DeHon, 1981); if these ridges existed, they were probably buried beneath the flows. Many may in fact have been obliterated by meteoritic bombardment. Hence the Tharsis area of Mars probably formed due to an ancient upwelling of the Martian mantle.

I propose that two models exist which explain the fracture trace data I have amassed and thus may indicate two possible origins for the Tharsis region: 1) a series of small domal uplifts combined to form the Tharsis dome; or 2) the dome is the result of a migrating hot spot.

Multiple Doming Model

The idea of a multi-centered doming of the crust has been proposed by Ramberg (1972) for gravity instability in layered systems, by Pitcher and Bussell (1977) for the emplacement of large batholiths in Peru, by Fletcher (1972) for domes found in the northern Appalachians and Scandanavian Caledonides, by Brun (1980) for a zone of mantled gneiss domes in Eastern Finland, and by Drury

(1977) for granitic diapirs in the Archean Greenstone Belt of Yellowknife, Canada. Ramberg's model, developed from centrifuge experiments, is based on the assumption that a low-density region exists in the upper mantle (buoyant layer). Domes, parallel ridges, and diapiric structures form as this low-density region rises to the surface through dense plastic rocks. Mohr and Wood (1976) further advanced this idea to explain the spacing of volcanoes in island arcs and rift systems. Figure 26 shows the results of one of Ramberg's centrifuge experiments. This experiment developed a linear set of domes in wax similar to the suspected centers of the Tharsis dome.

The results of Ramberg's experiment suggest how the early stages of the Tharsis region evolved. Figure 27 illustrates a model that I developed based upon Ramberg's work. In stage 1 (Figure 27a), a diapiric mass forms under the Tharsis region and migrates upward thinning the overlying crustal rocks. The rising mass follows a pre-Tharsis North-West (315°) trend of crustal weakness and is elongated in that direction. Due to the large size of this mass compared to the planetary radius, the magma does not rise as one "solid" unit. Instead smaller diapiric masses splinter off and follow the preexisting crustal weakness trend (stage 2, Figure 27b). In this model these smaller uplifts occur at approximately the same time. Each of these smaller domes penetrate the overlying thinned crustal rocks resulting in the formation of several



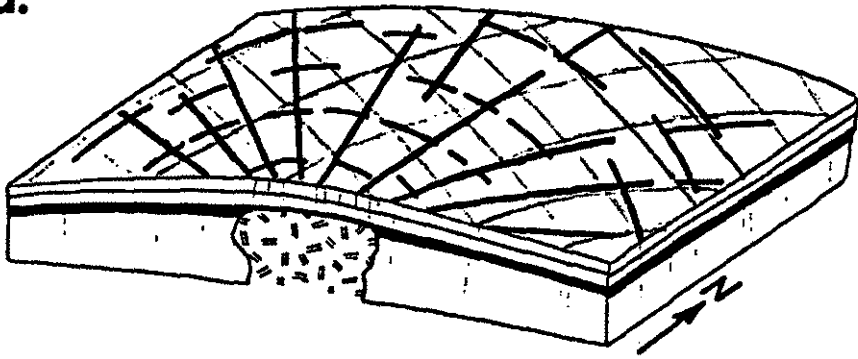
Figure 26 Parallel domes developed in (1978)

Figure 27

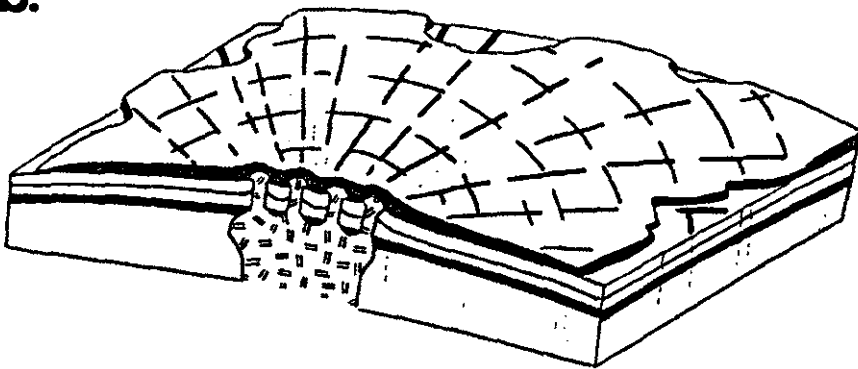
a) Early stage in the development of the Tharsis dome. Upward-rising diapiric mass fractures the primordial crust resulting in an early stage of crustal failure. Radial fracture patterns develop from this uplift similar to fractures developed by Withjack and Scheiner (1982).

b) At a later stage, smaller diapiric mass rise to the surface following older preexisting weaknesses. Each of these smaller domes in turn fracture the surface. Volcanic lava flows bury older fracture systems.

a.



b.



volcanic centers displaying radial fracture patterns. Many volcanic domes and lava plains form around each center, each being partially or totally obliterated by younger flows. Since Mars displays no evidence of lateral plate motion, the volcanic flows remain centered over this large source of magma and form extensive areas of volcanic deposition (Figure 27c).

In stage 4 (Figure 27d), the dome continues to build, not only from the migration of the magma upward, but in combination with the huge build-up of volcanic plains. Smaller satellite volcanoes and compressional (wrinkle) ridges appear on the flanks of the dome between periods of alternating volcanic and tectonic deformation.

Although Ramberg's ideas are not fully accepted in the published domain, they do show equal spacing of the uplifting centers and permit the formation of compressional ridges concentric with the uplift centers. Both of these features are not necessary for my four-stage model to be valid but they do emphasize the similarity between these two models derived from independent data sets.

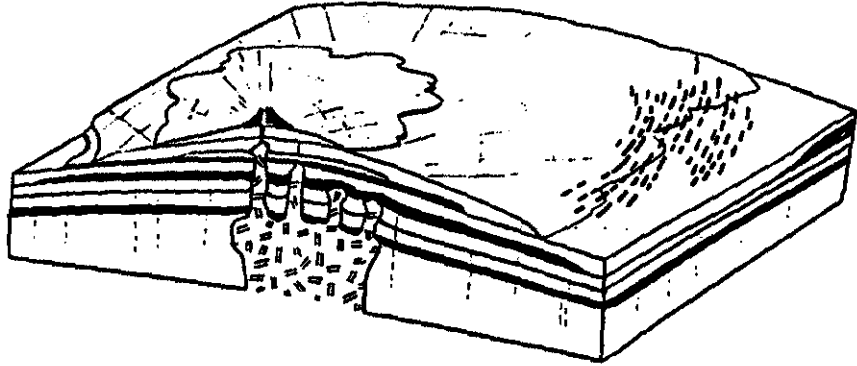
Ascent of magma to the surface would utilize preexisting basement weaknesses (Anderson and Grew, 1977). In order to test this idea, I constructed a model modified from the procedures developed by Withjack and Scheiner (1982) for single uplifting domes. An experiment was conducted to see if the observed fracture pattern found on Tharsis could be duplicated by a model. (For complete

Figure 27

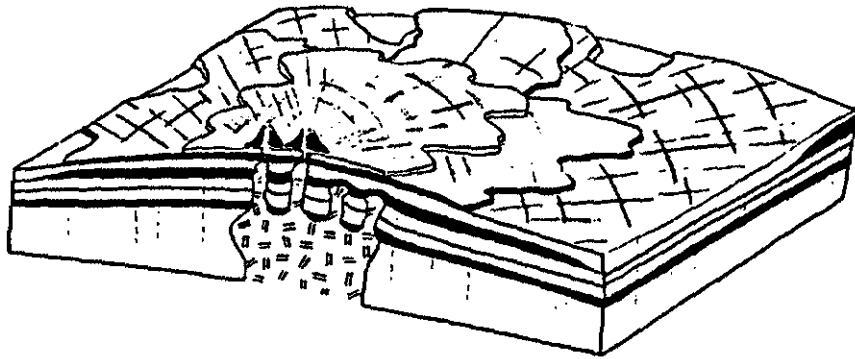
c) As this material reaches the surface, volcanic centers rise. These volcanic centers result in extensive deposition of volcanic lava plains obliterating a lot of the visible surface fractures.

d) Since Mars exhibits no lateral plate motion i.e. Plate Tectonics, the volcanoes remain fixed over the hotspots. More volcanic plains are formed until the volcanic centers are depleted of their source magma. Martian ridges are formed sometime between stage A thru D.

c.



d.



details and results of the experiment, see Appendix 5). Even though the experiment failed to construct the observed fracture patterns found in the Tharsis region, several conclusions can be drawn: 1) single domal uplifts form very pronounced radial patterns; 2) when more than one uplift is attempted the first fractures to appear are radial to the centers; 3) a strong dominant fracture appears between the subsequent uplifting centers as the radial pattern subsides; 4) the slower the uplift, the more pronounced the radial pattern becomes; and 5) the more rapid an uplift is between three or more uplifting centers, the more the outer uplifting centers maintain their radial pattern and the radial patterns associated with the center uplift(s) are gradually reduced. Although it is unclear whether my experiment accurately modelled the Martian situation, the results might indicate that the multi-centered domal model might not produce the fracture visible in the Tharsis area. Multiple radial fracture sets may indicate sequential rather than coincident uplift centers (described in the next section). More work is needed to establish the reliability of my physical experiments.

Sequential Doming Model

The second hypothesis is one of sequential intrusion of magmatic diapirs formed by a laterally migrating hotspot which was not fixed in place in the mantle. In this model,

the Tharsis dome could be a Martian analog to a rift system like the Baikal (Bahat, 1981) or the East African rifts (Fairhead, 1976; Phillips and Lambeck, 1980) found on Earth. Bahat (1981) concluded that an upward moving diapiric mass was responsible for the initial fracturing of the Baikal Rift and that the original mass has moved to the east following pre-existing fracture pattern. This scenario was applied to the Tharsis region of Mars. A similar diapiric mass could have developed under the Tharsis region. As the magma intruded upwards, the overlying crust fractured into two conjugate (perpendicular) trends: 1) North-West (315°) and 2) North-East (45°). This fracturing developed an Earth-like Martian rift system over the magmatic mass (Bott, 1981). However, for some unknown reason (i.e. Martian crust too thick; the planet cooled too fast) lateral plate motions never began. Instead the original magmatic mass laterally migrated towards the north-west following the newly formed North-West (315°) trend. Magma continued to migrate laterally in the North-West direction until it intersects a vertical weak zone in the overlying crust. This weak zone permitted the magma to rise vertically through the overlying crust. Vertical migration of the magma lead to the emplacement and doming of younger volcanic plains. The extensive deposition of volcanic plains resulted in the rapid formation of the Tharsis dome.

Since both models were constructed around the

assumption of an underlying basement weakness trend (355°), it is hard to speculate on which one best explains the observed data because no strong stratigraphic evidence exists to place relative ages upon any of the radial fracture sets. Each model involves the vertical rising of magma and radial fracturing of a thin, overlying crust. The only major difference in the two mechanisms is the timing of the magmatic uplifts. The sequential doming model would result in simultaneous vertical migration of magma; whereas, the migrating hotspot model would take a pulsating, stepped approach. Both models would follow the pre-Tharsis fracture weakness (315°) recognized in this study, as well as the development of the radial fracture pattern associated with the uplift centers.

Martian Ridges

One aspect of the Tharsis region which I have not examined in depth is the formation of the ridges that are found on the flanks of the Tharsis dome. Numerous authors (Saunders and Gregory, 1980; Gifford, 1980; Fernandez-Chicarro and Masson, 1980; Walters and Maxwell, 1980; Eppink and Saunders, 1982; Maxwell, 1982 and Willemann and Turcotte, 1982) have all attempted to explain the origin of Martian ridges. They seem to agree that the ridges are the result of compressional forces associated with the Tharsis uplift. Fernandez-Chicarro and

Masson (1980) predated the compressional ridges to graben formation. Walter and Maxwell (1980) agreed and concluded that the ridges were the result of a pulsating type of uplift.

Maxwell (1982) calculated the orthogonal to the ridges and estimated that 60% of the ridges are orthogonal to a center located 1°N , 122°W . This center lies between UC 1 and UC 2 of this study. Because their orthogonal directions fell somewhere in this general region, it is speculated that the Martian ridges formed sometime between the formation of uplifting center 1 and uplifting center 2.

CONCLUDING STATEMENT

The analytical procedures that have been attempted in this study have shown to provide significant results for the Tharsis region. However, there are several problems inherent in any study of this magnitude. Scale problems occur when examining and measuring features on an area one-third the size of a planet. Often small features will be overshadowed by larger features. There are also problems with the inability of ground checking your results, insufficient geological control, and insufficient tectonic control. To conduct a more in-depth study, a better understanding of geological as well as tectonic features is required. Scott and Tanaka (1981) recently developed a better stratigraphic map for Tharsis. This map was however not used in this study because it did not cover the entire study area.

Two different mechanisms were proposed to explain the formation of the Tharsis Dome: 1) multicentered doming and 2) sequential doming due to a migrating hotspot. Although each scenario is possible, neither mechanism can be proven or disproven in this study. Only with a stronger knowledge of similar forces on Earth, further research, or further exploration of the Martian surface by manned or unmanned spacecrafts can we test these hypothesis.

REFERENCES

- Abel-Rahman, M.A.; Hay, A.M., Sampling and Statistical Analysis of Multi-Model Orientation Data, Basement Tectonic Contri. 12, 73-86, (1978)
- Anderson, C.L., Grew, P.C., Stress Corrosion Theory of Crack Propagation and Applications to Geophysics, Rev. Geophys. Space Phys., 15, No.1, 77-104, (1977)
- Anguita, F., Herman, F., A Propagating Fracture Model Versus a Hot Spot Origin for the Canary Islands, Earth Planet. Sci. Lett., 27, 11-19, (1975)
- Arthyskov, E.V., Stresses in the Lithosphere Caused by Crustal Thickness Inhomogeneties, . Geophys. Res., 78, No. 32, 7675-7708, (1973)
- Artyushkov, E. V., Mechanisms of Continental Riftogenesis, Tectonophysics, 73, 9-14, (1981)
- Atkinson, B.K., Subcritical Crack Propagation in Rocks: Theory, Experimental Results and Applications, J. of Struct. Geol., 4, No. 1, 41-56, (1982)
- Babcock, E.A., Sheldon, L.G., Structural Significance of Lineaments Visible on Aerial Photos of the Athabasca Oil Sands Area Near Fort Mackay, Alberta. Bull. of Can. Petrol. Geol., 24, No. 3, 457-470, (1976)
- Bahat, D., Certain Mechanical Aspects in Comparative Continental Rifting with a Special Reference to the Baikal Rift, Geol. Mag., 118, No. 3, 271-280, (1981)
- Banerdt, W.B., Phillips, R.S., Sleep, N.H., Saunders, R.S., Thick Shell Tectonics on One-Plate Planets: Application to Mars, J. of Geophys. Res., 87, No. B12, 9723-9735, (1982)
- Binder, A.B., and McCarthy, D.W., Jr., Mars: The Lineament System: Science, 172, 279-281, (1972)
- Blasius, K.R., Cutts, J.A., Topography of Martian Central Volcanoes, Icarus, 45, 87-112, (1981)
- Bonatti, E., Harrison, C.G., Hot Lines in the Earth's Mantle, Nature, 263, 402-404, (1976)

- Bonatti, E., Easter Volcanic Chain (Southeast Pacific): A Mantle Hot Line, J. of Geophys. Res., 82, No. 17, 2457-2478, (1977)
- Boorder, H., Structural-Geological Interpretation of SLAR Imagery of the Colombian Amazonas, Inst. of Mining Metallurgy, Sect. B, 90, 145-151, (1981)
- Bott, M.H.P., Kusznr, N.J. Stress Distributions Associated with Compensated Plateau Uplift Structures with Applications to the Continental Splitting Mechanism, Geophys. J. Roy. Astron. Soc., 56, 451-459, (1979)
- Bott, M.H.P., Crustal Doming and the Mechanism of Continental Rifting, Tectonophysics, 73, 1-8, (1981)
- Bridgewater, D.S., Sutton, J., Watterson, J., Crustal Downfolding Associated with Igneous Activity, Tectonophysics, 21, 57-77, (1974)
- Brun, J.P., The Cluster-Ridge Pattern of Mantled Gneiss Domes in Eastern Finland: Evidence for Large Scale Gravitational Instability of the Proterozoic Crust, Earth Planet. Sci. Lett., 47, 441-449, (1980)
- Burke, K.C., Wilson, J.T., Hot Spots on the Earth's Surface, Scient. Amer., 235, 46-57, (1976)
- Carr, M.H., Tectonism and Volcanism of the Tharsis Region of Mars, J. Geophys. Res., 79, No. 26, (1974)
- Carr, M.H., The Surface of Mars, Yale University Press, New Haven, Connecticut, 1981
- Carr, M.H. (et al), Viking Orbiter Views of Mars, N.A.S.A., SP-441, C.R. Spitzer (Editor) (1980)
- Casella, C.J., Evolution of the Lunar Fracture Network, Geol. Soc. Amer. Bull., 87, 226-234, (1976)
- Christofferson, E., Hamil, M.M., A Radial Pattern of Sea-Floor Deformation in the Southwestern Caribbean Sea, Geol., 6, 341-344, (1978)
- Christensen, E.J., Balmino, G., Development and Analysis of a Twelfth Degree and Order Gravity Model of Mars, J. Geophys. Res., 84, No. 814, 7943-7953, (1979)
- Cloos, E., Experimental Analysis of Fracture Patterns, Geol. Soc. Amer. Bull., 66, 241-256, (1955)

- Cloos, E., Experimental Analysis of Gulf Coast Fracture Pattern, A.A.P.G., 52, No. 3, 420-444, (1968)
- Cochran, J.R., Talwani, M., Free Air Gravity Anomalies in the World's Oceans and Their Relationship to Residual Elevation, Geophys. J. Roy. Astron. Soc., 50, 495-552, (1977)
- Crosby, G.W., Radial Movements in Western Wyoming Salient of the Cordilleran Overthrust Belt, Geol. Soc. of Amer. Bull., 80, 1061-1078, (1969)
- Crough, S.T., Thermal Origin of Mid-Plate Hot-Spot Swells, Geophys. J. R. Astro. Soc., 55, 451-469, (1978)
- Crough, S.T., Hotspot Epeirogeny, Tectonophysics, 61, 321-333, (1979)
- Crumpler, L.S., Aubele, J.C., Structural Evolution of Arsia Mons, Pavonis Mons, and Ascreus Mons: Tharsis Region of Mars, Icarus, 34, 496-511, (1978)
- DeHon, R.A., Martian Volcanic Materials: Preliminary Thickness Estimates, J. Geophys. Res., 87 No. B12, 9821-9828, (1982)
- DeHon, R.A., Thickness Distribution of Tharsis Volcanic Material, Nasa Tech. Mem. 84211, 144-146, (1981)
- Dietz, R.S., Menard, N.W., Hawaii Swell, Deep, and Arch, Subsidence of the Hawaiian Islands, J. Geol., 61, No. 2, 99-113, (1953)
- Dokka, R.K., Late Cenozoic Extension of NE Baja Calif., MCX, Geol. Soc. Amer. Bull., 93, No. 5, 371-378, (1982)
- Donath, F.A., Analysis of Basin-Range Structure, South-Central Oregon, Geol. Soc. Amer. Bull., 73, 1-16, (1962)
- Downs, G.S. et al, New Radar-Derived Topography for the Northern Hemisphere of Mars, J. Geol. Res., 87, No. B-12, 9747-9754, 1982
- Drury, S.A., Structures Induced by Granite Diapers in the Archean Greenstone Belt at Yellowknife, Canada: Implications for Archaean Geotectonics, J. Geol., 85, 345-358, (1977)
- Eppink, J.F., Saunders, R.S., Patterns of Ridges and Scraps

- on Mars., Nasa Tech. Mem. 85127, 66-67, (1982)
- Fairhead, J.D., The Structure of the Lithosphere Beneath the Eastern Rift, East Africa, Deduced from Gravity Studies, Tectonophysics, 30, 269-298, (1976)
- Fairhead, J.D., A Gravity Link Between the Domally Uplifted Cainozoic Volcanic Centers of North Africa and its Similarity to the East African Rift System Anomaly, Earth Planet. Sci. Lett., 42, 109-113, (1979)
- Fielder, G., Lunar Tectonics, Quart. J. Geol. Soc. Lond., 119, 64-94, 1963
- Fielder, G., Fryer, R.J., Gash, P.J., Whit-Ford, J.L., Wilson, L., Lineament Patterns on the Moon, Mars, and Mercury, New Basement Tectonics Contr., 44, 379-387, (1974)
- Fernandez-Chicarro, A., Masson, P., A Possible Origin of the Ridged Plains of Mars, Nasa Tech. Mem. 82385, 107-109, (1980)
- Fletcher, R.C., Application of a Mathematical Model to the Emplacement of Mantled Gneiss Domes, Amer. J. Sci., 272, 197-216, (1972)
- Frey, H., Thaumasia: A Fossilized Early Forming Tharsis Uplift, J. Geophys. Res., 84, No. 83, 1009-1023, (1979)
- Frost, R.T.C., Tectonic Patterns in the Danish Region (as Deduced from a Comparative Analysis of Magnetic, Landsat, Bathymetric and Gravity Lineaments), Geologic in Mijnboun, 56, No. 4, 351-362, (1977)
- Gass, I.G., Geological and Geophysical Parameters of Mid-Plate Volcanism, Phil. Trans. Roy. Soc. Lond. A 288, 588-597, (1978)
- Gass, I.G., The Evolution of Volcanism in the Junction Area of the Red Sea, Gulf of Aden and Ethiopian Rifts, Phil. Trans. Roy. Soc. Lond. A 267, 369-381, (1970)
- Gifford, A.W., Ridge-Rings on Mars, Nasa Tech. Mem. 82385, 90-92, (1980)
- Ginberg, M., Martian Valley Orientation and Regional Structural Control, Nasa Tech Mem. 82385, 95-97, (1980)
- Gintov, O.B., Guterman, V.G., Pseudodisplacements in Zones

- of Cross-Cutting Fractures, Geologiya i /Geofizika, 22, No. 3, 145-150, (1981)
- Goody, R.M., Walker, J.G., Atmospheres, Foundations of Earth Science Series, Prentice-Hall, (1972), 150 pages.
- Greeley, R., Spudis, P.D., Volcanism on Mars, Rev. Geophys. Space Phys., 19, No. 1, 13-41, (1981)
- Gzovsky, M.H., Grigoryev, A.S., Gushchenko, O.J., Mikhailova, A.N., Nikonov, A.A., Osokina, D.N. Problems of the Tectonophysical Characteristics of Stress, Deformations, Fractures, and Deformation Mechanisms of the Earth's Crust, Tectonophysics, 18, 167-205, (1973)
- Harp, E.L., Fracture System of Mars, Proc. First Int'l. Conf. on the New Basement Tect., 5, 389-408, (1976)
- Hartmann, W.K., Martian Surface and Crust: Review and Synthesis, Icarus, 19, 550-575, (1973)
- Head, J.W., Volcanism on Mars, Nature, 294, 305-307, (1981)
- Jackson, E.D., Shaw, H.R., Stress Fields in Central Portions of the Pacific Plate: Delineated in Time by Linear Volcanic Chains, J. Geophys. Res., 80, No. 14, 1861-1874, (1975)
- Johnson, A.C., Lineament Analysis: An Exploration Method for the Delineation of Structural and Stratigraphic Anomalies, New Basement Tecton. Contr., 50, 449-452, (1974)
- Katterfel'd, G.N., Global and Regional Systems of Lineaments on the Earth, Mars, and the Moon, New Basement Tect. Contr., Chpt. 10, No. 43, 369-377, (1974)
- Katterfel'd, G.N., Charushin, G.W., Global Fracturing on the Earth and Other Planets, Geotectonics, No. 6, 333-337, (1970)
- Kochel, R.C., Burgese, C.N., Structural Control of Geomorphic Features in Kasei Valles Region of Mars, Nasa Tech. Mem. 85127, 288-290, (1982)
- Kochel, R.C., Structural Control of Sapping Valley Network Along Valles Marineris, Mars, Nasa Tech. Mem. 85127, (1982)

- Kosygin, Y., Yushmonov, V.V., Maslov, L.A., Formation Mechanism and Location of Concentric Complexes (Ring Structures), Geologiya i Geofizika, 22, No. 6, 20-27, (1981)
- Lambeck, K., Comments on the Gravity and Topography of Mars, J. Geophys. Res., 84, No. B11, 6241-6247, (1979)
- Lowman, P.D., Crustal Evolution in Silicate Planets: Implications for the Origin of Continents, J. Geol., 84, 1-26, (1976)
- Lutz, T.M., Foland, K.A., Meridional Pattern of the Oceanic Rift System, Geol., 6, 179-183, (1978)
- Malykh, A.V., Ryazanov, G.V., On the Relationship of the Zones of Intensified Fracturing of the Sedimentary Mantle to the Faults in the Basement Complex in the Southeastern Part of the Tunguska Syncline, Soviet Geol. Geophys., 21, No. 11, 60-63, (1980)
- Mareschai, J.C., Uplift by Thermal Expansion of the Lithosphere, Geophys. J. Roy. Astron. Soc., 66, 535-552, (1981)
- Masson, P., Structure Pattern Analysis of the Noctis Labyrinthus-Valles Marineris Region of Mars, Icarus, 30, 49-62, (1977)
- Masson, P., Contribution to the Structural Interpretation of Valles Marineris-Noctis Labyrinthus-Claritas Fossae Regions of Mars, Moon and the Planets, 22, 211-219, (1980)
- Maxwell, T.A., Plain Ridges: Indicators of Compressional Stress on the Moon, Mars, and Mercury, Nasa Tech. Mem. 85127, 277-278, (1982)
- McGill, G.E., Planetary Fracture Patterns: Influence of Inheritance of Stress Analysis, Nasa Tech. Mem. 81776, 80-82, (1980)
- McMillian B., Venkatakrisnan R., A Computer program for Statistical Analysis of Lineament, Unpublished manuscript, (1985)
- Middlemost, E.A.K., Evolution of Volcanic Islands, Lithos, 6, 123-132, (1973)
- Mohr, P.A., Wood, C.A., Volcano Spacing and Lithospheric Attenuation in the Eastern Rift of Africa, Earth Planetary Sci. Lett., 33, 126-144, (1976)

- Mohr, P.A., Surface Structure and Plate Tectonics of Africa, Tectonophysics, 15, 3-18, (1972)
- Molnar, P., Atwater, T., Relative Motion of Hotspots in the Mantle, Nature, 246, 288-291, (1973)
- Moore, J.McM., Jackson, N., Structure and Mineralization in the Cligga Granite Stock, Cornwall, Geol. Soc. Lond., 133, 467-480, (1977)
- Morgan, W.J., Deep Mantle Convection Plumes and Plate Motions, A.A.P.G., 56, No. 2, 203-213, (1972)
- Muller, O.H., Pollard, D.D., The Stress State Near Spanish Peaks, Colorado Determined from a Dike Pattern, Pageoph., 115, 69-86, (1977)
- Mutch, T.A., Arvidson, R.E., Head, J.W., Jones, K.L., Saunders, R.S., The Geology of Mars, Princeton University Press, Princeton, New Jersey, 1976
- Nakamura, K., Volcanoes as Possible Indicators of Tectonic Stress Orientation-Principle and Proposal, J. Volcan. Geotherm. Res. 2, 1-16, (1977)
- Nakamura, K., Jacob, K.H., Davies, J.N., Volcanoes as Possible Indicators of Tectonic Stress Orientation-Aleutians and Alaska, Pageoph., 115, 87-111, (1977)
- Nakamura, K., Uyeda, S., Stress Gradient in Arc-Back Regions and Plate Subduction, J. Geophys. Res., 85, No. B11, 6419-6428, (1980)
- Nettleton, L.L., Regionals, Residuals, and Structures, Geophys., 19, No. 1, 1-22, (1954)
- Neuken, G., Wise, D.U., Mars: A Standard Crater Curve and Possible New Time Scale, Science, 194, No. 4272, 1381-1387, (1976)
- Norman, J.W., Fracture Analysis in the Determination of Sub-Unconformity Structure - A Photogeological Study, J. Petroleum Geol., 1, No. 1, 43-63, (1978)
- Norman, J.W., Photogeological Fracture Trace Study of Controls of Kimberlite Intrusion in Lesto Basalts, Trans. Instn. Min. Metall., Sect. B, 78-90, (1977)
- Norman, J.W., Photogeological Fracture-Trace Analysis as a

- Subsurface Exploration Technique, Trans. Instn. Min. Metall., Sect, B, No. 85, 1351-1362, (1976)
- Nur, A., The Origin of Tensile Fracture Lineament, J. Struct. Geol., 4, 31-40, (1982)
- Parmentier, E.M., Turcotte, D.L., Numerical Experiments on the Structures of Mantle Plumes, J. Geophys. Res., 80, No. 32, 4417-4424, (1975)
- Petrasko, A.K., Hodge, D.S., Shaw, R., Mechanics of Emplacement of Basic Intrusions, Tectonophysics, 46, 41-63, (1978)
- Phillips, R.J., Saunders, R.S., The Isostatic State of Martian Topography, J. Geophys. Res., 80, No. 20, 2893-2898, (1975)
- Phillips, R.J., Lambeck, K., Gravity Fields of the Terrestrial Planets: Long Wave Lengths Anomalies and Tectonics, Rev. Geophys. Space Phys., 18, No. 1, 27-76, (1980)
- Phillips, R.J., Saunders, R.S., Conel, J.E., Mars: Crustal Structure Inferred from Bouguer Gravity Anomalies, J. Geophys. Res., 78, No.23, 4815-4820, (1973)
- Plescia, J.B., Saunders, R.S., Tectonic History of the Tharsis Region, Mars, J. Geophys. Res., 87, No. B12, 9775-9791, (1982)
- Plescia, J.B., Roth, L.E., Saunders, R.S., Tectonic Features of Southeast Tharsis, Nasa Tech. Mem. 85127, 68-70, (1982)
- Pitcher, W.S., Bussell, M.A., Structural Control of Batholithic Emplacement in Peru: A Review, J. Geol. Soc. Lond., 133, 149-256, (1977)
- Podwysocki, M.H., Gold, D.P., The Surface Geometry of Inherited Joint and Fracture Trace Patterns Resulting from Active and Passive Deformation, Goddard Space Flight Center Report, X-923-74-222, (1974)
- Pretorius, J.P., Partridge, T.C., The Analysis of Angular Atypicality of Lineaments as an Aid to Mineral Exploration, J.S. African Inst. Mining Metallurgy, 74, 367-369, (1974)

- Reches, Ze'ev, Analysis of Joints in Two Monoclines in Israel, Geol. Soc. Amer. Bull., 87, 1654-1662, (1976)
- Ramberg, H., Theoretical Models of Density Stratification and Diapirism in the Earth, J. Geophys. Res., 77, No. 5, 877-889, (1972)
- Ramberg, H., Gravity, Deformation and the Earth's Crust, Chapter 11, Academic Press, 246-321, (1981)
- Roth, L.E., Downs, G.S., Saunders, R.S., Shubert, G., New-Radar Derived Topography for the Northern Hemisphere of Mars, J. Geophys. Sci., 87, No. B12, 9747-9754, (1982)
- Roth, L.E., Downs, G.S., Saunders, R.S., Radar Altimetry of South Tharsis, Mars, Icarus 42, 287-316, (1980)
- Rumsey, I.A.P., Relationship of Fractures in Unconsolidated Superficial Deposits to those in the Underlying Bedrock, Mod. Geol., 3, 25-41, (1971)
- Salvatori, R., Bianchi, R., Coradini, M., Fulchignoni, M., Statistical Approach to the Fracture Pattern of the Tharsis Region of Mars, Nasa Tech. Mem., 84211, 386-388, (1981)
- Sanford, A.R., Analytical and Experimental Study of Simple Geologic Structures, Geol. Soc. Amer. Bull., 70, 19-52, (1959)
- Sapronov, N.L., Magma-Conduction Reactures in the South of the Tunguska Syncline, Geologiya i Geofizika, 22, No. 3, 53-60, (1981)
- Saunders, R.S., Mars Structural Studies, Nasa Tech Mem. 84211, 375-376, (1981)
- Saunders, R.S., Gregory, T.E., Tectonic Implications of Martian Ridge Plains, Nasa Tech. Mem., 82385, 93-94, (1980)
- Sawatzky, D.L., Raines, G.L., Geologic Uses of Linear-Feature Maps Derived from Small-Scale Images, Basement Tect. Contr., 15, 91-100, (1978)
- Schultz R.A., Malin, M.C., Martian Global Tectonics, Nasa Tech. Mem. 85127, 291, (1982)
- Scott, D.H., Volcanoes and Volcanic Provinces: Martian

- Western Hemisphere, J. Geophys. Res., 87, No. B12, 9839-9851, (1982)
- Scott, D.H., and Carr, M.H., U.S. Geological Survey Misc. Inv. Map I-1083, 1978
- Scott, D.H., Tanaka, L., Mars: Paleostratigraphic Restoration of Buried Surfaces in Tharsis Montes, Icarus, 45, 304-319, (1981)
- Scott, D.H., Tanaka, K.L., Ignimbrites of Amazonis Planitia Region of Mars, J. Geophys. Res., 87, No. B12, 1179-1190, (1982)
- Shaw, H.R., The Fracture Mechanisms of Magma Transport from the Mantle to the Surface, in Physics of Magmatic Processes, Chapt. 6, 201-264, Princeton Univ. Press, (1980)
- Shepherd, J., Gaskell, J.C., Analysis of Fractures and Fissures Versus Mineralization Trends in the Drake Volcanics, New South Wales, Australia, Trans. Instn. Min. Metall., B9-B15, (1977)
- Shul'ts, S.S., Planetary Fractures and Tectonic Deformation, Geotronics, No. 4, 203-207, (1971)
- Sjogren, W.L., Lorell, J., Wong, L., Downs, W., Mars Gravity Field Based on a Short-Arc Technique, J. Geophys. Res., 80, No. 20, 2899-2908, (1975)
- Sjogren, W.L., Mars Gravity: High-Resolution Results from Viking Orbiter 2, Science, 203, 1006-1009, (1979)
- Solomon, S.C., The Geophysics of Mars: Whence the Tharsis Plateau?, Nature, 294, 304-305, (1981)
- Solomon, S.C., Head, J.W., Tharsis: An Alternative Explanation, (abstract) in Reports of the Planetary Geology Program 1979-1980, Nasa Tech. Mem. 81776, 71-73, 1980
- Solomon, S.C., Head, J.W., Evolution of the Tharsis Province of Mars: The Importance of Heterogeneous Lithospheric Thickness and Volcanic Construction, J. Geol. Res. 87, No. B12, 9755-9774, 1982
- Solomon, S.C., Head, J.W., Lunar Mascon Basins: Lava Filling, Tectonics, and Evolution of the Lithosphere, Rev. Geophys. Space Phys., 18, No. 1, 107-141, (1980)

- Spitzer, Cary, Viking Orbiter Views of Mars, By the Viking Orbiter Imaging Team, NASA SP-441, (1980)
- Spohn, T., Schubert, G., Convective Thinning of the Lithosphere: A Mechanism for Rifting and Mid-Plate Volcanism on Earth, Venus and Mars, Tectonophysics, 94, 67-90, (1983)
- Stevenson, D.J., Models of the Earth's Core, Science, 214, No.4521, 611-618, (1981)
- Turcotte, D.L., Membrane Tectonics, Geophys. J. R. Astr. Soc. 36, 33-42, 1974
- Turcotte, D.L., Willemann, R.J., Role of Membrane Stresses in the Support of Planetary Topography. J. Geophys. Res., 86, No.5, 3951-3959, (1981)
- USGS Topographic Map of Mars, Map M-25M-3-RMC, 1976
- Vogt, P.R., Volcano Spacing, Fractures, and Thickness of the Lithosphere, Earth Planet. Sci Lett., 23, 337-348, (1974)
- Vogt, P.R., Volcano Height and Plate Thickness, Earth Planet. Sci. Lett., 23, 337-348, (1974)
- Vogt, P.R., Plumes, Subaxial Pipe Flow, and Topography along the Mid-Oceanic Ridge, Earth Pt. Sci. Lett., 29, 309-325, (1976)
- Walcott, R.I., Flexure of the Lithosphere at Hawaii, Tectonophysics, 9, 435-446, (1970)
- Walters, R.S., Maxwell, T.A., Ridge-Rille Intersections in the Tharsis Province of Mars, Nasa Tech. Mem., 84211, 383-385, (1981)
- Walters, R.F., Contouring by Machine: A User's Guide, A.A.P.G., 53, No.11, 2324-2340, (1969)
- Walters, T.R., Maxwell, T.A., Strain Estimates for the Ridged Plains of Mars: Evidence of Compression in the Coprates Quadrangle, Nasa Tech. Mem. 85127, 279-281, (1982)
- Watts, A.B., Cochran, J.R., Gravity Anomalies and Flexure of the Lithosphere Along the Hawaiian-Emperor Seamount Chain, Geophys. J. Roy. Astron. Soc., 38, 119-141, (1974)

- Whitford-Stark, J.L., Tharsis Volcanoes: Separation Distances, Relative Ages, Sizes, Morphologies, and Depths of Burial, J. Geophys. Res., 87, No. B12, 9829-9838, (1982)
- Wilhelm, D.E., Comparison of Martian and Lunar Geologic Provinces, J. Geophys. Res., 79, No.26, 3933-3941, (1974)
- Willemann, R.J., Turcotte, D.L., The Role of Lithospheric Stress in the Support of the Tharsis Rise, J. Geophys. Res., 87, No. B12, 9793-9801, (1982)
- Wilson, J.T., Mantle Plumes and Plate Motions, Tectonophysics, 19, 149-164, (1973)
- Windley, B.F., Davies, F.B., Volcano Spacing and Lithospheric/Crustal Thickness in the Archaean, Earth Planet Sci. Lett., 38, 291-297, (1978)
- Wise, D.U., Golombek, M.P., McGill, G.E., Tectonic Evolution of Mars, J. Geophys. Res., 84, No. B14, (1979)
- Wise, D.U., Golombek, M.P., McGill, G.E., Tharsis Province of Mars: Geologic Sequence, Geometry, and a Deformation Mechanism, Icarus, 38, 456-472, (1979)
- Wise, D.U., Funicello, R., Parotto, M., Origins of Regional Scale Lineaments Swarms as Suggested by Fracture Domain Analysis of Italy, Nasa Tech. Mem. 81776, 83-85, (1980)
- Withjack, M.D., Scheirner, C., Fault Patterns Associated with Domes - An Experimental and Analytical Study, A.A.P.G. Bull. 66, No. 3, 302-316, (1982)
- Woronow, A., Cratering Record in the Inner Solar System, Nasa Tech. Mem. 82385, 174-176, (1981)

APPENDIX 1

Terminology of Martian Features

Appendix 1

Central vent volcanoes	Similar to cinder cones on Earth. Found throughout the Martian surface.
Complex flows	(Lobate plains) Complex overlapping flow plains normally void of ridges. Believed to be the result of volcanism characterized by sporadic flows with lower rates of effusion.
Fossae	An area of extensive fracturing usually centered around one direction.
Patera	Term to describe various "saucer-shaped" features with associated channels and radiant surface features. These features usually display complex central caldera.
Questionable plains	Plains that include units that are obliterated by erosion, fracturing and mass wasting.
Shields	Classified central volcanoes found on Earth with complex calderas and flank slopes of a few degrees.
Simple flow	(Ridged plains) Simple flow plains which display low, uniform topographic relief. Normally found associated with Martian wrinkle ridges.
Tholii	Volcanic domes with steep slopes. Believed to consist of more viscous lavas than shield volcanoes.
Undifferentiated flows	Plains that lack any features indicating volcanic origin. (i.e. no flow lobes, volcanoes, etc.) may be the result of eolian processes.

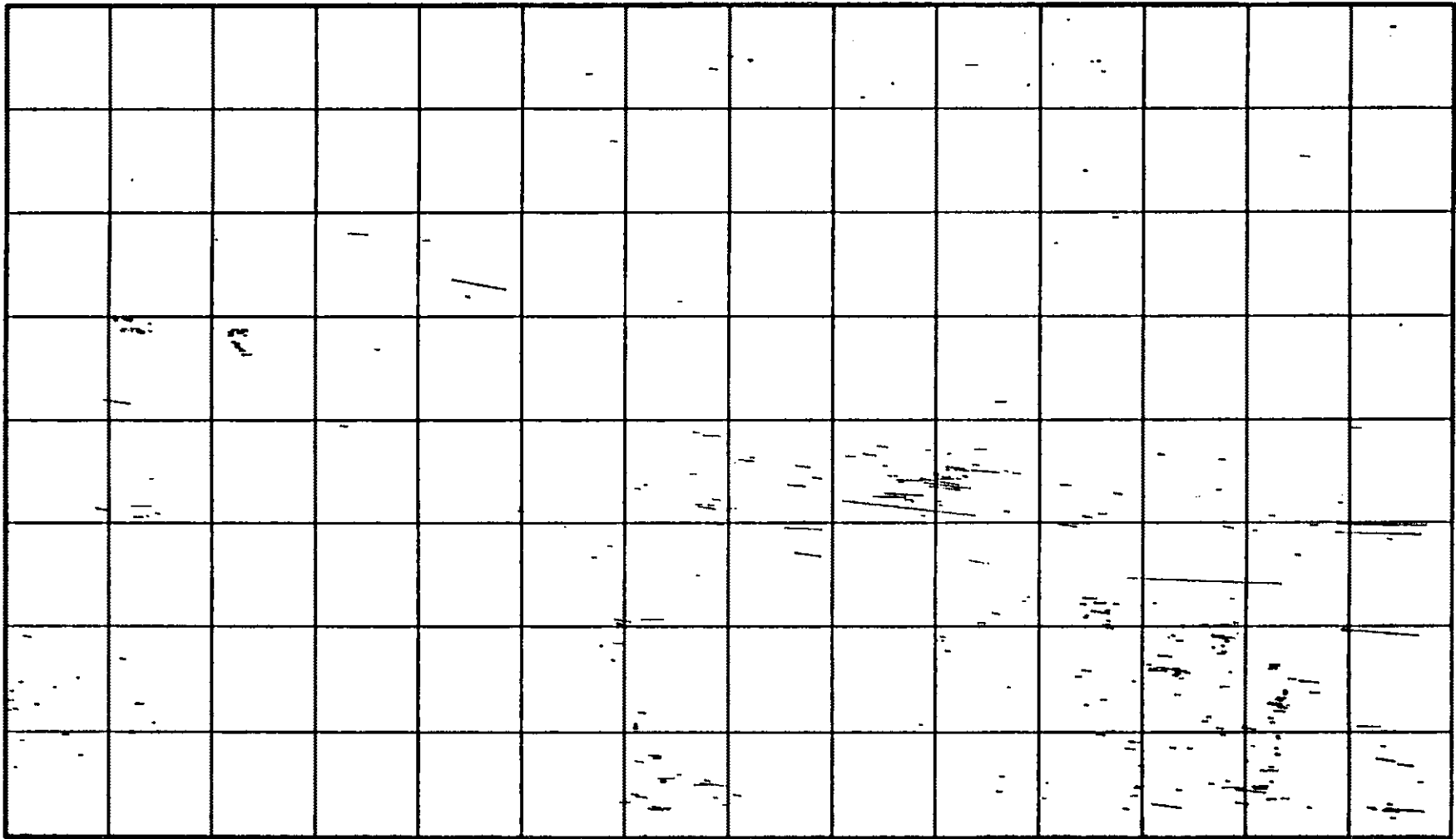
Valles

Regions believed to be the result
of fluvial activity from melting
ground ice.

Compiled from: Greeley and Spudis (1981) and DeHon (1982).

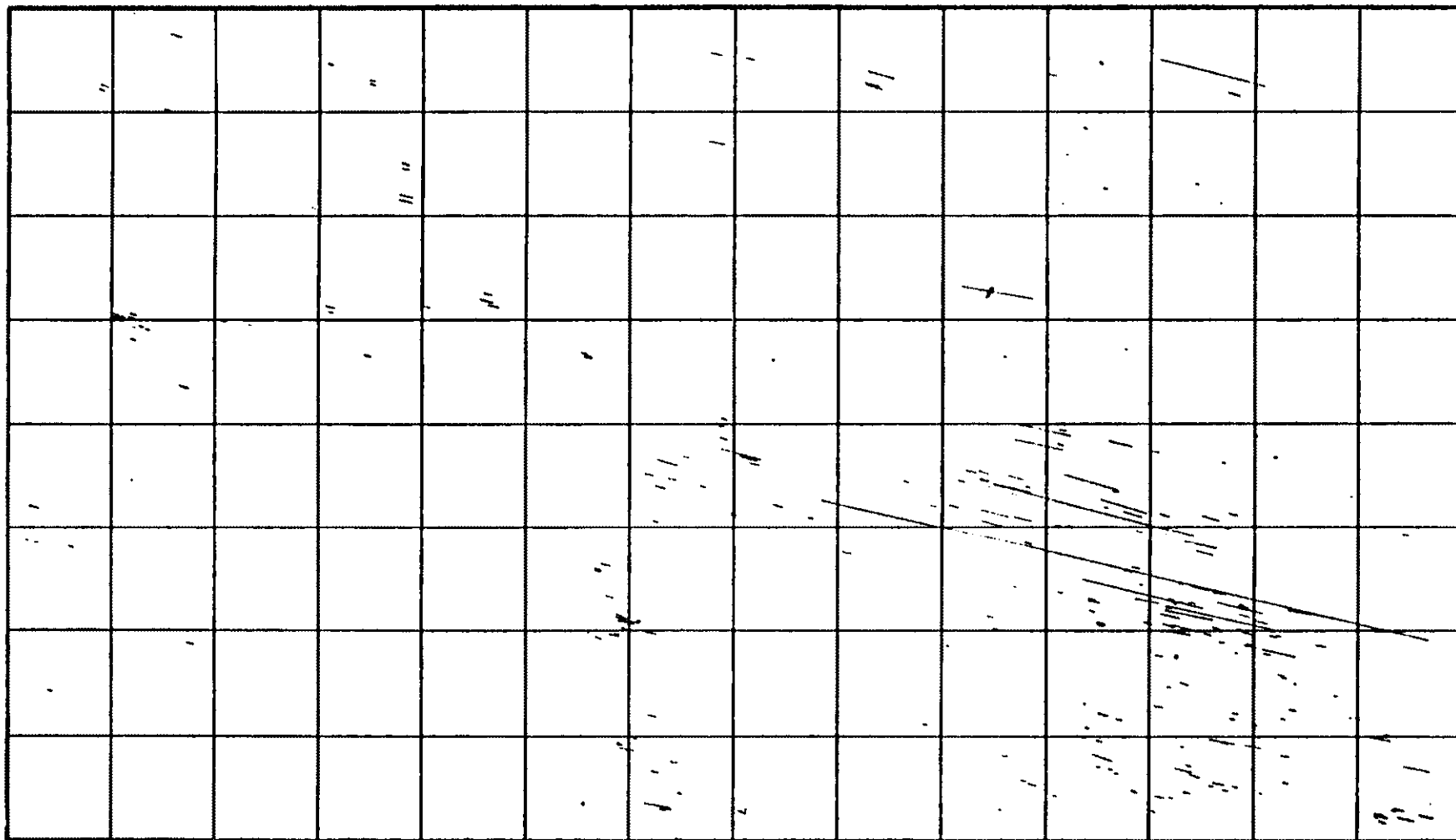
APPENDIX 2

Lineament data for 10 degree intervals



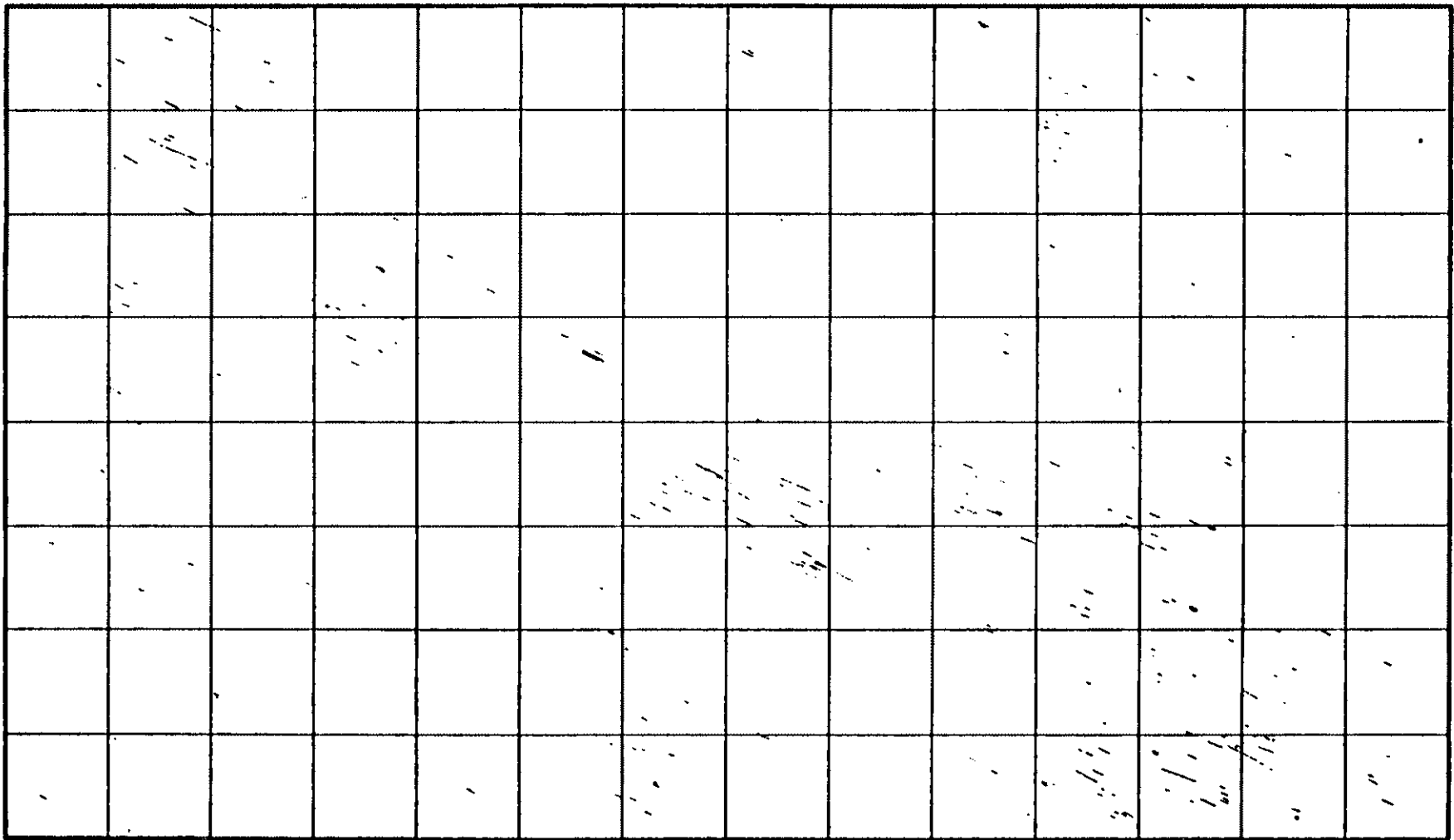
ALL FRACTURES

CELL SIZE • 50.0 50.0
 DEGREE RANGE • 270.0 TO 280.0
 LENGTH RANGE • 0.00 TO 5000.00



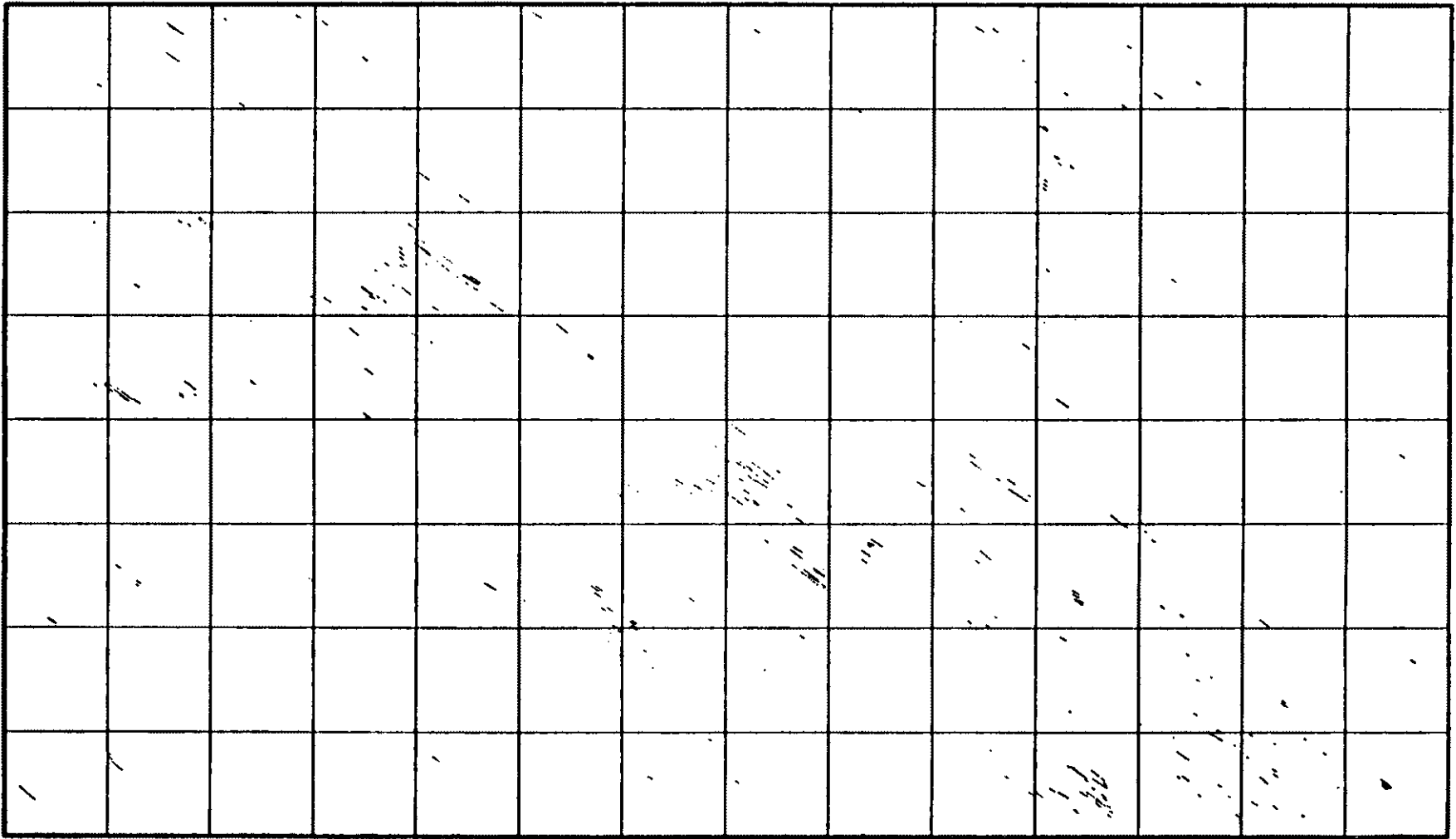
ALL FRACTURES

CELL SIZE: 50.0
 DEGREE RANGE : 280.0 TO 290.0
 LENGTH RANGE : 0.00 TO 5000.00



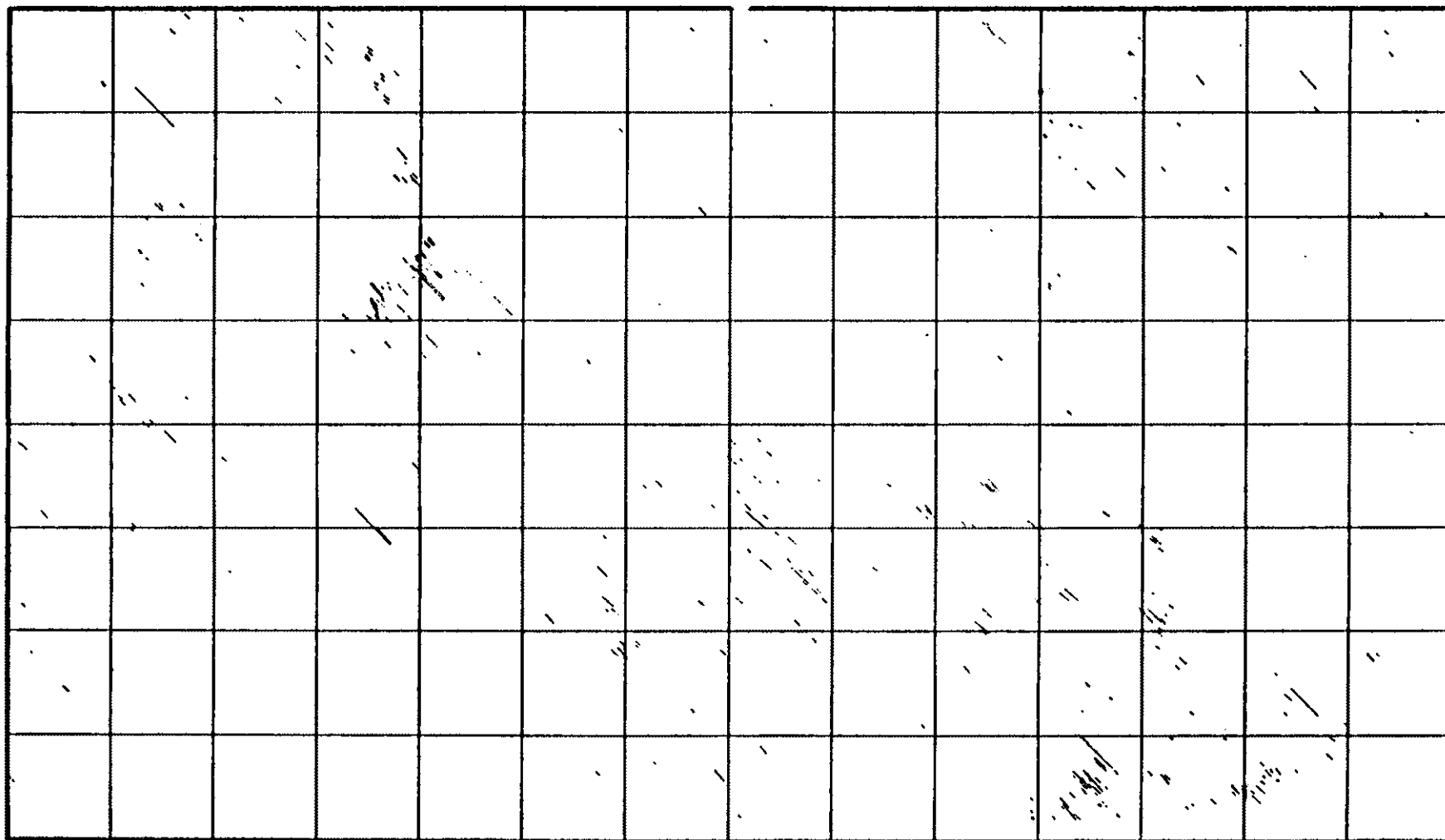
ALL FRACTURES

CELL SIZE: 50.0 50.0
 DEGREE RANGE : 290.0 TO 300.0
 LENGTH RANGE : 0.00 TO 5000.00



ALL FRACTURES

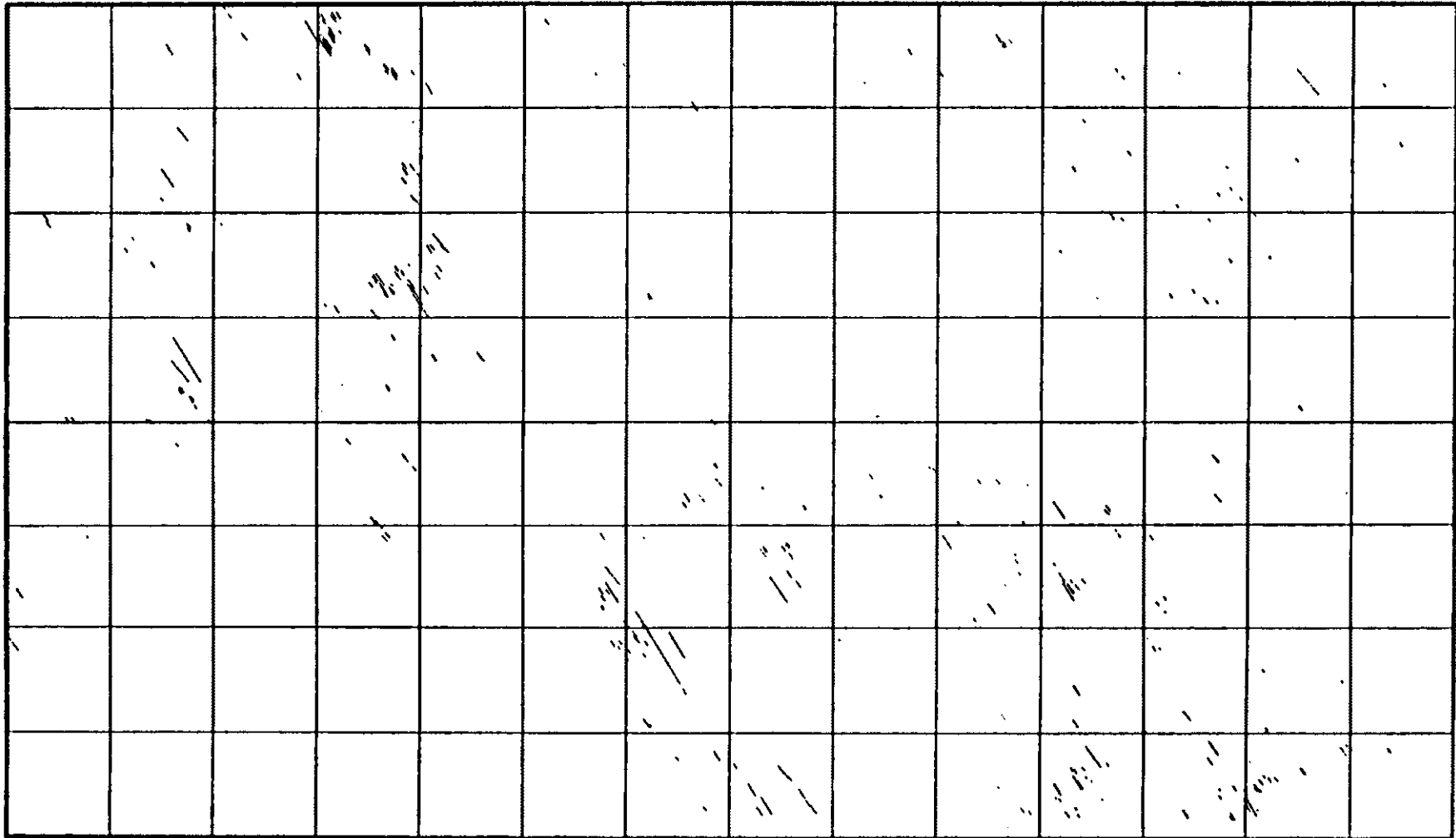
CELL SIZE : 50.0 50.0
 DEGREE RANGE : 300.0 TO 310.0
 LENGTH RANGE : 0.00 TO 5000.00



ALL FRACTURES

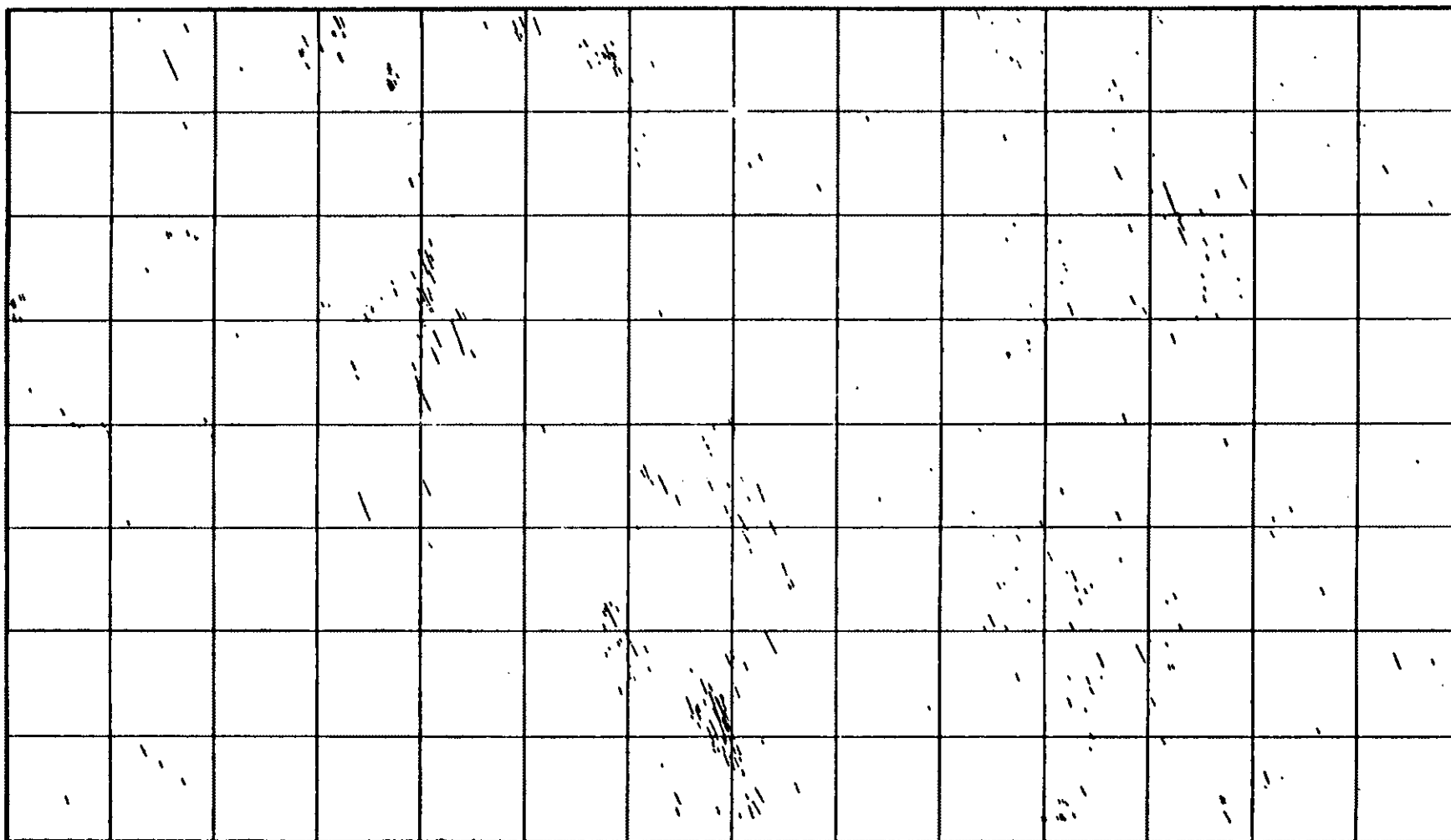
CELL SIZE: 50.0
 DEGREE RANGE: 310.0 TO 320.0
 LENGTH RANGE: 0.20 TO 5000.00

50.0



ALL FRACTURES

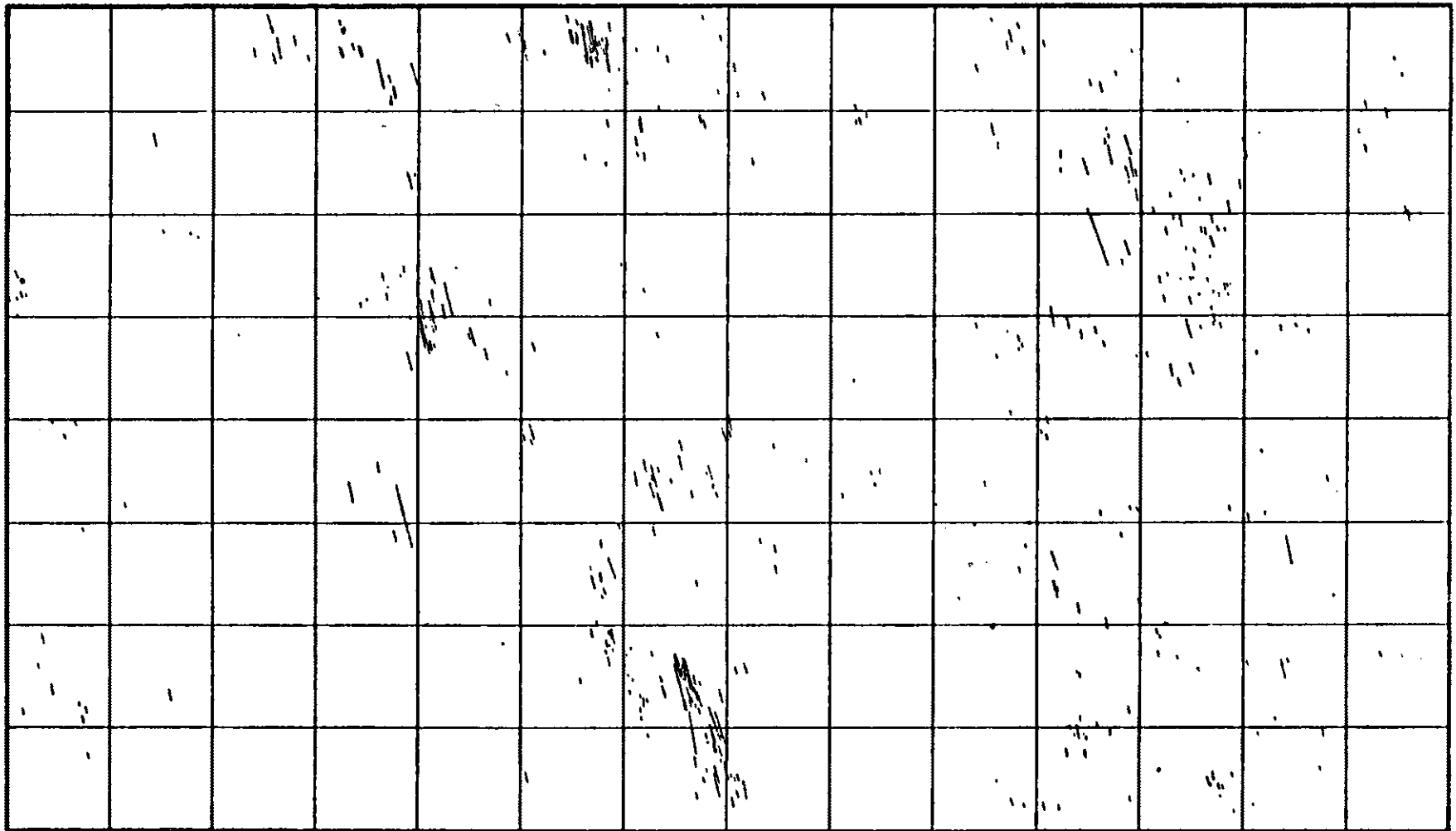
CELL SIZE • 50.0 50.0
 DEGREE RANGE • 320.0 TO 330.0
 LENGTH RANGE • 0.20 TO 5000.00



ALL FRACTURES

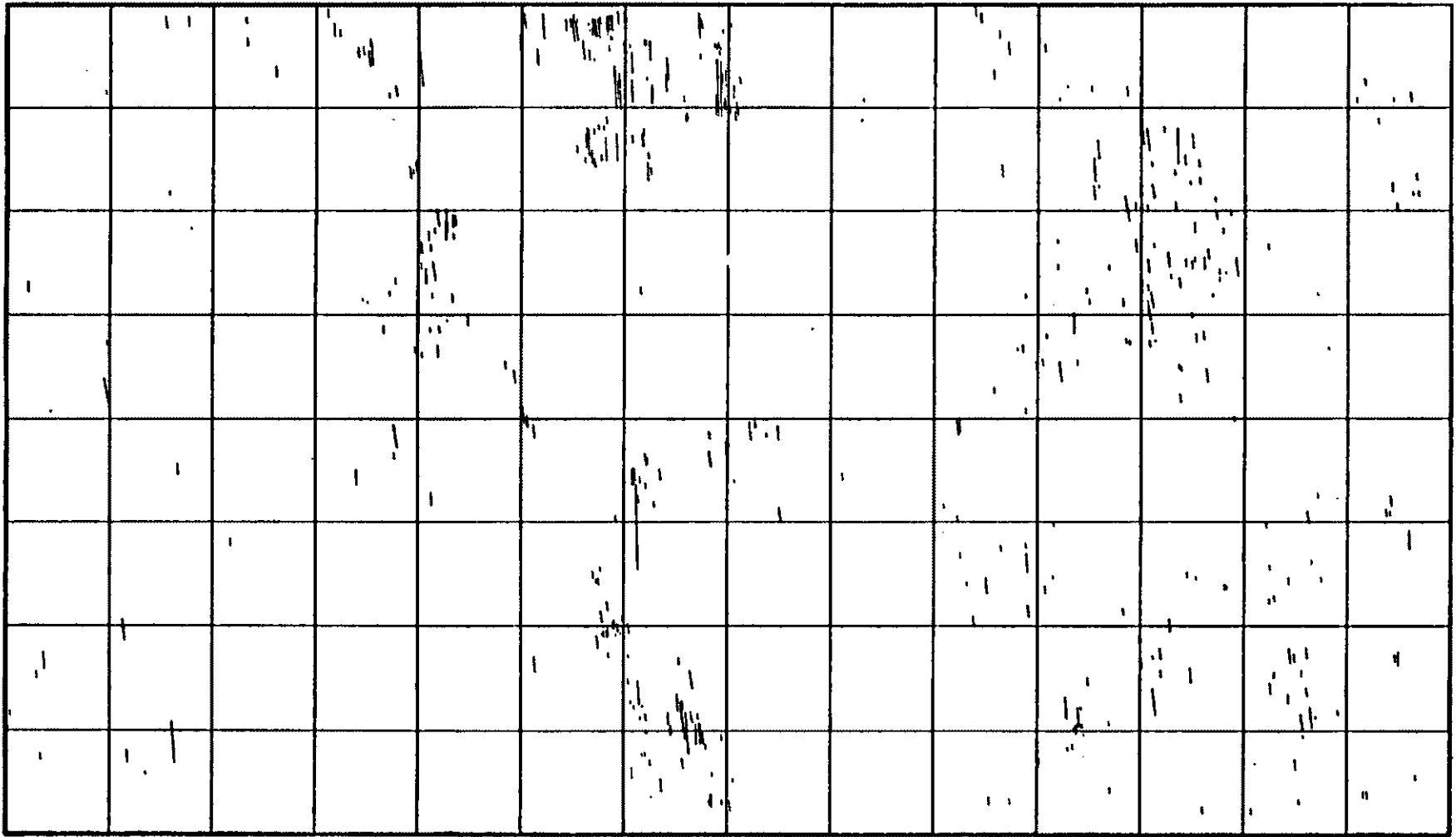
CELL SIZE • 50.0
 DEGREE RANGE • 330.0 TO 340.0
 LENGTH RANGE • 2.00 TO 5000.00

50.0



ALL FRACTURES

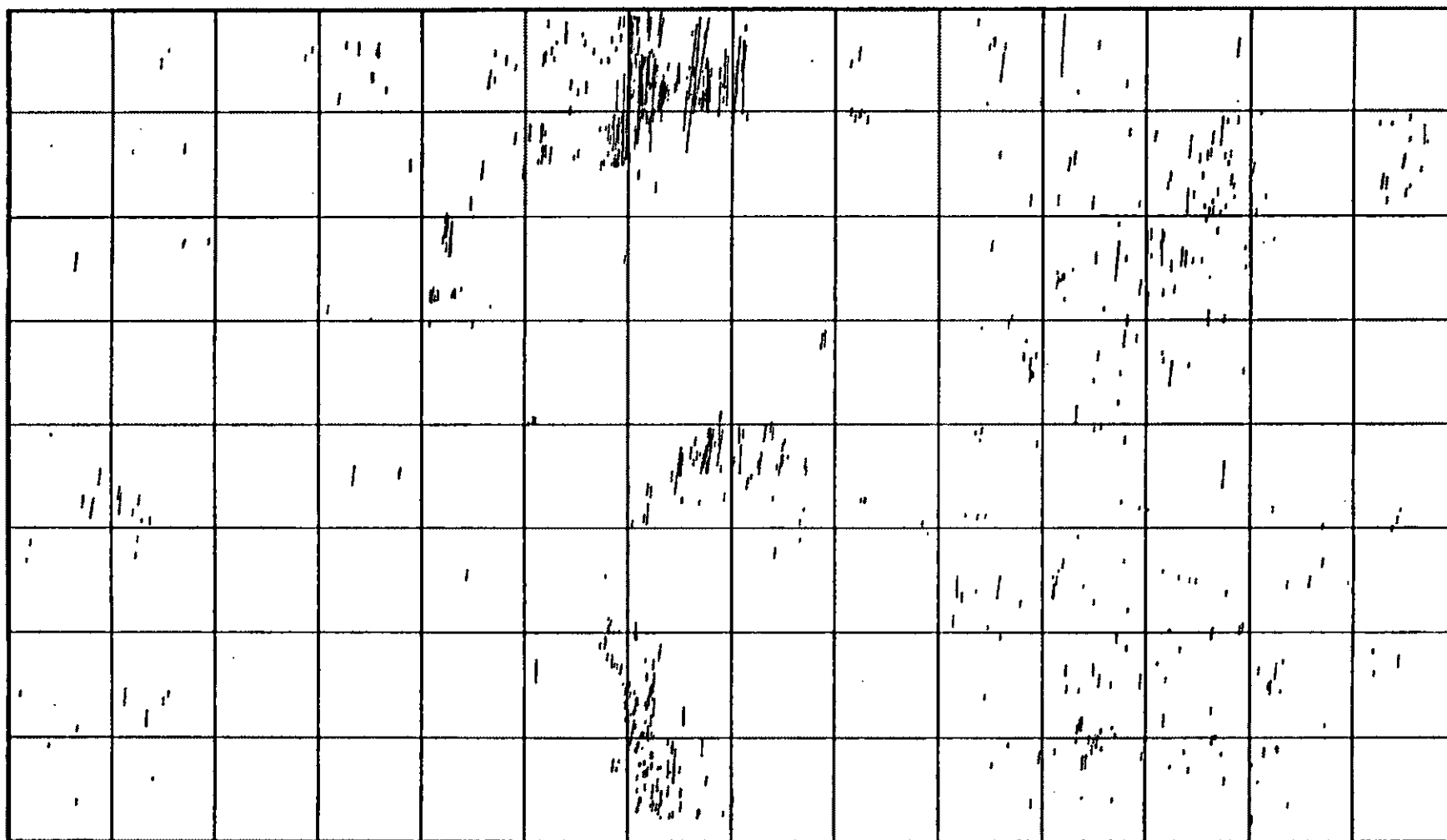
CELL SIZE • 50.0 50.0
 DEGREE RANGE • 340.0 TO 350.0
 LENGTH RANGE • 2.00 TO 5202.20



ALL FRACTURES

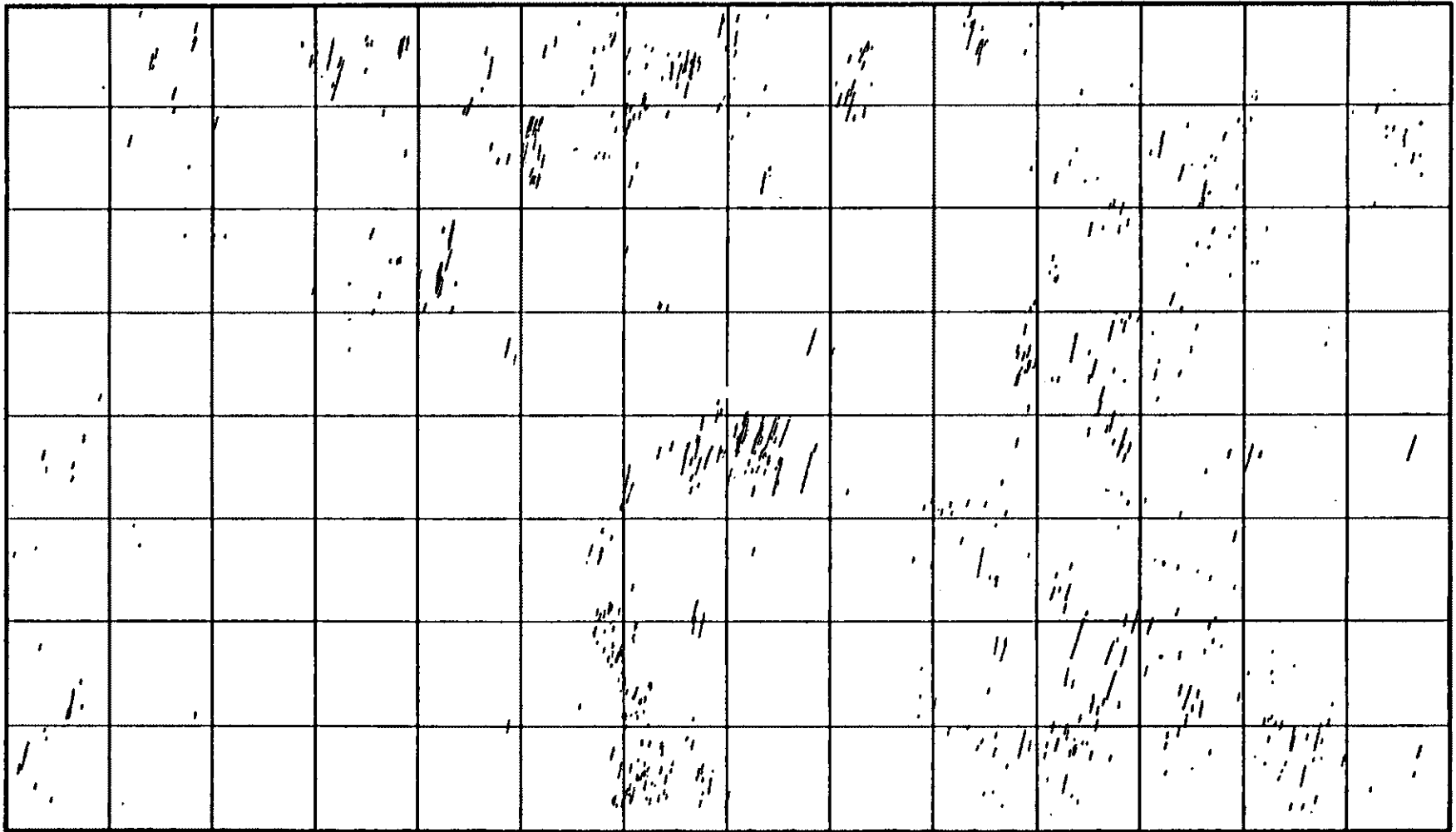
CELL SIZE • 50.0
 DEGREE RANGE • 350.0 TO 360.0
 LENGTH RANGE • 2.20 TO 500.00

50.0



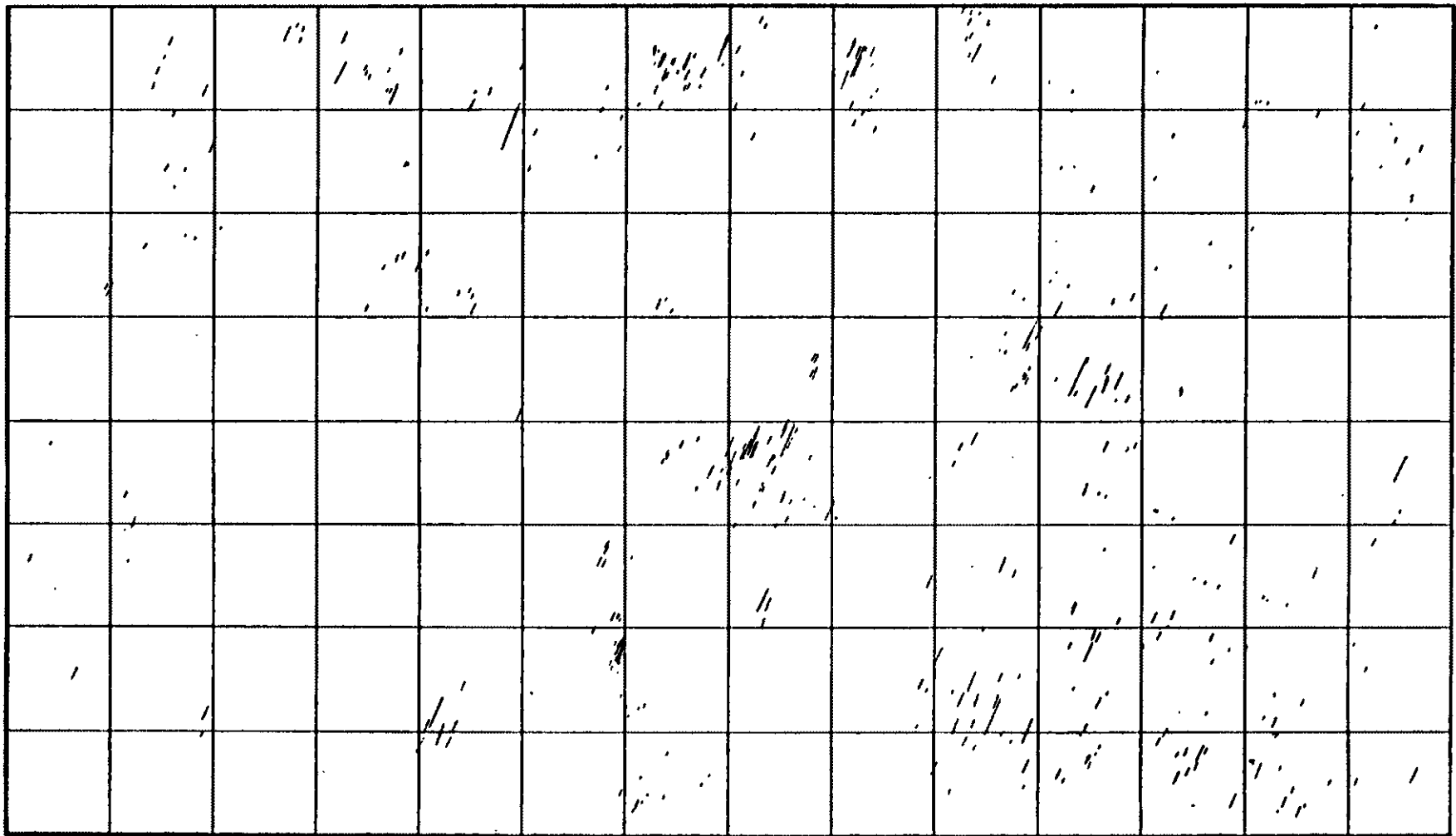
ALL FRACTURES

CELL SIZE: 50.0 50.0
 DEGREE RANGE: 0.0 TO 10.0
 LENGTH RANGE: 0.00 TO 5000.00



ALL FRACTURES

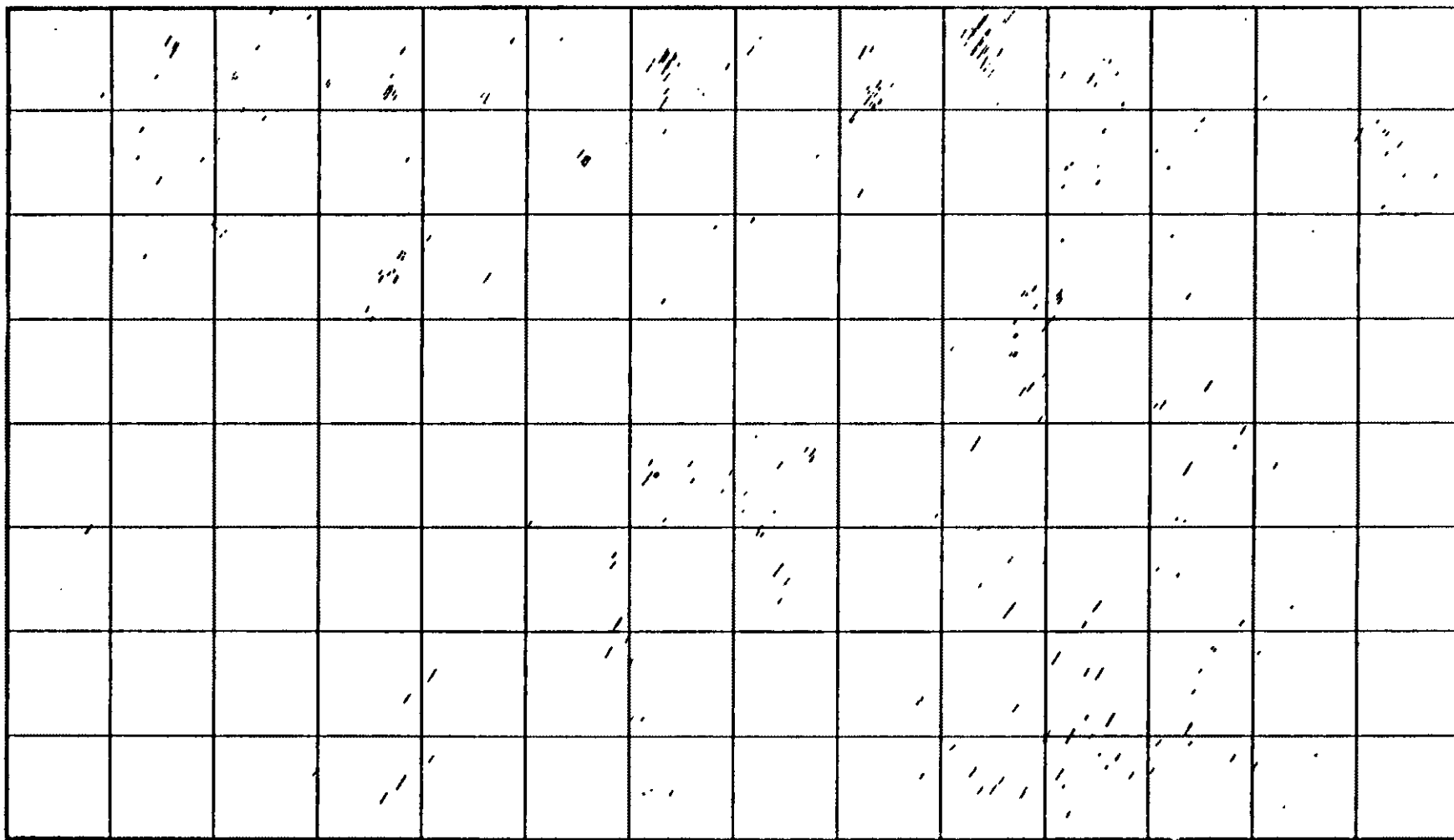
CELL SIZE • 50.0 50.0
 DEGREE RANGE • 10.0 TO 20.0
 LENGTH RANGE • 0.20 TO 5200.00



ALL FRACTURES

CELL SIZE • 50.0
 DIRECTION RANGE • 20.0 TO 30.0
 LENGTH RANGE • 0.20 TO 500.00

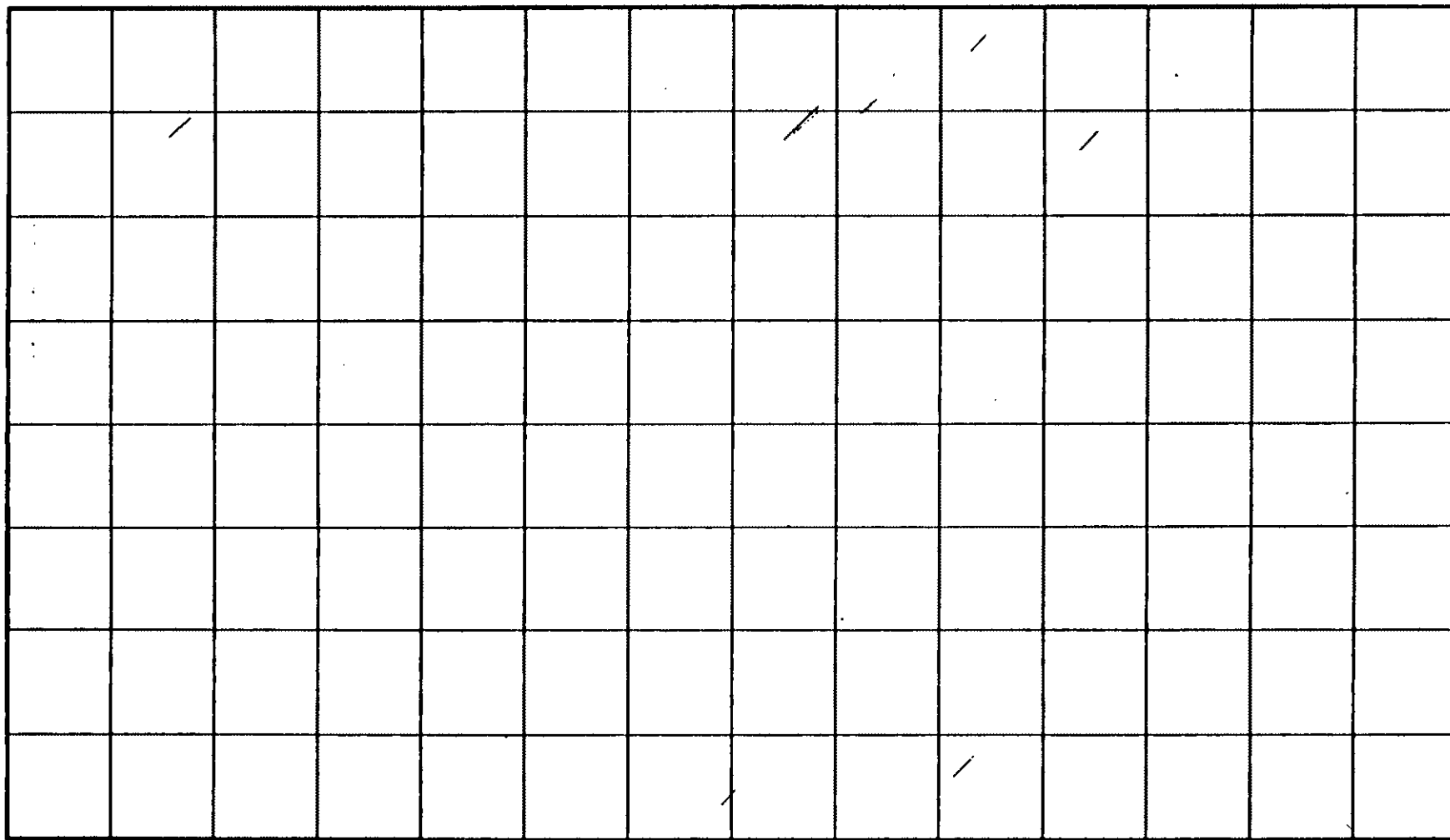
50.0



ALL FRACTURES

CELL SIZE • 50.0
 DEGREE RANGE • 30.0 TO 40.0
 LENGTH RANGE • 0.00 TO 10.00

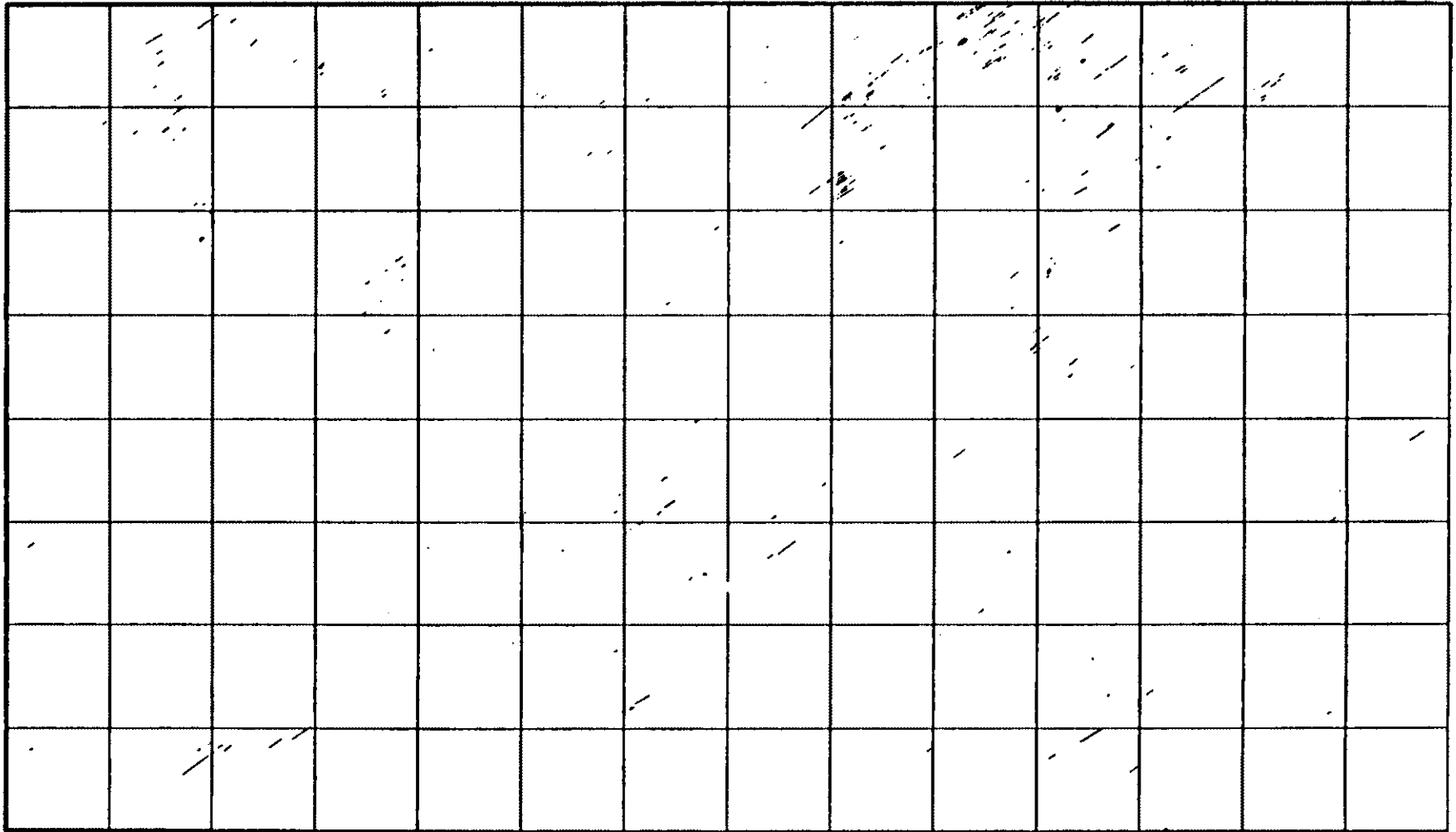
50.0



ALL FRACTURES

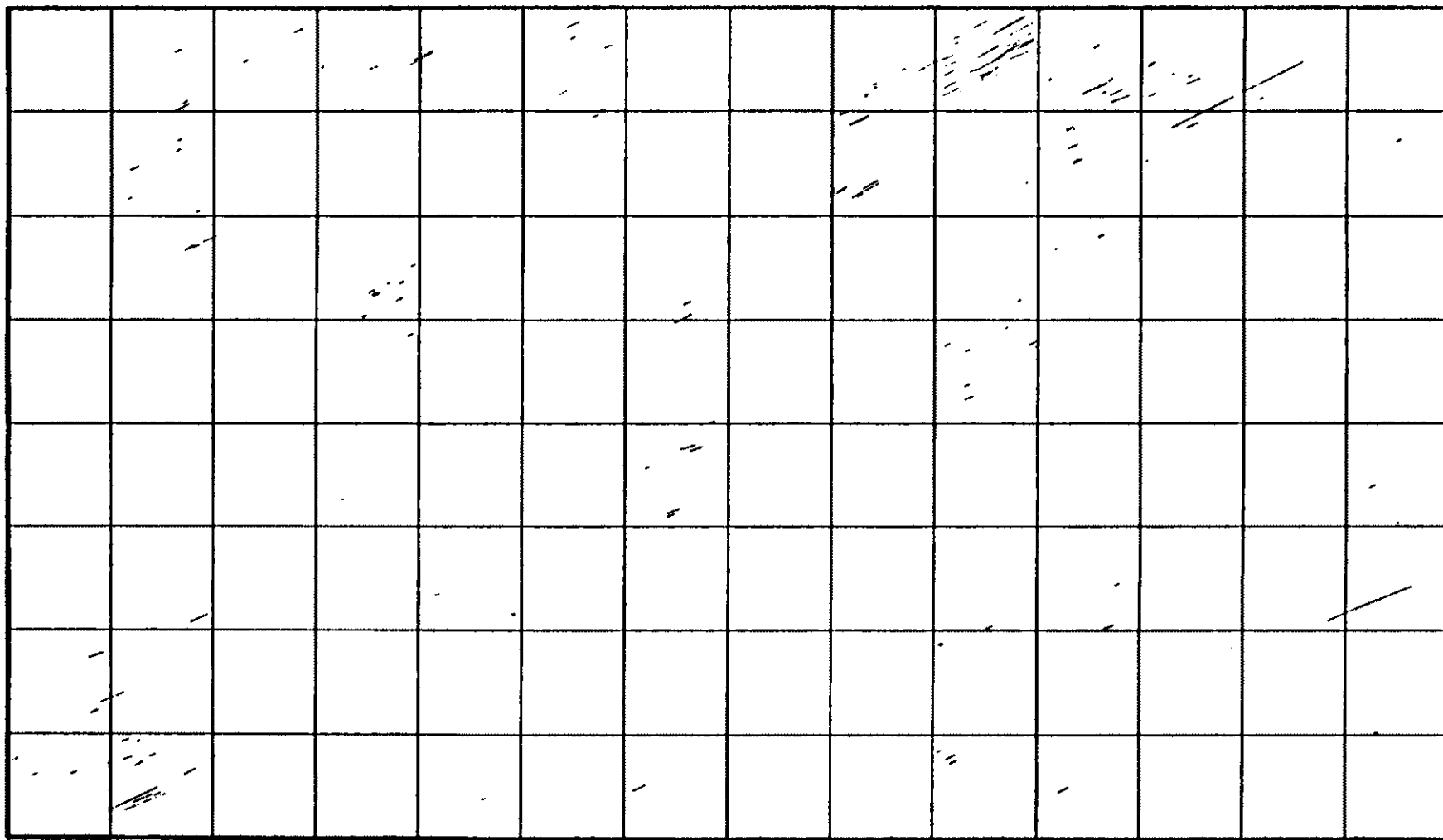
CELL SIZE • 50.0
 DEGREE RANGE • 40.0 TO 50.0
 LENGTH RANGE • 10.00 TO 25.20

50.0



ALL FRACTURES

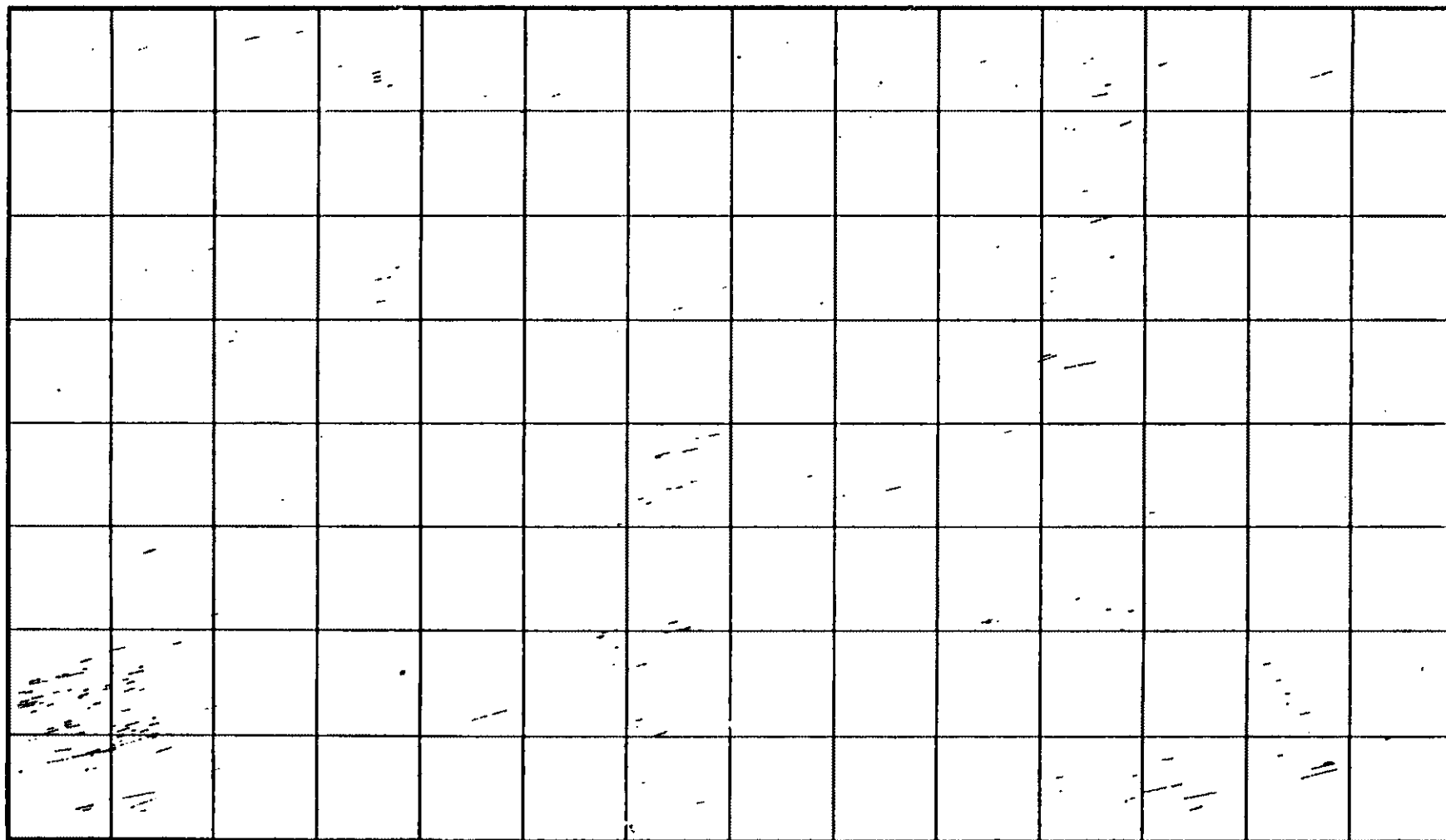
CELL SIZE: 50.0 50.0 50.0
 DEGREE RANGE : 50.0 TO 60.0
 LENGTH RANGE : 0.00 TO 5000.00



ALL FRACTURES

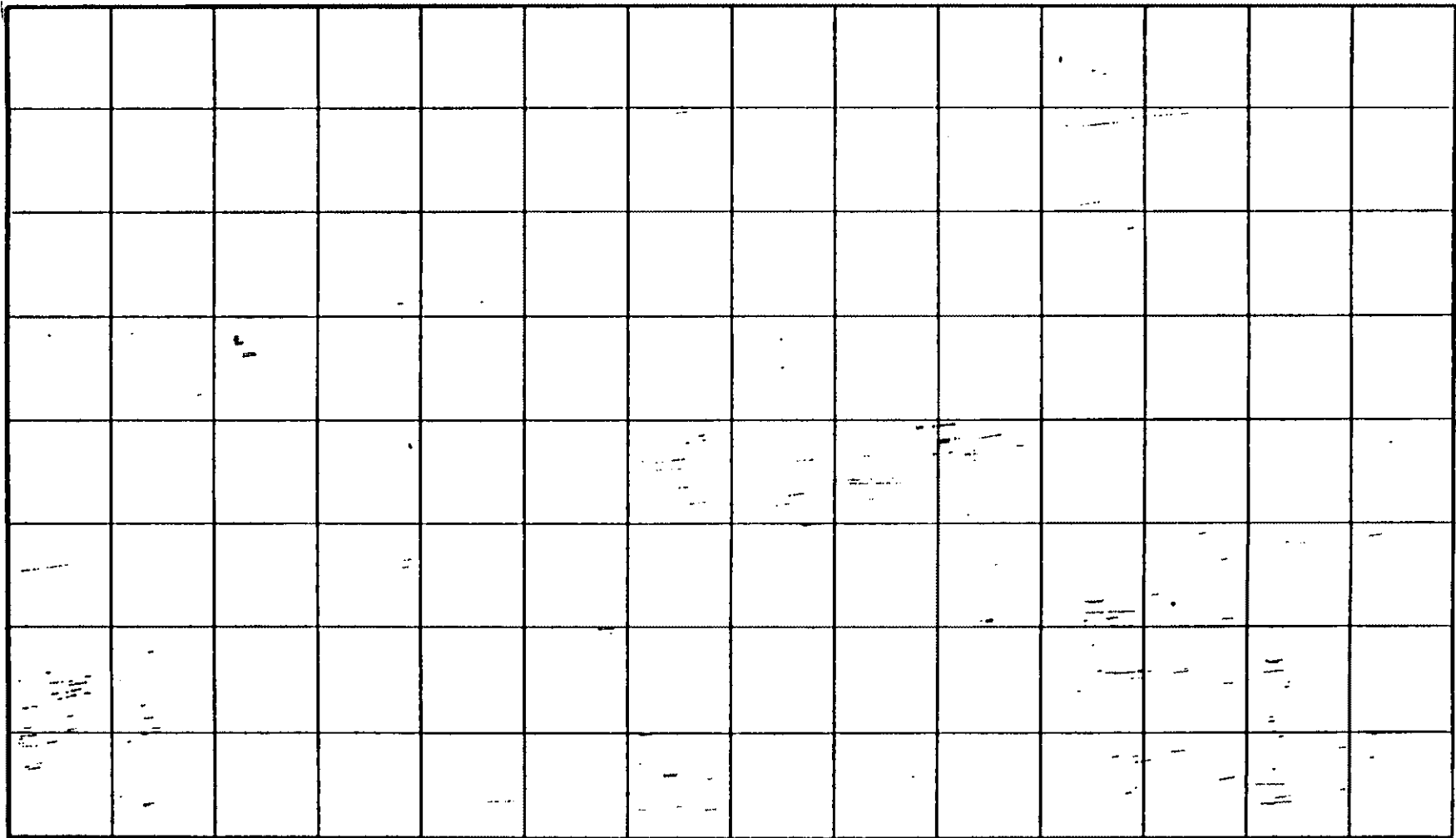
CELL SIZE • 50.0
 DEGREE RANGE • 60.0 TO 70.0
 LENGTH RANGE • 0.00 TO 500.00

50.0



CELL SIZE: 50.0
 DEGREE RANGE: 70.0 TO 90.0
 LENGTH RANGE: 0.00 TO 5000.00

50.0

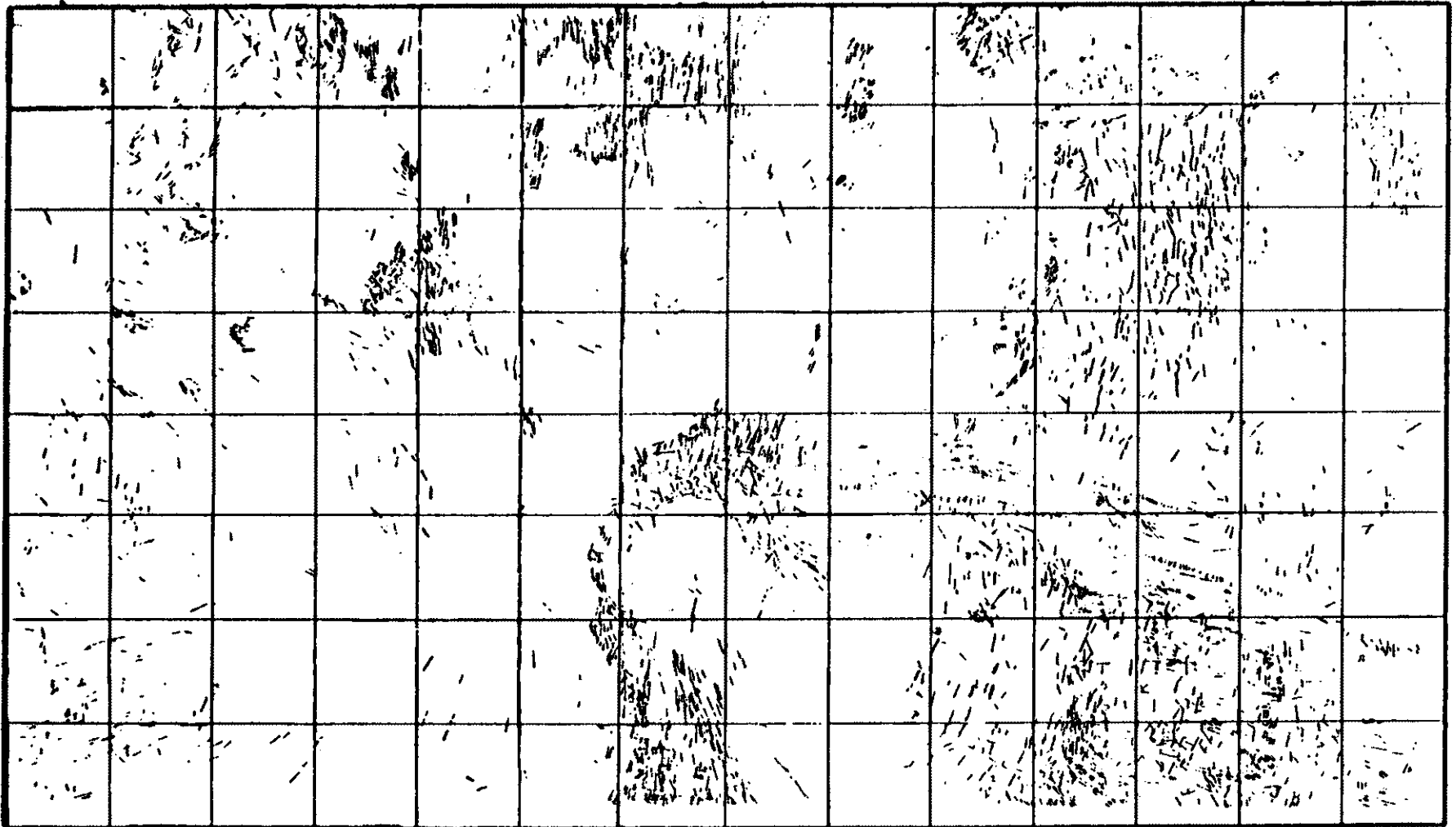


ALL FRACTURES

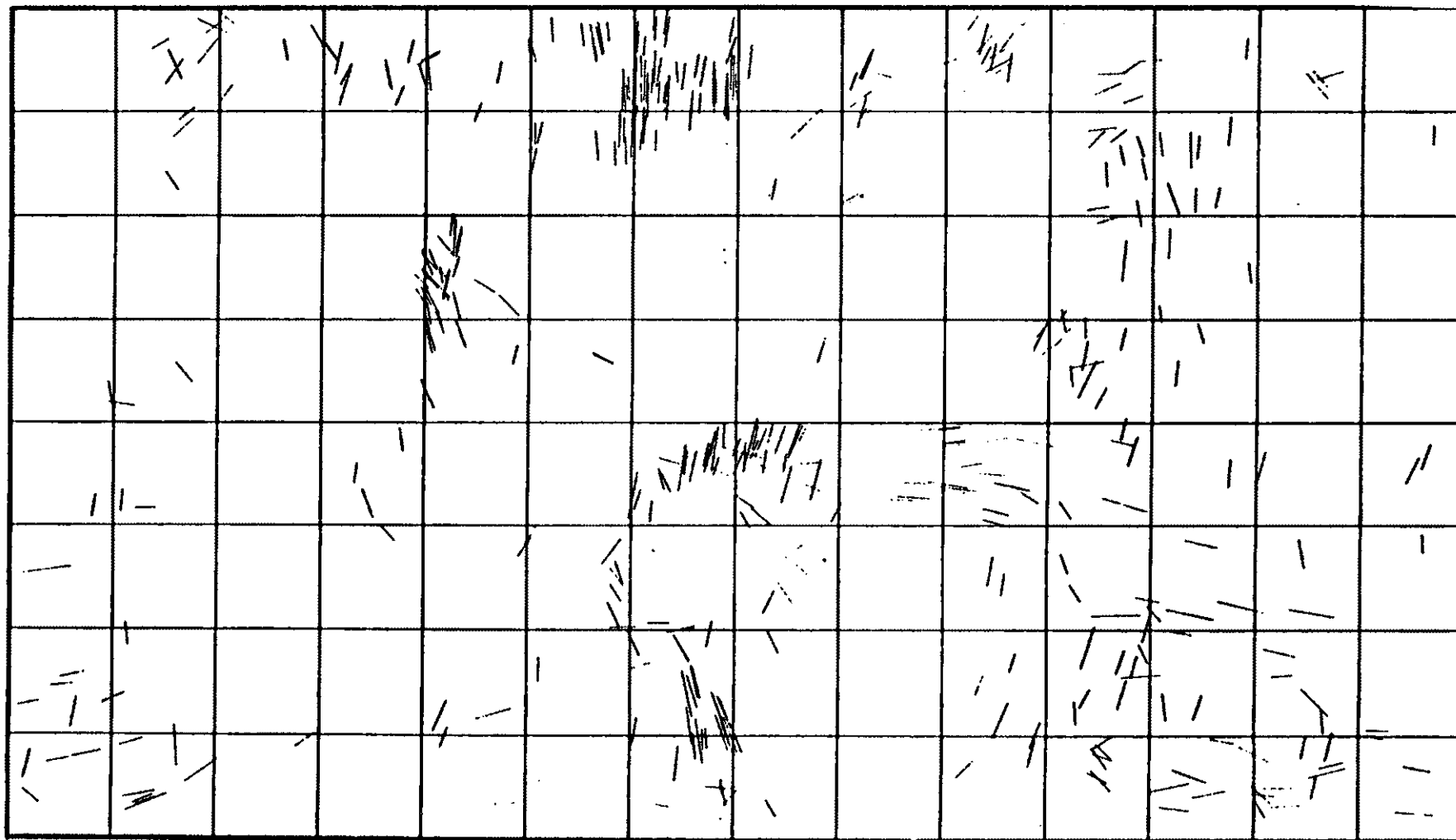
CELL SIZE: 50.0 50.0
 DEGREE RANGE: 92.0 TO 90.0
 LENGTH RANGE: 0.00 TO 5000.00

APPENDIX 3

Lineament data divided by lengths



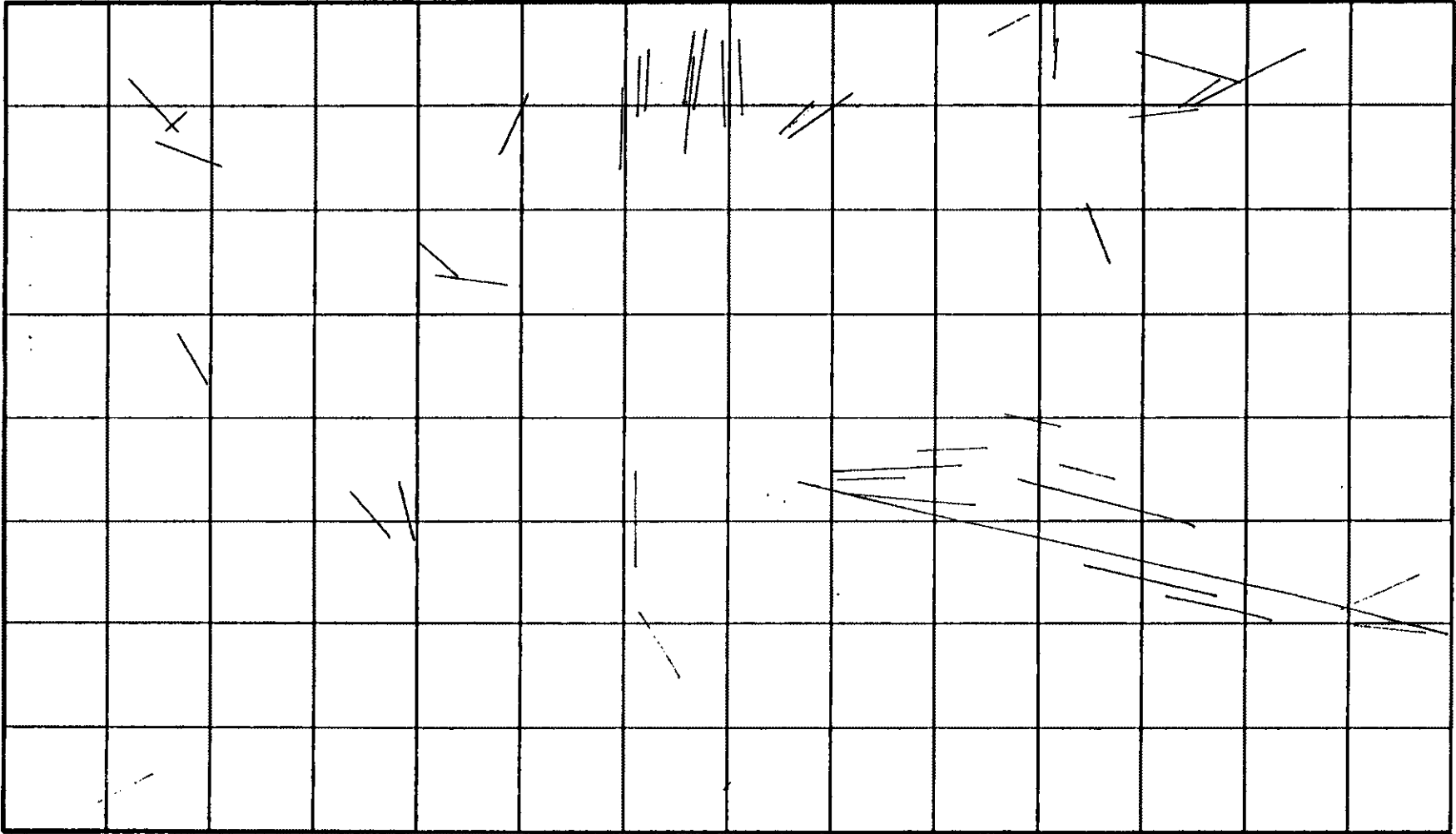
ALL FRACTURES 0 to 10mm



ALL FRACTURES

CELL SIZE • 50.0
 DEGREE RANGE • 0.0 TO 360.0
 LENGTH RANGE • 10.00 TO 25.00

50.0



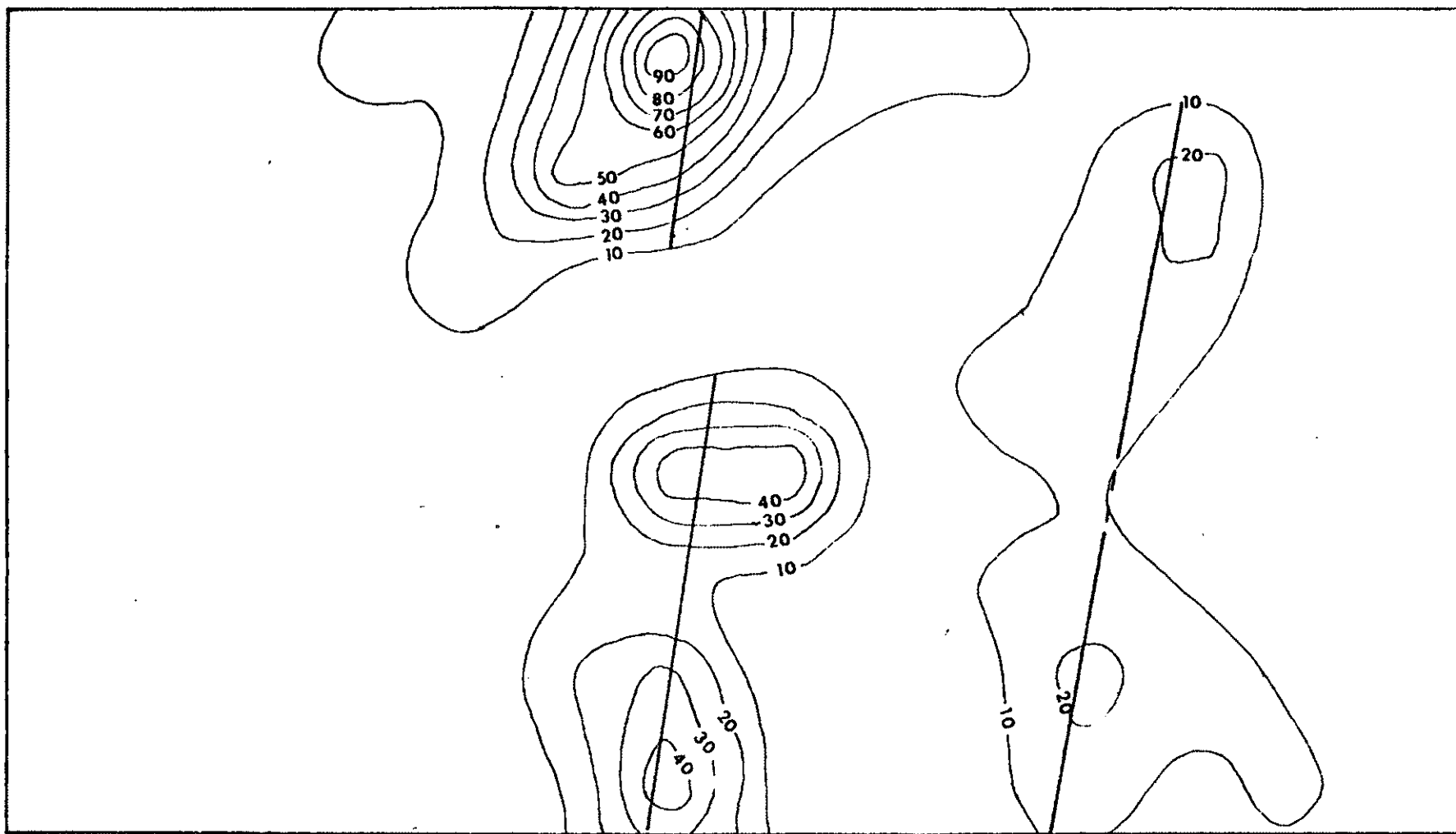
ALL FRACTURES

CELL SIZE: 50.0
 DEGREE RANGE: 0.0 TO 360.0
 LENGTH RANGE: GREATER THAN 25.20

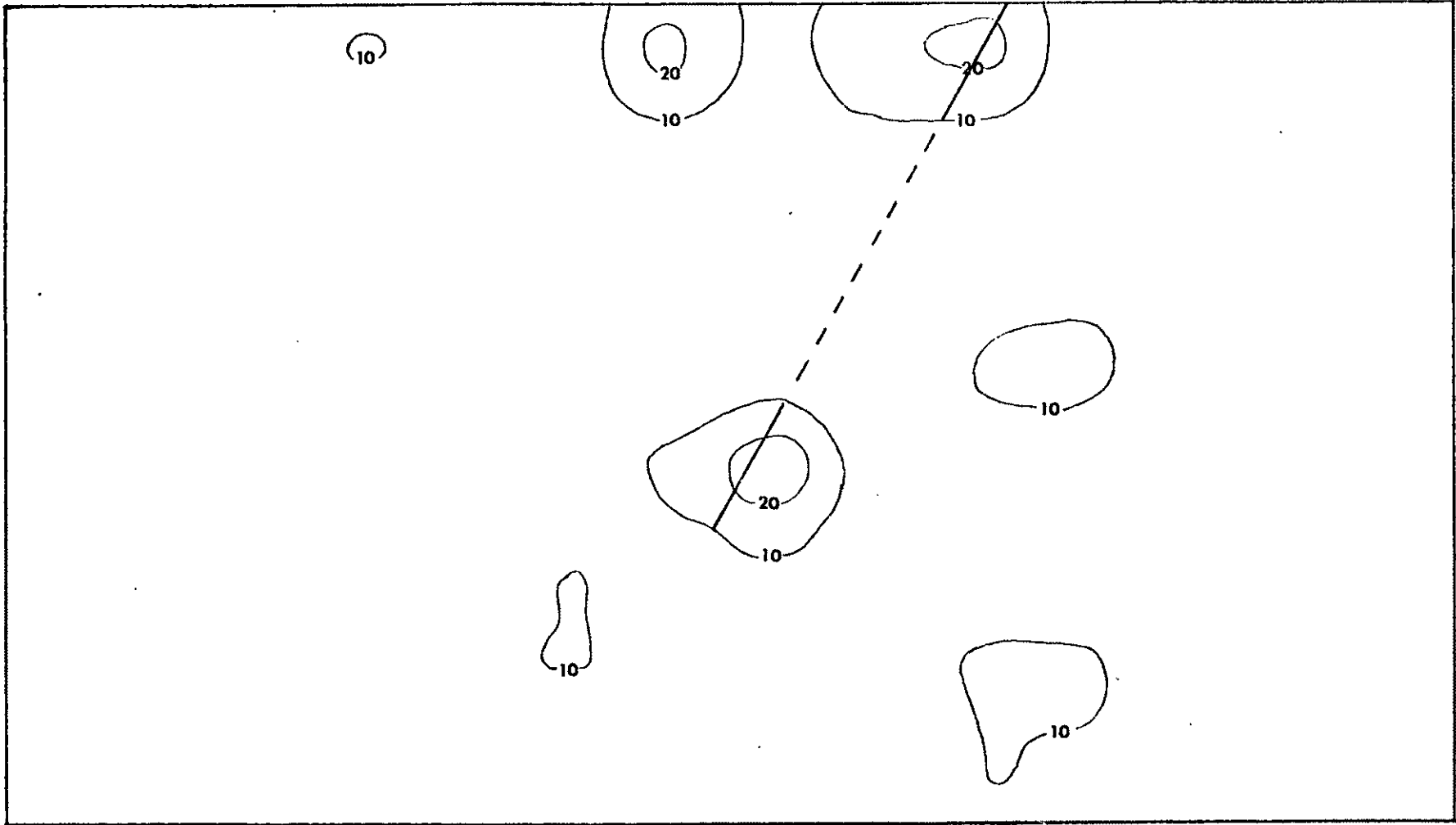
50.0

APPENDIX 4

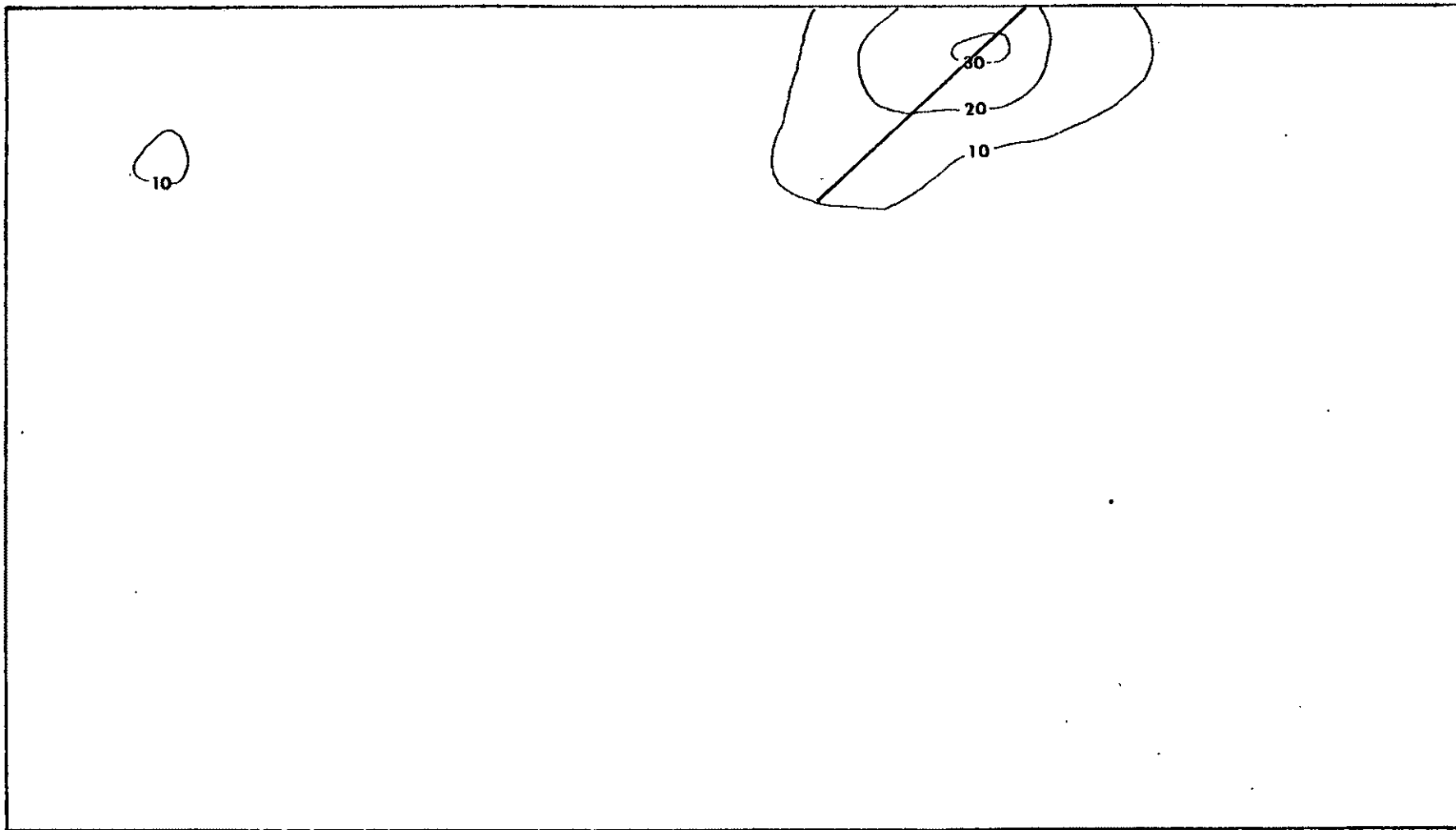
Density Distribution Plots



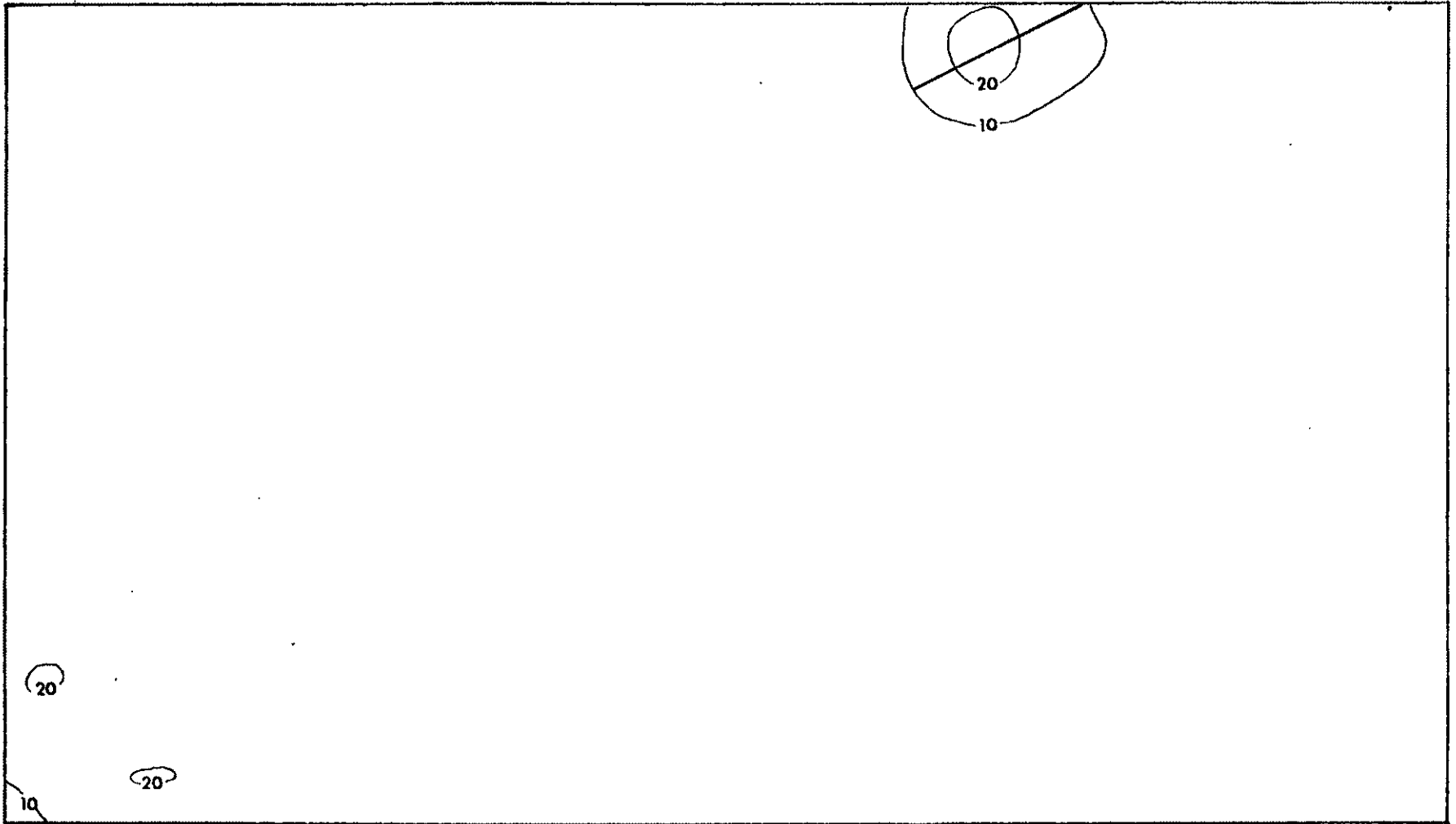
0-20 Degrees



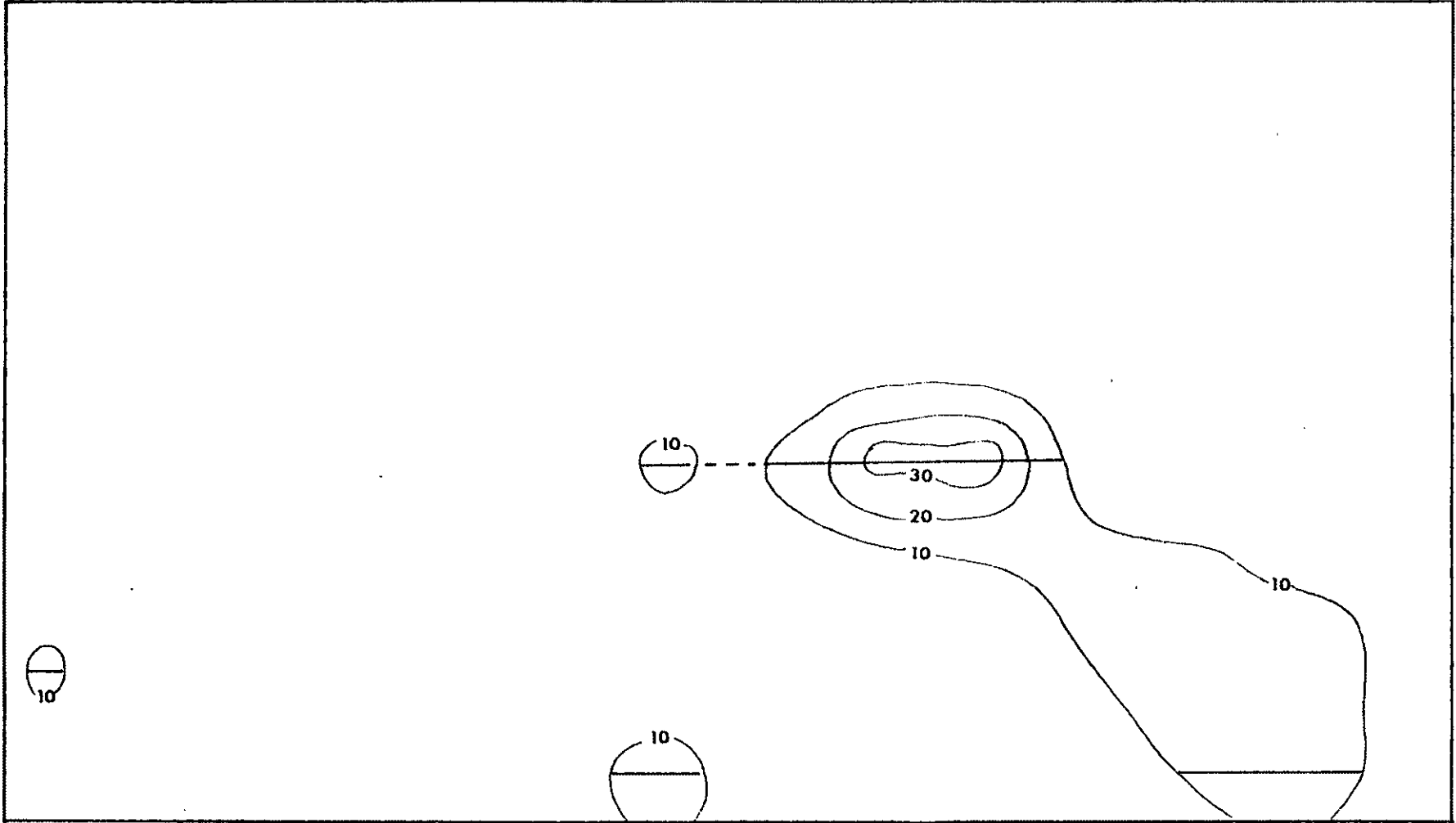
20-40 Degrees



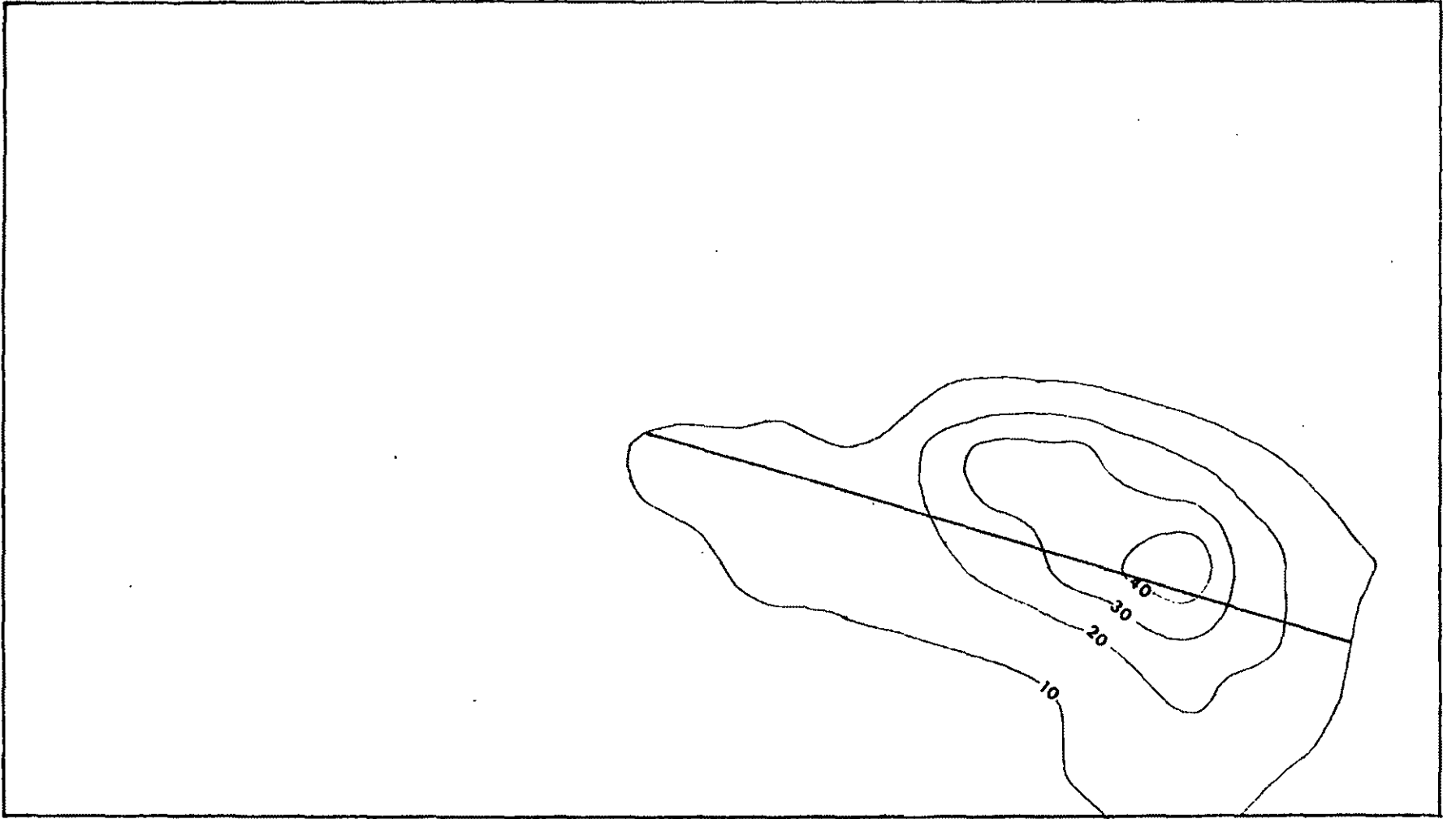
40-60 Degrees



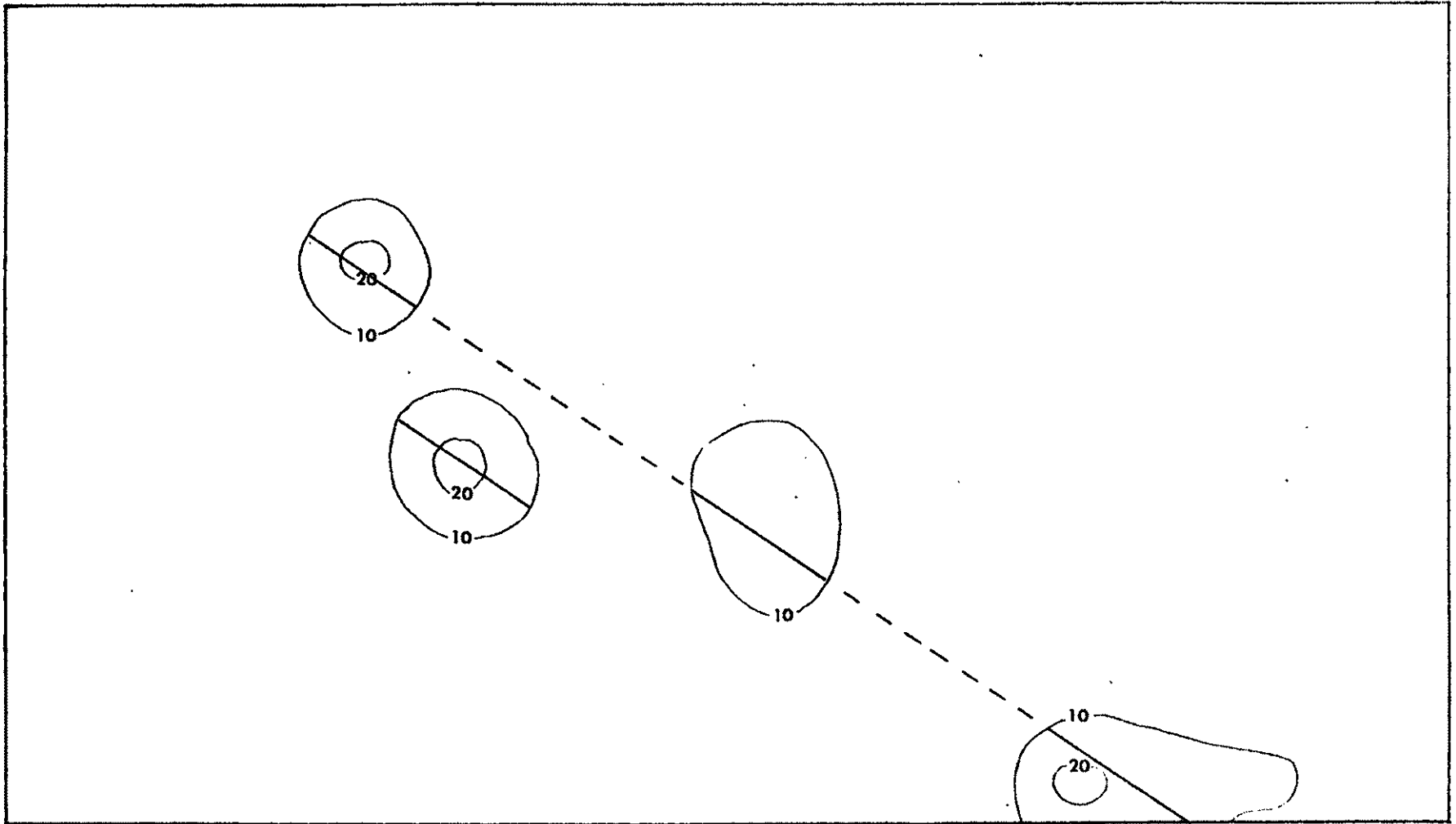
60-80 Degrees



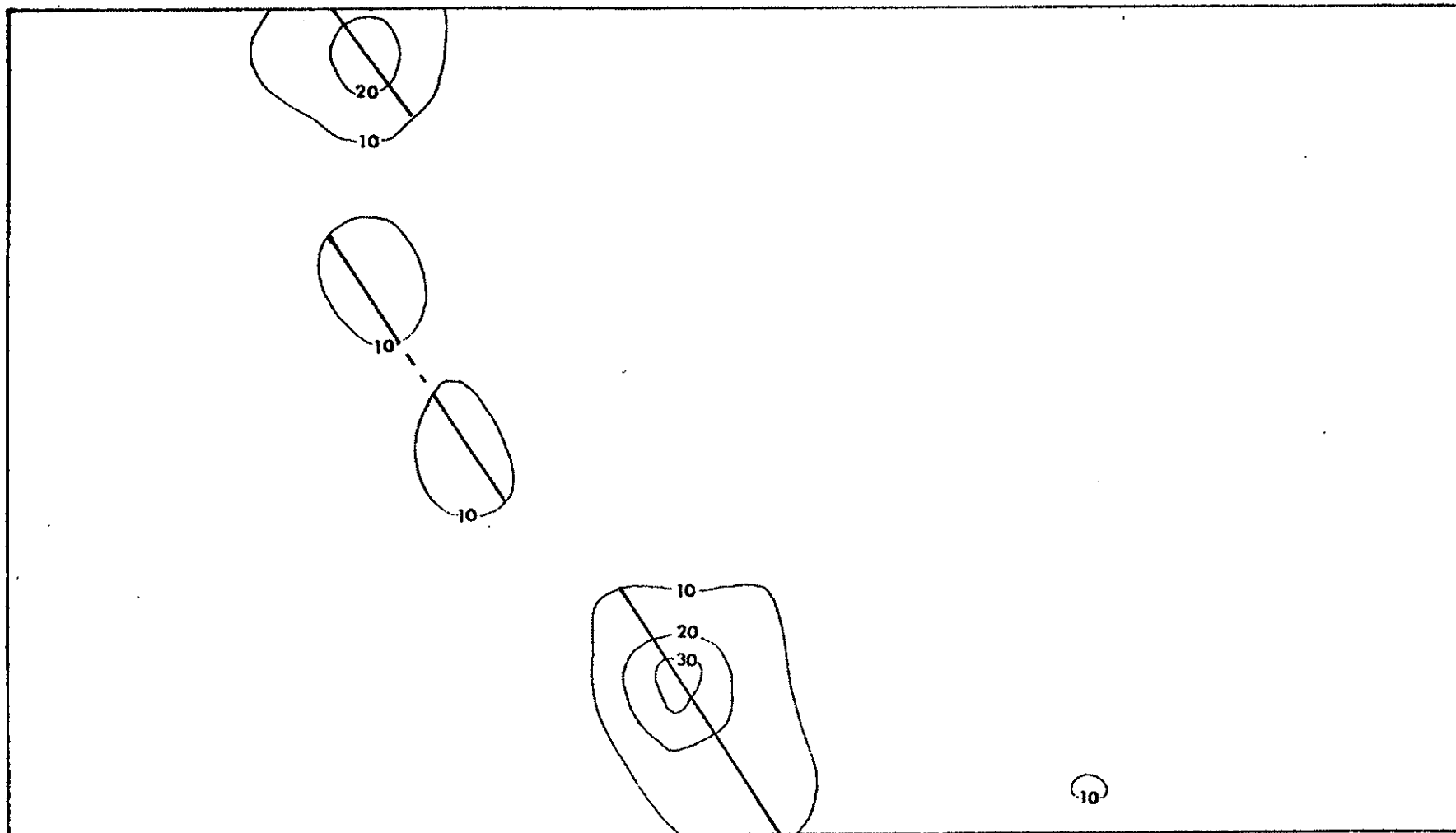
80-280 Degrees



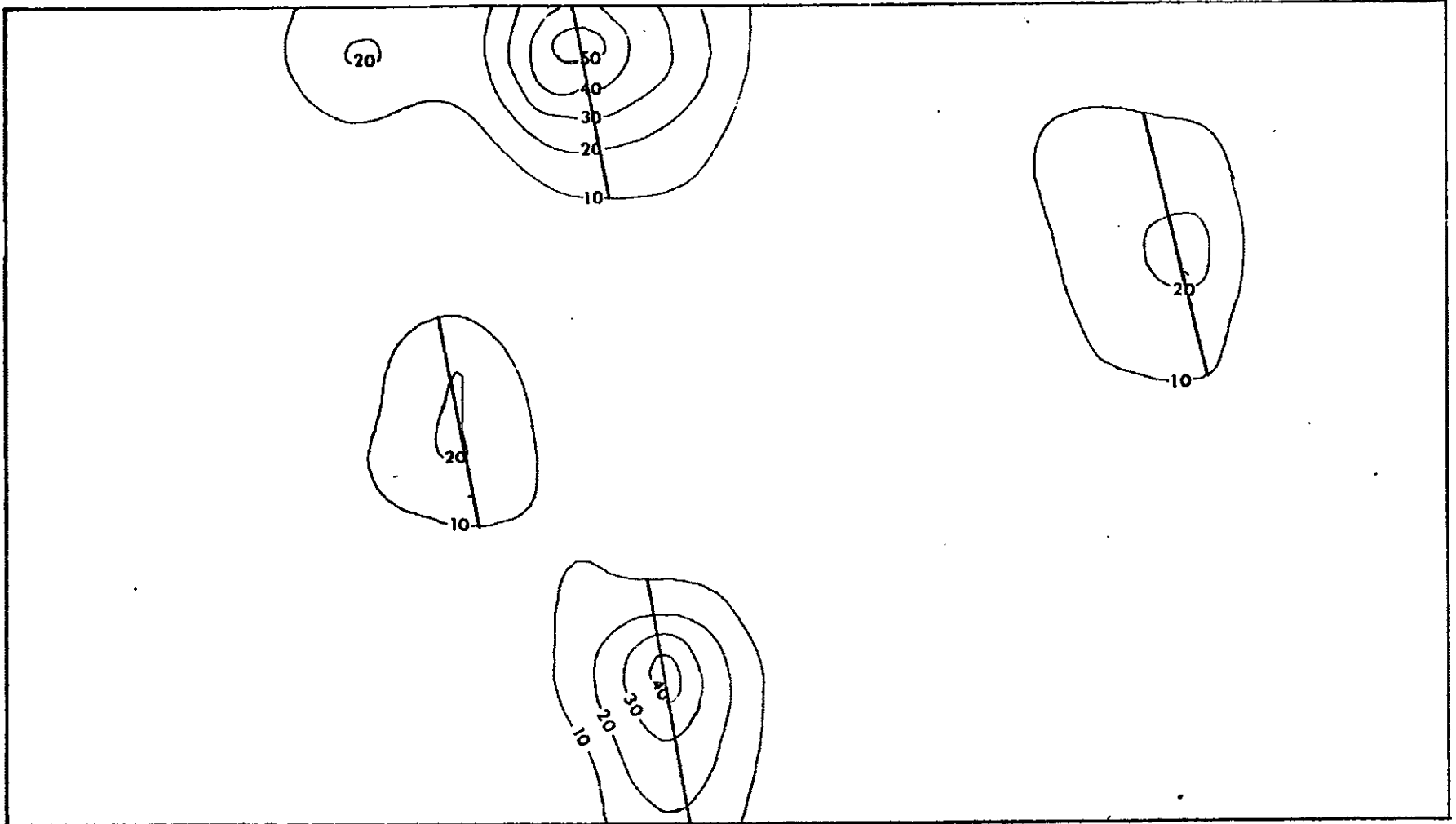
280-300 Degrees



300-320 Degrees



320-340 Degrees



340 - 360 Degrees

APPENDIX 5

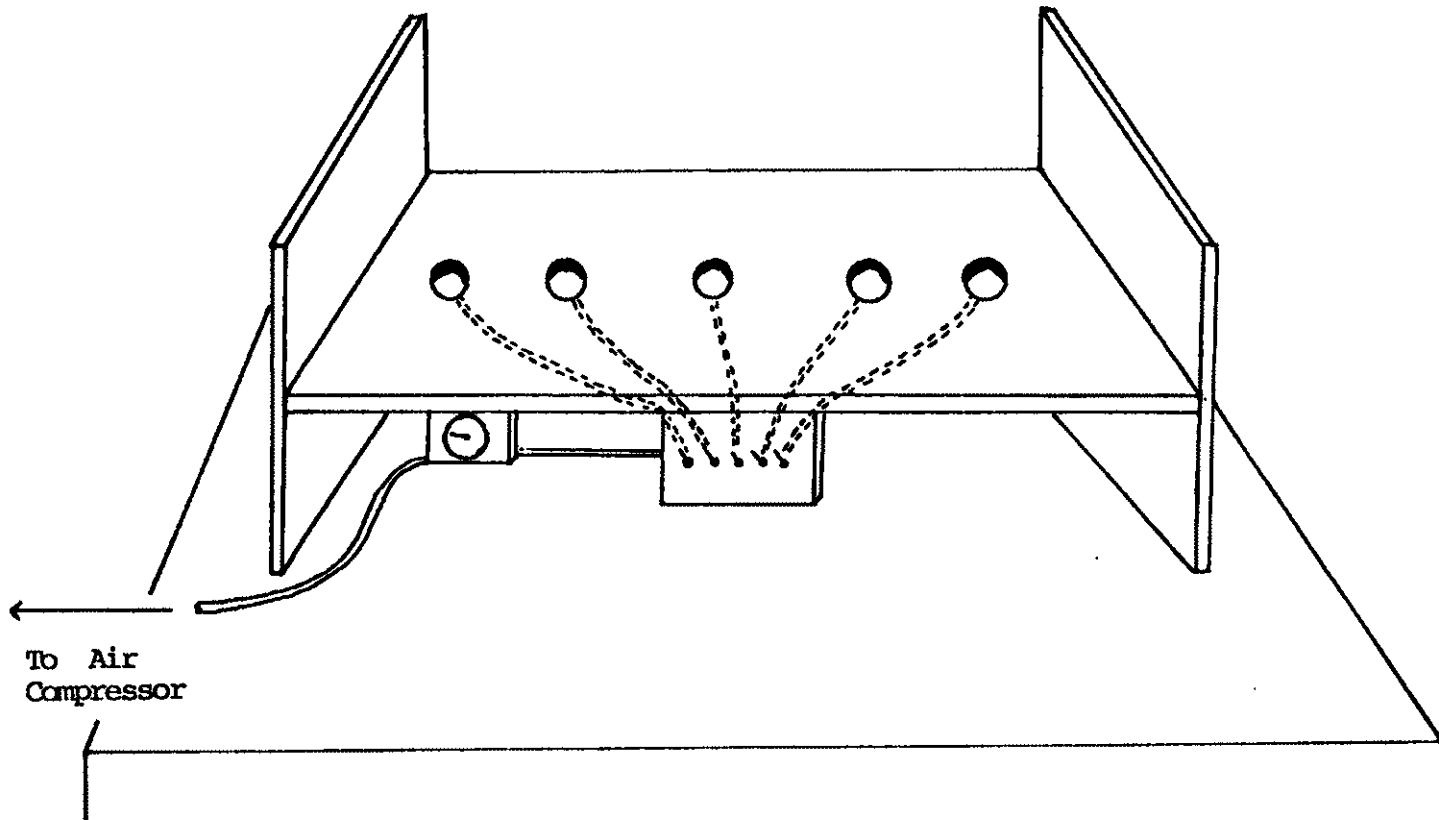
Uplifting Experiment

An experiment was constructed to study the fracture patterns associated with multiple uplifting domes. The experiment was modified from the procedures developed by Withjack and Scheiner (1982) for single, uplifting domes.

Figure 28 is an illustration of the apparatus used in this study. The base and sides of the apparatus were constructed from half-inch plexiglass. The base contained five evenly spaced holes representing different uplifting centers. Attached under each of these uplifting centers (UC's) were five rubber balloons of equal dimensions. Each of the UC's were connected to an air compressor by polyurethane tubing. Individual valves feed each UC with an air pressure gauge in line to assure proper, constant air flowage. A 35mm camera is fixed above for photographing.

Thirty five runs of the experiment were attempted using different combinations of three materials; 1) modeling clay; 2)plaster; and 3)sand. Each run was mixed in a styrofoam tray and dried in an oven at 70°F. The trays were then fastened to the base of the apparatus by celophane tape over an UC. Compressed air was then pumped thru the valves to the UC.

Figure 28 Appratus used in fracture trace experiment.
Model after Withjack and Schneider (1984)



Although this experiment failed to construct the fracture pattern found in the Tharsis region, several conclusions can be drawn:

- 1) Single domal uplifts form very pronounced radial patterns.
- 2) When more than one uplift is attempted: 1) the first fractures to appear are radial to the centers, (Figure 3) a strong dominant fracture appears between the uplifting centers and the radial pattern subsides.
- 3) The slower the uplift the more pronounced the radial pattern. When an uplift is rapid between three or more uplifting centers, the outer uplifting centers maintain their radial pattern, and the radial pattern associated with the center uplift is gradually reduced.